

A COMPARISON OF SPHERICAL GRIDS FOR
NUMERICAL INTEGRATION OF ATMOSPHERIC MODELS

by

DAVID L. WILLIAMSON

B.S. The Pennsylvania State University
(1963)

M.A. The Pennsylvania State University
(1965)

SUBMITTED IN PARTIAL FULFILLMENT OF THE
REQUIREMENTS FOR THE DEGREE OF
DOCTOR OF PHILOSOPHY

at the

MASSACHUSETTS INSTITUTE OF TECHNOLOGY

April, 1969

Signature of Author
Department of Meteorology, April 10, 1969

Certified by
Thesis Supervisor

Accepted by
Chairman, Departmental Committee on Graduate Students



A COMPARISON OF SPHERICAL GRIDS FOR
NUMERICAL INTEGRATION OF ATMOSPHERIC MODELS

by

DAVID L. WILLIAMSON

Submitted to the Department of Meteorology on April 10, 1969
in partial fulfillment of the requirement for the degree of
Doctor of Philosophy.

ABSTRACT

The properties of spherical grids are reviewed and compared with one another. A quasi-homogeneous spherical geodesic grid is introduced to eliminate many of the undesirable features of other grids. The spherical geodesic grid is first compared with the other grids for integrating the nondivergent barotropic vorticity equation. Initial conditions are used for which an analytic solution exists. The spherical geodesic grid produces the best solution. The only observable error in the contoured output is a small phase error.

Methods of developing difference approximations for the primitive barotropic model over triangular grids are first considered in cartesian geometry. Comparative integrations show that the six-point differences associated with triangular grids produce better solutions than square differences with similar resolution and the same order of truncation error.

Conservative difference schemes are introduced for the primitive barotropic model over the spherical geodesic grid. The small variation in the grid interval means that conservative schemes which are second order over regular grids are first order over the spherical geodesic grid. This truncation error can be made insignificant by taking a fine enough mesh. Comparative integrations indicate that the spherical geodesic grid produces results that are at least as good as those produced by the schemes currently being used for numerical weather prediction.

Thesis Supervisor: Edward N. Lorenz

Title : Professor of Meteorology

TABLE OF CONTENTS

I	INTRODUCTION	5
II	SPHERICAL GRIDS	7
	2.1 Conformal coordinates	7
	2.2 Spherical coordinates	11
	2.3 Spherical geodesic grid	15
	Figures for Chapter II	20
III	NONDIVERGENT BAROTROPIC MODEL ON THE SPHERE	25
	3.1 Finite Difference Approximations	25
	3.2 Initial Conditions	29
	3.3 Errors in initial time step	29
	3.4 Twelve-day integrations	33
	Figures for Chapter III	37
IV	PRIMITIVE BAROTROPIC MODEL ON A PLANE	44
	4.1 Conservative difference approximations	49
	4.2 Individual approximations	53
	Pressure Gradient	55
	Mass Flux	57
	Momentum Flux	59
	4.3 Homogeneous grid	59
	4.4 Truncation error	63
	4.5 Fourth order schemes	65

4.6	Boundary conditions	67
4.7	Numerical integrations	69
	Figures for Chapter IV	73
V	PRIMITIVE BAROTROPIC MODEL ON THE SPHERE	81
5.1	Conservative difference approximations	82
5.2	Numerical experiments	89
	Gravity Waves	90
	Neamtan Waves	92
5.3	Initial tendencies	97
5.4	Truncation error	102
	Figures for Chapter V	109
VI	CONCLUSIONS	122
6.1	Conclusions	122
6.2	Suggestions for further research	126
	Acknowledgements	128
	Appendices	129
1	Relations used to simplify truncation error expressions	129
2	Computation of \vec{C}_i	134
	References	136
	Biography	140

CHAPTER I

INTRODUCTION

The advent of today's large fast computers has made it practical to experiment with atmospheric models defined over the entire sphere. A spherical domain eliminates the need for artificial side boundaries which introduce spurious results into the regions near them and also makes it possible for general circulation models to study the interactions between the tropics and mid-latitudes as well as between hemispheres.

There are two main methods used today to model the atmosphere over a sphere: expansion into spherical harmonics and discrete approximations over grid points. In the first method, or spectral method, all the variables of the governing equations are represented by a series of spherical harmonics. The prognostic equations then become prognostic equations for the amplitude of each spherical harmonic and the evolution of these amplitudes is calculated in time. In the grid point method the variables of the governing equations are replaced by a discrete set of variables defined at a set of grid points over the sphere. The continuous differential operators of the governing equations are replaced by discrete operators defined over the grid points. The evolution of the discrete variables is then calculated in time.

The first spectral integration was carried out by Bjer (1964) for the vorticity equation. Ellsaesser (1956) performed comparison

integrations between the grid point and spectral methods for a slightly more general model. He concluded that for these simple models the spectral method produces better results than the grid point method. However, for models based on the complete meteorological equations the desirability of the spectral method becomes questionable. Robert (1966) performed a successful integration of the complete equations; however, not all the physical processes occurring in the atmosphere were included.

Satisfactory methods of handling phenomena such as precipitation have not been developed for spectral models. Robert (1968) is currently studying them. This lack of such methods plus the large number of interaction coefficients necessitated by the desirability of fine resolution have led almost all experimenters modeling the general circulation to use grid point methods. For this reason, the remainder of this report will deal with grid point methods.

Fundamental problems which naturally arise with grid point methods are the definition of the grid points themselves and the development of discrete approximations to be applied at these grid points. Various grid systems over a sphere and accompanying difference schemes have been suggested in the last decade and tried with varying degrees of success. As will be seen in the next chapter, these schemes all have some undesirable property. One property which few of these schemes possess yet which seems desirable is homogeneity. A new quasi-homogeneous grid is also introduced in the next chapter. In the following chapters difference approximations are developed for atmospheric models and evaluation experiments are compared with experiments using other schemes.

CHAPTER II

SPHERICAL GRIDS

The nets of points suggested to date for use with discrete approximations fall into three main categories: nets based on conformal map coordinates, nets based on spherical coordinates, and quasi-homogeneous nets independent of the coordinate systems. We consider each category in turn.

2.1 Conformal coordinates

In order to use mappings for numerical studies, the domain of interest, in our case the sphere, is projected onto a section of a plane. A net of points is then defined on the projection. This net can be considered as the projection of a net of points originally on the sphere. Following Kurihara (1965b) we refer to these points on the sphere as the original grid.

Conformal mappings are used in meteorology in order to preserve the general form of the hydrodynamical equations when written in terms of the map coordinates. The difficulties of using conformal mappings for spherical studies arise from the impossibility of mapping the entire sphere conformally onto a finite section of a plane.

The use of a uniform grid on a Mercator projection is clearly unsatisfactory for spherical integrations. With such a grid, the original grid interval becomes infinitely small at high latitudes and the pole, at infinity, cannot be reached. Kuo and Nordo (1959) have

used a grid, similar to the one proposed by Richardson (1922), with square meshes of variable size on a Mercator map. Their grid increment was doubled at 60° and again at two higher latitudes. The pole was represented by an extra row of six points which were close but not at the infinite pole. Kuo and Nordo integrated the quasi-nondivergent model developed by Kuo (1956) over one hemisphere using Green's method. Initial conditions were for mean zonal flow with a somewhat random disturbance superimposed. The integration was carried out for six days using a $1\frac{1}{2}$ hour time step. It was not possible to continue the computations for a longer period because a computational instability developed after the fifth day. This instability was apparently connected with the change in grid size at 60° . The instability plus the inability to properly handle polar phenomena make this type of grid unsuitable for spherical integrations.

Smagorinsky, Manabe, and Holloway (1965) have integrated the primitive equations over one hemisphere using a uniform mesh on a stereographic projection. Such a grid is not homogeneous over the hemisphere. The original grid increment varies by a factor of two from pole to equator. It seems possible to integrate over an entire sphere using two such grids, one for each hemispherical projection. A square mesh on one projection has some points which lie outside the equator on that projection and which have a corresponding position inside the equator of the other projection. Such points do not in general correspond to grid points of the other projection and some sort of interpolation scheme is needed to provide values of the variables at these

points. If energy conservative schemes are desired they are very difficult to formulate using these interpolated values. Also, as will be seen in the next paragraph, great care must be taken in the interpolation formulation to eliminate spurious small scale features from appearing in the integrations.

In order to obtain a more homogeneous grid, Phillips (1957) proposed using a stereographic map for high latitudes and a Mercator map for low latitudes, connected at middle latitudes by overlapping grids. With this system, the original grid interval changes by only a factor of 1.4. Phillips (1959) performed a numerical test to check the stability of his system since the scheme was too complicated to examine theoretically. He integrated the primitive equations for a barotropic atmosphere for a period of two days using Eliassen type finite-differencing. The initial conditions were defined to be a Haurwitz wave of wave number four. Haurwitz (1940) has shown that in a non-divergent barotropic atmosphere, such a wave will move from west to east without change of shape with a known constant angular velocity equal to 13° per day for the initial conditions chosen by Phillips. Because of divergence due to the free surface in Phillips' model, the rate of progression of his flow pattern should be less than that given by Haurwitz.

The wave in the numerical experiment moved about 9° per day, in rough agreement with what was expected. The fields remained quite smooth. The isolines agreed well with one another where the two maps overlapped except for two small areas. Two small temporary "wiggles"

appeared during the course of the integrations. They appeared only near the top boundary of the Mercator grid, the stereographic grid values being quite smooth at all times. Phillips concluded that the "wiggles" were some peculiar type of truncation error.

A further study by Phillips (1962) suggested that these truncation errors can be eliminated by changing the finite difference formulation. After reformulating the differences he repeated the same barotropic forecast as in the first test. The new system did avoid the peculiar truncation errors near the boundaries. This forecast was continued to three days. The fields were perfectly smooth and resembled the initial data very closely. Phillips¹ later carried out a 12 day integration with no trouble.

Even though with careful formulation, difference schemes work over this grid, the basic idea of interpolating between two grids at mid-latitudes where much is happening does not appeal to most investigators. Also, the problem of formulating energy conservative schemes is very difficult and has not been treated successfully to date. Because of these difficulties caused by the impossibility of conformally mapping the entire sphere onto a finite section of the plane, investigators turned to grids based on the sphere itself and to polar spherical coordinates.

¹Private communication

2.2 Spherical coordinates

The immediately obvious grid of this class is one with grid points at intersections of equally spaced latitude and longitude lines. In this case, as the pole is approached, the meridians converge and the linear distance between grid points in the longitudinal direction approaches zero. This convergence places a severe restriction on the maximum allowable time increment through linear stability conditions. Such a grid is also far from homogeneous.

Most grids in this class have been designed to avoid the small time step required by the convergence of grid points in the polar areas. The atmospheric general circulation models that are presently being integrated over the entire earth all use grids of this kind.

Gates and Riegel (1962) designed a grid, similar to that proposed by Pfeffer (1960), to avoid the small time step. In their grid, the latitudinal increment was fixed while the longitudinal increment increased by multiples at higher latitudes. The increment was first increased at 45° , then again at 70° , 75° , 80° , and 85° .

As a first test of their grid system, Gates and Riegel integrated a non-divergent barotropic model for a period of several days. Initial conditions were for a wave that should move with an angular velocity of 20° per day without change of shape. Since the analytic solution for their model is known, numerical errors can be determined exactly. After a ten day period of integration, their solution had a pronounced distortion in the form of a backward tilt. This tilt first appeared near the latitude where the longitudinal increment was first doubled. Thus the

phase truncation error is a function of the longitudinal grid increment and increases where the grid interval increases.

This artificial tilt in the wave structure being modeled produces erroneous momentum transports which in turn produce a wrong distribution of the easterlies and westerlies in the solution. Thus general circulation models with this type of error produce statistics inconsistent with the original continuous model. This would be a serious flaw in general circulation model approximations.

In an effort to reduce this wave distortion in middle latitudes, Gates and Riegel (1963a) changed the grid so that the longitudinal increment first doubled at 75° . The numerical test was repeated. The distortion at mid latitudes was eliminated, but the effect of the increment increase at higher latitudes was not considered, there being little happening there.

As additional tests, Gates and Riegel (1963b) integrated the barotropic model, the two-level quasi-geostrophic model, and the two-layer balanced model of variable static stability. The equations were all formulated in terms of a streamfunction for the non-divergent part of the wind and a potential function for the irrotational part. Initial conditions were atmospheric data for OOGCT, 7 December 1957. No difficulties due to the doubling of the grid increment were reported.

A disadvantage of this grid, in addition to the differential phase truncation error, is that the time increment is still limited by the convergence of the longitudinal grid increment up to 70° where the linear grid interval is less than half its value at the equator.

Kurihara (1965b) has defined a grid in which the longitudinal grid increment changes more gradually with increasing latitude. In fact the linear grid increment actually increases with increasing latitude. Kurihara defines $N+1$ equally spaced latitude circles from the pole to the equator. He places $4N$ grid points around the equator. At each successively higher latitude the number of grid points is decreased by four, resulting in four points next to the pole and one point at the pole.

Kurihara (1965b) carried out successful test computations using a barotropic primitive equation model. However his scheme was quite complicated, involving a number of interpolations. In a later paper (Kurihara and Holloway, 1967), he avoided these complications by using difference equations formulated by means of the so-called box method. Integrations with a nine-level model produced seemingly satisfactory results. These results, however, are not useful for comparison with other schemes because of the complexity of the continuous model.

Gary (1968) performed rather extensive comparisons between difference schemes which have been used for general circulation models over Kurihara's grid and over Gates and Riegel's grid. These integrations will be considered in more detail in later sections for comparisons of our schemes with those currently being used for numerical experiments. It suffices to state here that he found Kurihara's "uniform" grid less satisfactory than the Gates and Riegel type.

Grimmer and Shaw (1967) attempted to eliminate the differential phase truncation error by using a variable time step. In their scheme, the longitudinal grid increment remains constant and the time step is decreased with increasing latitude to maintain linear stability. Because of the variable time step, at any point in the integration, the time-levels reached by the various rows are different. Linear interpolation in time is used to provide values at the same time level for the application of the difference operators. This interpolation provides a certain amount of smoothing.

With test integrations using Phillips' (1959) initial conditions, Grimmer and Shaw found that their schemes worked quite well. However, they also conclude that their system is not ideal. The resolution near the pole is excessive and synoptic developments there do not warrant such detail. A large fraction of the computer time is used computing in high latitudes. In one experiment more than half the computer time was spent integrating the two northernmost rows, which represent only about two percent of the area of the sphere.

As is seen above, all the grids and accompanying difference approximations that have been developed to date have some undesirable property. In an attempt to eliminate these undesirable properties we introduce a quasi-homogeneous grid and accompanying discrete approximations for models of the type used for general circulation studies.

2.3 Spherical geodesic grid

Many people have noted the similarity between a sphere and Buckminster Fuller's Geodesic Domes, constructed from plane triangles (see Mc Hale, 1962, for a collection of photographs of such domes). This close similarity leads one to believe a spherical grid can be defined in a similar fashion. A similar division of the globe was used for geomagnetic studies by Vestine et al. (1963). The name spherical geodesic grid follows from defining the grid as a collection of geodesics, or arcs of great circles.

This type of grid has several inherent advantages. Since the grid is quasi-homogeneous the maximum allowable time step is not limited by the closeness of grid points in one small region of the domain of interest. The grid does not have points lined up on latitude circles. This feature might be desirable for statistical studies as points lined up on latitude circles might lead to spurious results in zonally averaged quantities. The grid also has the advantage of not being based on the coordinate system used. This means that parallel integrations can be performed with several orientations of the grid points. If the results agree with one another, it can be assumed the grid did not cause a systematic error. In the following we give a review of the grid as formulated in Williamson (1968).

The spherical geodesic grid consists of a number of almost, but not quite, equal-area, equilateral spherical triangles covering the entire sphere. There are many methods of defining such a grid. Basic

to those considered here is an icosahedron, the geometric solid with 20 equilateral-triangular faces, constructed inside a sphere with its twelve vertices on the sphere. We denote the 20 triangles of the icosahedron as major triangles. The vertices of the major triangles can be connected by great circles to form 20 congruent major spherical triangles covering the sphere (Fig. 2.1). These major spherical triangles are then subdivided into smaller grid triangles.

One possible grid is defined by dividing the major triangles into smaller congruent triangles and projecting these onto the sphere. Let each side of a major triangle be divided into n equal segments, where $n = 2^m$ for some integer $m \geq 1$. Perpendicular lines are constructed from the division points to the opposite sides, as in Fig. 2.2. Each major triangle then contains $3n(n-2)/4$ complete congruent equilateral plane triangles, with n half triangles along each edge. The vertices of these smaller triangles are projected onto the surface of the sphere by a ray from its center and connected by great circles to form the spherical grid triangles.

A second possible grid, the one used for the integrations presented here, is defined as follows. Examination of an icosahedron shows that it can be separated into five sets of four triangles. For convenience we place the end vertices of each set at the north and south poles as in Fig. 2.3. (This restriction is easily removed.) With this orientation, the north and south poles are common to all five sets of four triangles.

The sides of the major spherical triangles are now divided into n equal arcs (again $n = 2^m$). In this case, three sets of great circles do not always intersect at one point as straight lines do in the plane case. Hence the two sets shown as solid lines in Fig. 2.3 are used to define the grid points in ACD. These points are projected across AC to define the points in ACE. The points in the other two triangles of the set are defined in the same manner using the south pole for reference instead of the north. The grid triangles are formed by connecting the points with great circles (solid and broken lines in Fig. 2.3). Note that again the sides of the major spherical triangles do not coincide with sides of the grid triangles. The latitudes and longitudes of the grid points can be found in a straightforward manner by applying standard formulas of spherical trigonometry. The details are given in Appendix 1 of Williamson (1968). Once the positions of the grid points are found for this orientation of the grid, any point can be made the pole by a simple rotation (Appendix 2 of Williamson, 1968). Figs. 2.4 and 2.5 show the two orientations of the grid used in this study. In the figures, circles represent grid points located on the side of a major triangle, and crosses indicate points interior to major triangles. In Fig. 2.4 the poles are at vertices of major triangles, and sides of major triangles run in the zonal bands 27 to 33° and -27 to -33° . In the second orientation (Fig. 2.5), the poles are near the centers of major triangles and there is no narrow zonal band containing sides of major triangles all around the earth.

Each major triangle contains $3/4 n(n-2)$ complete grid triangles and each edge bisects n triangles. Therefore the grid consists of $15 n^2$ triangles. All but 12 grid points are vertices of six triangles, the 12 points are vertices of five triangles. Hence, if N is the number of grid points

$$6 \times (N - 12) + 5 \times 12 = 3 \times 15 n^2$$

and the number of grid points is given by

$$N = \frac{15}{2} n^2 + 2.$$

We define an average area \bar{A} to be the area a spherical triangle would have if the area of $15 n^2$ of them equalled the area of the earth, i.e.,

$$\bar{A} = 4\pi r^2 / 15 n^2$$

where r is the radius of the earth. Similarly, a mean grid interval \bar{h} can be defined to be the length of a side of an equilateral triangle having area \bar{A} .

$$\bar{h}^2 = 4\bar{A} / \sqrt{3}$$

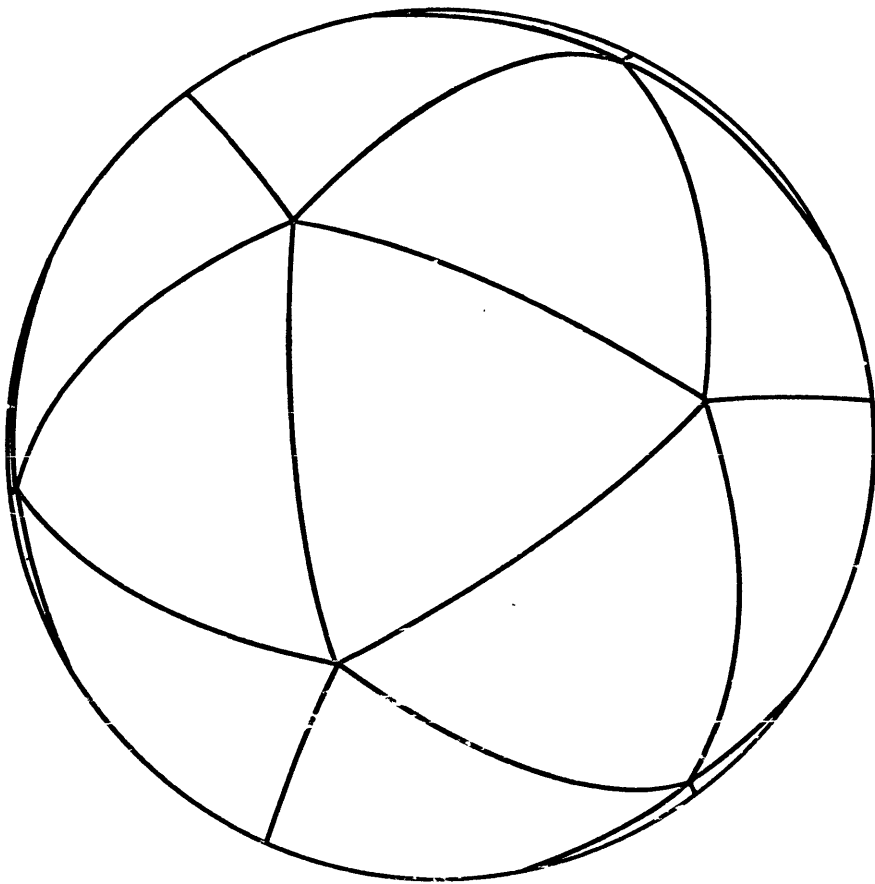
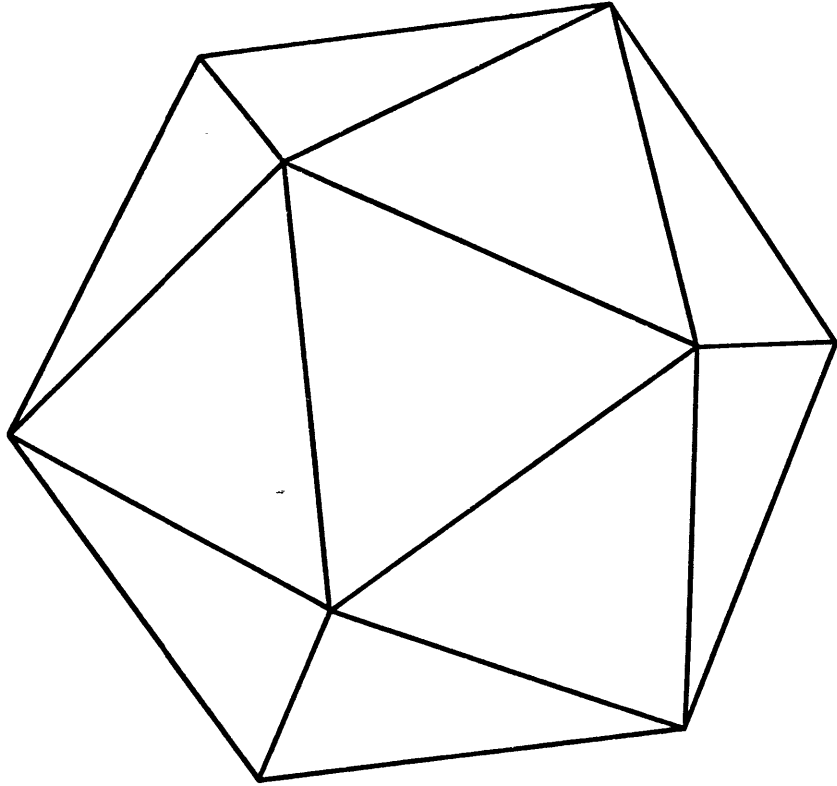
Table 1 provides the appropriate values for several values of n taking $r = 6370$ km. We refer to $n = 8$ as a 10° grid and $n = 16$ as a 5° grid: The actual grid interval of the 10° grid varies from 8.59° in the vertices of major triangles to 10.82° in the centers. The grid interval of the 5° grid varies from 4.28° to 5.49° . These grids are there-

fore not homogeneous in the sense that all grid intervals are equal; however, such triangular grids are impossible to define if the grid interval is less than 63° .

Table 1

n	Number of Triangles	Number of Grid Points	\bar{A} km ²	\bar{h} km	Degrees
4	240	122	213×10^4	1911	19.8
8	960	482	53×10^4	1100	9.91
16	3840	1922	13×10^4	554	4.98
32	15360	7682	3.3×10^4	276	2.48

Fig. 2.1 An icosahedron and an icosahedron expanded
onto a sphere.



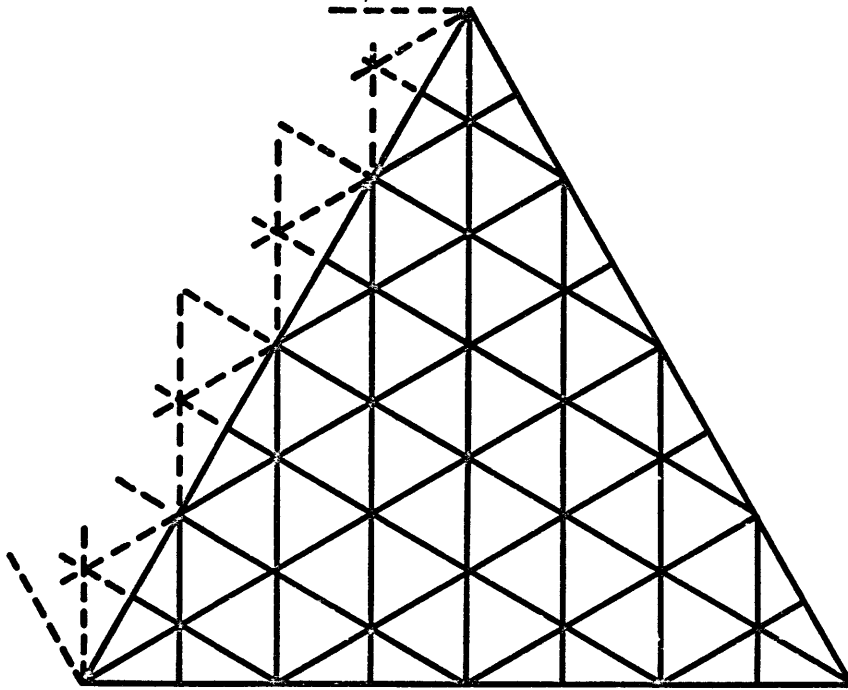


Fig. 2.2 Division of major plane triangle into smaller congruent triangles ($n = 8$).

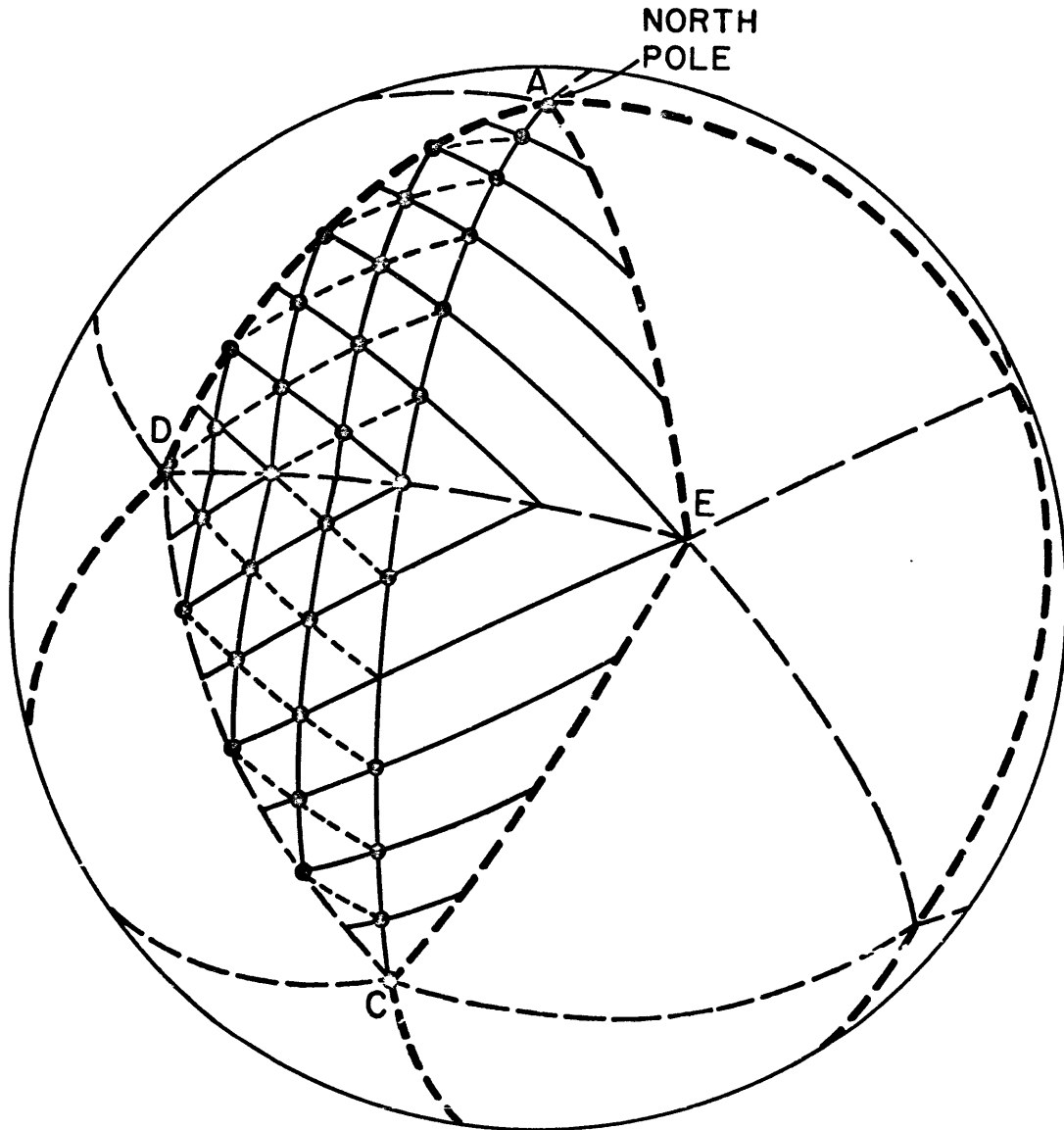


Fig. 2.3 Division of major spherical triangles into grid triangles ($n=8$). See text for explanation.



Fig. 2.4 Spherical geodesic grid with pole at a major triangle vertex. Circles represent grid points on sides of major triangles, crosses represent grid points interior to major triangles.

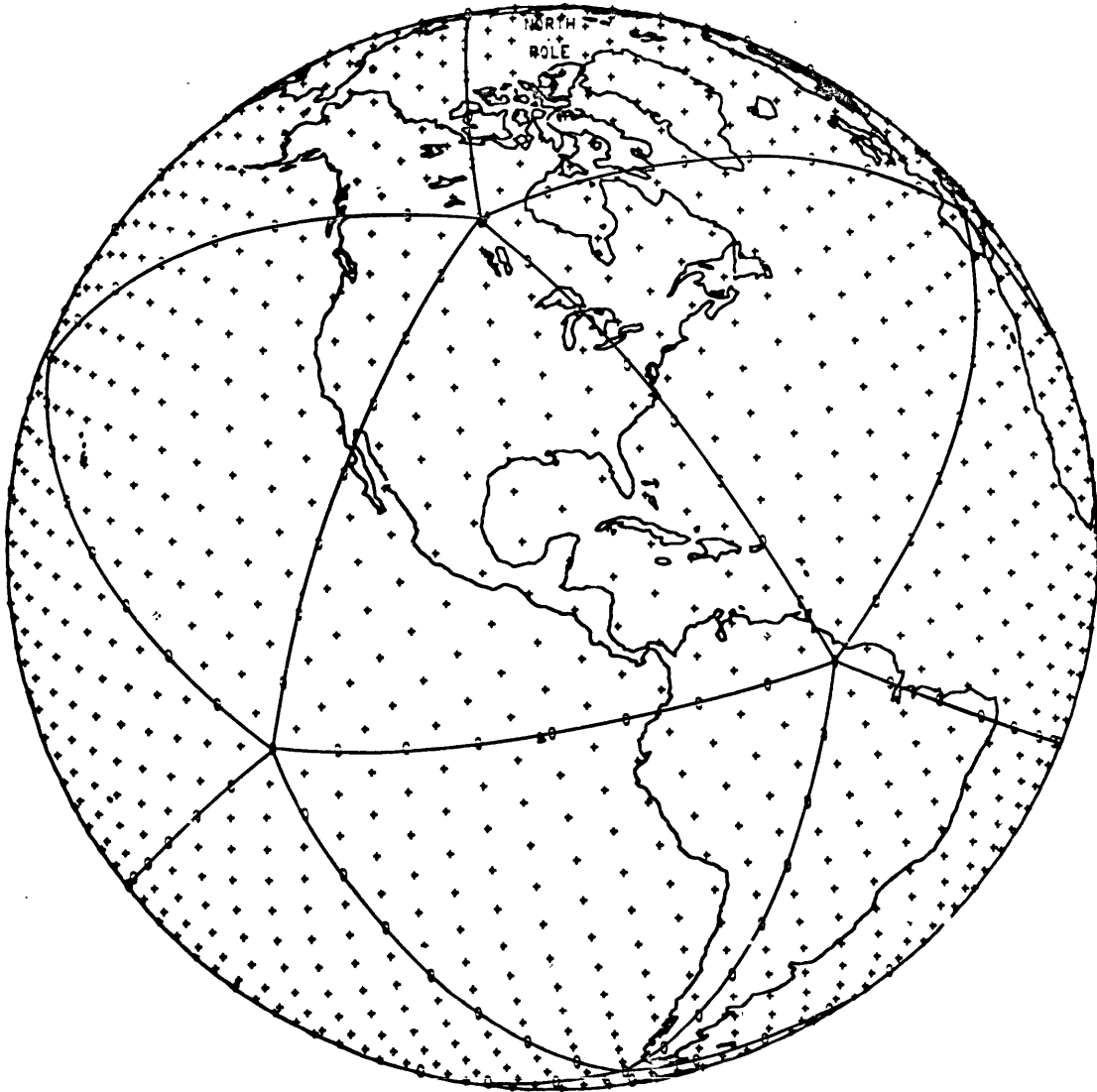


Fig. 2.5 Spherical geodesic grid with pole near
the center of a major spherical triangle.
See Fig. 2.4 caption.

CHAPTER III

NONDIVERGENT BAROTROPIC MODEL ON THE SPHERE

As a first test of the spherical geodesic grid, the barotropic model for nondivergent, frictionless flow is used

$$\frac{\partial \zeta}{\partial t} = -J(\psi, \zeta + f)$$
$$\zeta = \nabla^2 \psi$$

Here ζ is vorticity, ψ the streamfunction, f the Coriolis parameter, J the Jacobian operator, and ∇^2 the Laplacian.

This model was chosen for the test so that analytic initial conditions with a known solution (Neamtan, 1946) could be prescribed. In doing so, all errors except those due to the numerical methods employed are eliminated. A similar test over the grid of Vestine et al. (1963) was performed by Sadourny, Arakawa, and Mintz (1968).

3.1 Finite difference approximations

A finite difference form of the Jacobian or advection term has been proposed by Lorenz¹ for a grid of arbitrary triangles. Consider the polygon, with area A , formed by K triangles surrounding the grid point P_0 , such as in Fig. 3.1 with $K = 5$. The vertices of the polygon are P_1 to P_5 . Since the flow is nondivergent, integration of

¹Private communication, 1966.

the first equation over this region results in

$$\frac{\partial}{\partial t} \int_A \zeta \, dA = - \oint_S u_n (\zeta + f) \, ds$$

where u_n is the velocity normal to the boundary s . Two approximations are made in applying this equation to the grid. First, the area integral of the vorticity is replaced by $\zeta_o A$. Second, the absolute vorticity $\zeta^* = \zeta + f$ is assumed to be uniform along each side of the polygon and is given by the arithmetic mean of its values at the end points of the side. Then since $u_n = -\partial\psi/ds$, the difference form becomes

$$\frac{\partial \zeta_o}{\partial t} = \frac{1}{2A} \sum_{i=1}^K (\zeta_i^* + \zeta_j^*) (\psi_j - \psi_i) \quad (3.1)$$

where $j = i+1 \pmod{K}$.

It is immediately seen that if the total vorticity is defined to be the sum of the vorticity at the grid points weighted by the areas of the surrounding triangles, then total vorticity is conserved. It is also easy to show that kinetic energy and the square of vorticity are conserved.

If this scheme is applied to a rectangular grid by averaging the difference equations obtained from triangulation using either right diagonals or left diagonals, the result is seen to be Arakawa's (1966) scheme. The scheme applied to an equilateral triangular grid on a plane is second order.

As is always the case for models formulated in terms of a stream function, it is necessary to solve Poisson's equation. The method used in this test is a sequential relaxation. Thus a difference scheme for the Laplacian is needed. Such schemes have been formulated for triangular grids by MacNeal (1953) and Winslow (1966). We introduce another method. These methods all reduce to the same one for equilateral triangular grids on a plane.

Construct the polygon, with area a , formed by the perpendicular bisectors of the rays $P_0 P_i$ of the original polygon (Fig. 3.1). Integration of $\zeta = \nabla^2 \psi$ over a gives

$$\Gamma = \oint_{s'} u_s ds$$

Where Γ is the circulation around the boundary s' of a and u_s is the counterclockwise tangential velocity. Two approximations are used to apply this equation to the grid. First, replace the circulation by $\zeta_0 a$. Second, assume that the tangential velocity $u_s (= \partial\psi/\partial n)$ is constant on each segment of s' and equal to $(\psi_i - \psi_0) / |P_0 P_i|$. The difference approximation is then

$$\zeta_0 = \sum_{i=1}^K \omega_i (\psi_i - \psi_0) \quad (3.2)$$

where $\omega_i \equiv l_i / |P_0 P_i| a$ and l_i are the lengths of the line segments of s' .

The solution of Poisson's equation is obtained by a sequential relaxation. The direction of the sweep through the grid is complicated by its being nonrectangular and is not given here. It may be indicated by the usual equations:

$$\psi_o^{m+1} = \psi_o^m + \alpha R^m \tag{3.3}$$

$$R^m = \frac{1}{\sum_{i=1}^k \omega_i} \left\{ \sum_{i=1}^k \omega_i (\psi_i^j - \psi_o^m) - \beta_o \right\}$$

j is either m or $m+1$ depending on whether or not the i^{th} surrounding point has been affected by the $m+1$ pass, and α is an overrelaxation coefficient to be determined experimentally.

The forecast can be made by either advancing β using $\partial\beta/\partial t$ or by relaxing for $\partial\psi/\partial t$ from $\partial\beta/\partial t$ and advancing ψ . The latter method is used here. The initial guess for the relaxation in the first time step is a zero field. The second time step uses the $\partial\psi/\partial t$ field from the first step for the initial guess and the general time step uses an extrapolation from the fields at the two previous times for the first guess. The relaxation is continued until the residue R is less than some prescribed convergence limit ϵ at all points. See Thompson (1961) for information concerning standard relaxation procedures used in meteorology. Any suitable time stepping may be used. Centered time differences are

used in the following integrations with a forward time step initially.

3.2 Initial conditions

The nondivergent barotropic model is chosen for the first test of the spherical geodesic grid since it has known solutions in the form of waves travelling around the earth with constant angular velocity and without change of shape. By using such analytic initial conditions we can determine exactly the total error, sum of roundoff and truncation, of the numerical scheme. Since Gates and Riegel (1962) integrated the same model over a sphere, we can use their initial conditions to allow also a direct comparison between the two difference schemes. Their initial and verification fields of ψ are

$$\psi = -279.68 \sin \varphi + 136.65 \sin(6\lambda - \nu t) \sin \varphi \cos^6 \varphi \quad (3.4)$$

in units of $\text{km}^2 \text{sec}^{-1}$. The pattern moves eastward with angular velocity $\nu/6 = 20^\circ$ longitude per day. Fig. 3.2 shows the field given by (3.4).

3.3 Errors in initial time step

As a first step in the error analysis, the model was run for one time step starting at time zero and the errors were examined as a function of grid orientation, overrelaxation coefficient and convergence criterion.

The speed of the relaxation process for the 5° grid is shown in Fig. 3.3. The convergence limit $\epsilon = .125 \text{ m}^2 \text{ sec}^{-2}$ corresponds to approximately 0.07 percent of the maximum $\partial\psi/\partial t$. One corresponding curve from Gates and Riegel (1962) is given for comparison. The geodesic grid is seen to be more sensitive to variation of overrelaxation parameter than Gates and Riegel's grid. It is also seen to be slower; however, Gates and Riegel's results are for only one hemisphere with fewer points. The second orientation of the grid is systematically faster than the first. This was also observed in similar tests with a 10° grid. The fastest convergence is around $\alpha = 1.8$ for all except one case. Winslow (1966) reports an optimum value between 1.9 and 1.96 for linearized overrelaxation in a nonuniform triangular mesh on a plane. One should remember that the results in Fig. 3.3 apply only to the first time step with initial conditions (3.4). The relaxation is considerably faster with the extrapolated first guess. The scheme converges on the average in less than 20 iterations with $\alpha = 1.8$, $\epsilon = .125$, and the grid of Fig. 2.5.

The error in the computed solution of $\partial\psi/\partial t$ is shown in Fig. 3.4 for $\alpha = 1.7$, $\epsilon = .125$ and grid of Fig. 2.5. The error consists of cells of alternating sign around the hemisphere with negative error (computed minus analytic solution) west of the wave trough and positive west of the ridge. The maximum error of each cell is found between latitudes 20° and 25° , the area of maximum vorticity advection. This type of error field produces a systematic underestimate of the true vorticity advection.

Table 2 lists the largest positive and negative errors of $\partial\psi/\partial t$ at time $t = 0$. These values are about 40 percent larger than the corresponding values from Gates and Riegel's integrations. Also, our results exhibit a larger and less systematic variation. The actual error patterns are all like Fig. 3.4 for the other values of α and ϵ tested.

The errors in Table 2 and Fig. 3.4 are the accumulation of the errors of all the discrete approximations used. It is also of interest to examine the errors of each phase in the computation. We consider first the error in calculating the vorticity. Fig. 3.5 shows the vorticity field determined analytically. The error pattern from calculating the vorticity from (3.2) resembles Fig. 3.5 closely, negative cells of error coinciding with positive cells of vorticity. This implies that the values of ζ calculated by the difference scheme are too small, and the gradient is smaller than it should be. The ζ error is about 2.0 percent of the true values with grid orientation 1, and 2.4 percent with grid orientation 2. There is a slight distortion of the error pattern when a zero contour crosses a side of a major triangle.

The pattern of exact values of $\partial\zeta/\partial t$ is like that of Fig. 3.4, but with uniform cells. The error in the Jacobian approximation using exact values of ψ and ζ also resembles Fig. 3.4 with positive cells out of phase with those of $\partial\zeta/\partial t$, indicating that the values of $\partial\zeta/\partial t$ are too small. The error in $\partial\zeta/\partial t$ is about 5 percent. When the values of ζ obtained from (3.2) are used instead of the exact

Table 2

$\alpha \backslash \epsilon$.25		.125		.0625	
1.6	65.5	-65.5	66.7	-66.9	69.0	-69.1
	69.4	-69.5	66.5	-66.5	-	-
1.7	65.4	-65.2	67.5	-67.8	69.5	-69.7
	67.9	-67.8	65.4	-65.5	64.3	-64.4
1.8	65.7	-66.4	68.9	-69.3	70.6	-70.8
	63.4	-63.8	63.3	-63.5	63.5	-63.5
1.9	71.0	-71.7	71.4	-71.5	-	-
	64.1	-64.9	63.9	-64.3	64.1	-64.1

Maximum positive and negative errors of $\partial\psi/\partial t$ ($m^2 \text{ sec}^{-2}$) at $t = 0$.

The upper numbers are for grid Fig. 2.4 the lower ones for grid of

Fig. 2.5.

values, the error is increased to 13 percent. The error field is also more distorted at sides of major triangles in this case.

The values of $\partial \Psi / \partial t$ were found by relaxing the exact $\partial \mathcal{L} / \partial t$ field to compare with the values obtained in the previous section. The convergence properties are the same as those with the approximate $\partial \mathcal{L} / \partial t$ field. The error using exact $\partial \mathcal{L} / \partial t$ values is 50 percent of that using the approximate $\partial \mathcal{L} / \partial t$ values.

3.4 Twelve day integrations

Initial conditions (3.4) were integrated for 12 days using 1 hour time steps, $\delta = 1.8$, $\epsilon = .125$, and the grid shown on Fig. 2.5. The wave moved eastward without change of shape at a speed of 18.6° per day compared to 20° per day for the analytic solution. No figure showing the final field is included as the only observable difference between it and Fig. 3.2 would be the phase shift. The wave did not exhibit any tendency for the trough to tilt, as reported by Gates and Riegel (1965), even though the spherical geodesic grid is coarser with respect to the wave at higher latitudes.

Since the analytic solution to these initial conditions is simply a wave moving without change of shape, Ψ^2 integrated around latitude bands is constant with time. Other quantities, such as kinetic energy and square vorticity, also have invariant zonal averages for these initial conditions and, of course, invariant global averages for arbitrary initial conditions. Examination of the integrals of the numerical solution furnishes a good check on the

accumulation of truncation error in the amplitude of the wave as a function of latitude. Fig. 3.6 shows a plot of ψ^2 integrated over the entire earth and also over two latitude bands. The middle curve is the average over the entire earth; the upper, for 50 to 60°N, is typical for latitude bands above 40°; and the lower, 20 to 30°N, is typical for latitudes below 40° with little variation near the equator. The averages are obtained by a simple summation of values at the points in a latitude band without weighting the values by the areas represented by the points. The truncation error in this integration is not significant for this wave pattern.

A small oscillation appears in all the averages with a period of about 3.2 days. Since the computed wave moved with speed 18.6° per day, this oscillation can be attributed to truncation error depending on trough position with respect to the grid. To check the hypothesis, the same initial conditions were integrated for 12 days using a 10 degree grid (every other point of Fig. 2.5) with both one and two hour time steps. In both cases, the wave moved with a speed of 15° per day. The small oscillations again appeared in the averages with a period of 4 days, agreeing with the observed 15° speed.

If these small-scale oscillations are removed from Fig. 3.6, the mean is seen to increase in lower latitudes, decrease in higher latitudes, and remain steady over the whole globe for the 5° grid. These changes may be a manifestation of truncation error being a function of latitude. Since the wave initial condition is a function of longitude increment, and the grid interval is a function of linear

increment, the grid is relatively coarser in high latitudes with respect to the ψ field under consideration.

The integrations using the 10° grid showed the means of all latitude bands increasing with time. The increase was very small for lower latitudes and increased to about 2.5 percent in 12 days for the higher latitudes above 50° . The global average increased by less than 2 percent in the 12 days. The resolution of the 10° grid at high latitudes is quite poor with respect to the wave, there being slightly less than four grid triangles per wavelength at 55° and obviously fewer at higher latitudes.

An initial condition of wave number four was also integrated over the 5 degree grid of Fig. 2.5 using 1 hour time steps. The initial condition is that given by Phillips (1962) as

$$\psi = -318.45 \sin \varphi + 318.45 \cos^4 \varphi \sin \varphi \cos 4\lambda \quad (3.5)$$

in units of $\text{km}^2 \text{sec}^{-1}$. Such a wave moves eastward with a speed of 12.2 degrees per day. Again the actual final pattern after 12 days did not differ significantly from the initial pattern except for the phase shift.

In this case the truncation error in approximating the integration of ψ^2 by an unweighted average over grid points is no longer negligible. Continuous integration of ψ^2 would result in constant zonal averages. However, when the analytic values are summed only at grid points, the result (solid curves in Fig. 3.7) is

seen to vary with a period of about 7.4 days. Such a period corresponds to the pattern moving one wavelength with respect to the grid. The averages of the numerical solution are given as the dotted curves in Fig. 3.7. The slightly larger period of the numerical solution is caused by the phase truncation error of the scheme. If the truncation error associated with the integration over latitude bands is subtracted, the same comments can be made concerning the truncation error of the model as in the wave number six case.

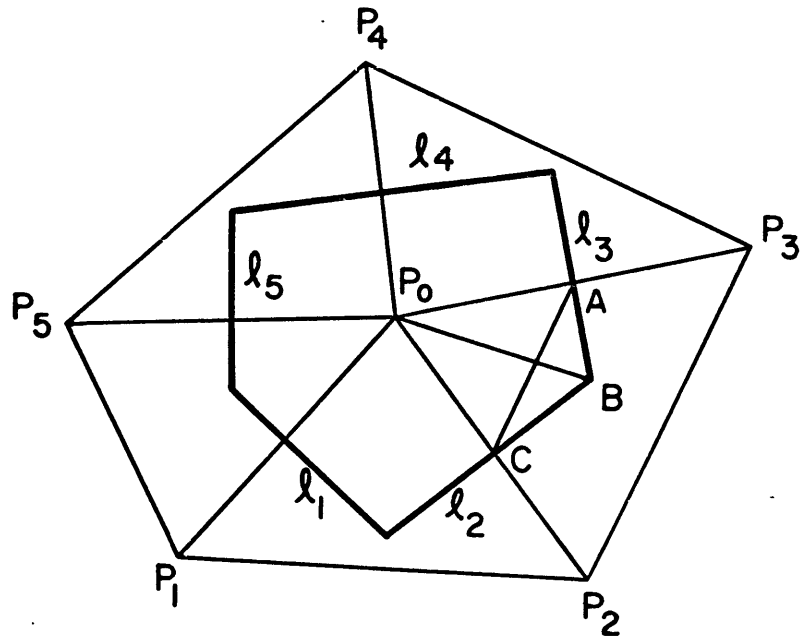


Fig. 3.1 Grid triangles and points for difference equations.

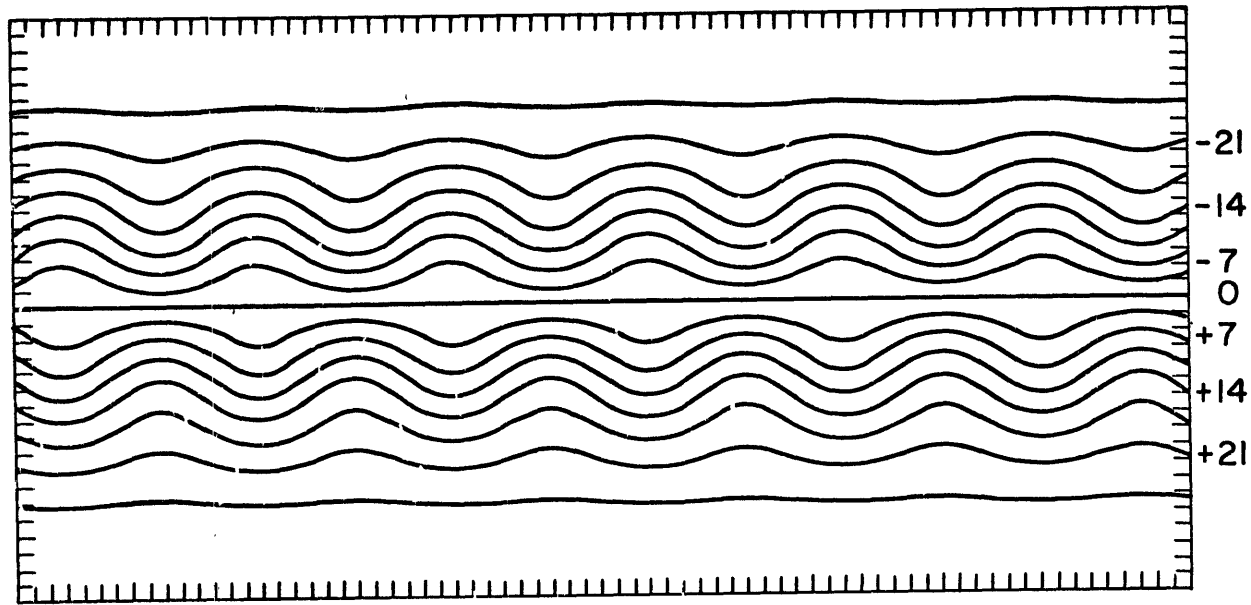


Fig. 3.2 Initial wave number six ψ field. Intersections of 5° latitude, longitude lines are projected onto a rectangular grid for the figure. The equator has zero ψ value. Contour interval is $3.5 \times 10^7 \text{ m}^2 \text{ sec}^{-1}$.

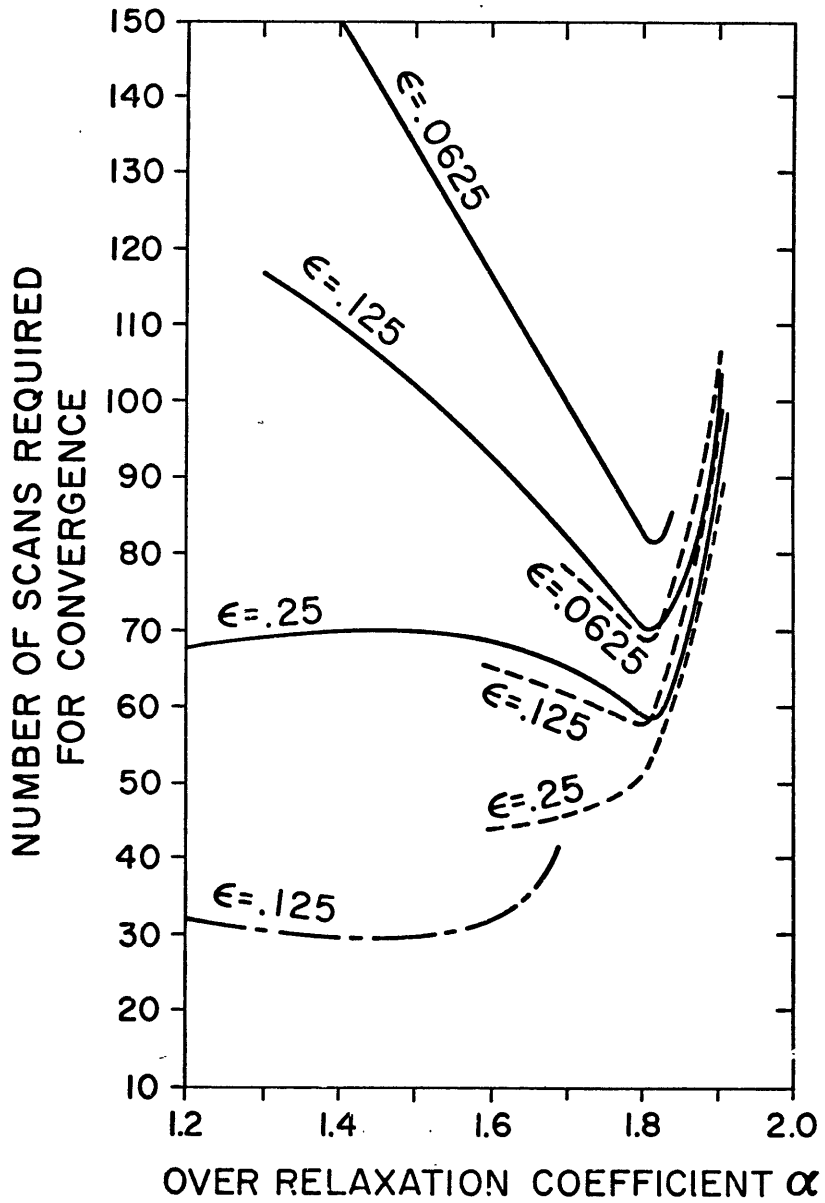


Fig. 3.3 Convergence speed of relaxation. Dashed lines are for the grid of Fig. 2.5, solid lines are for that of Fig. 2.4. The dash-dot line is a corresponding curve from Gates and Riegel converted to our coordinates.

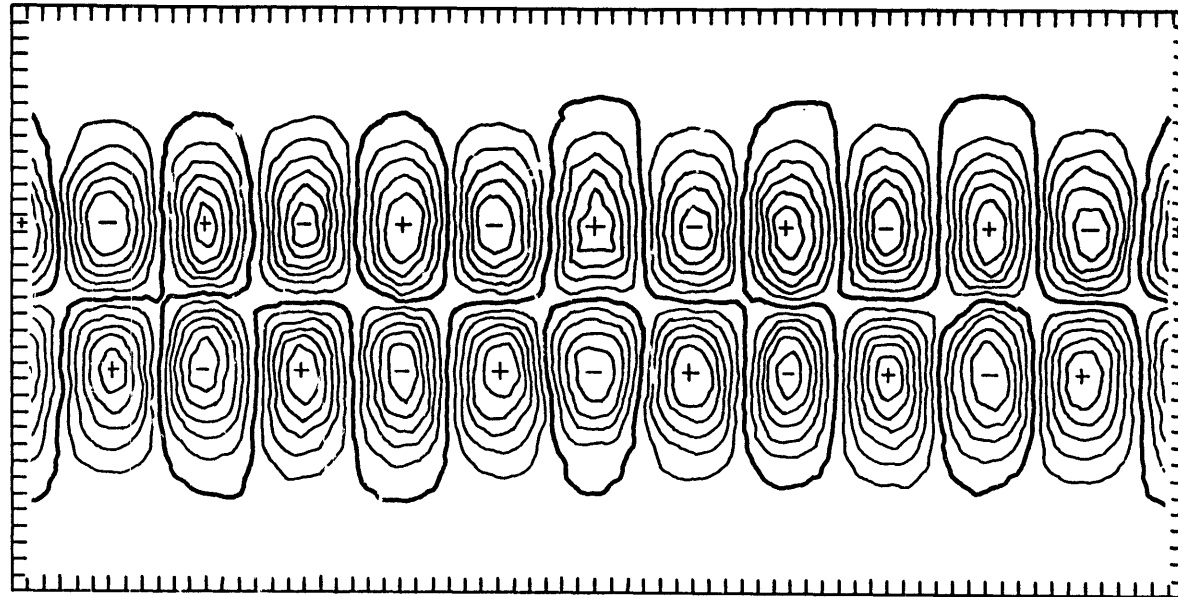


Fig. 3.4 $\partial\psi/\partial t$ error at time $t=0$, $\alpha = 1.7$, $\epsilon = .125$, and for grid of Fig. 2.5.
 The dark line is the zero contour; contour interval is $10 \text{ m}^2 \text{ sec}^{-2}$.

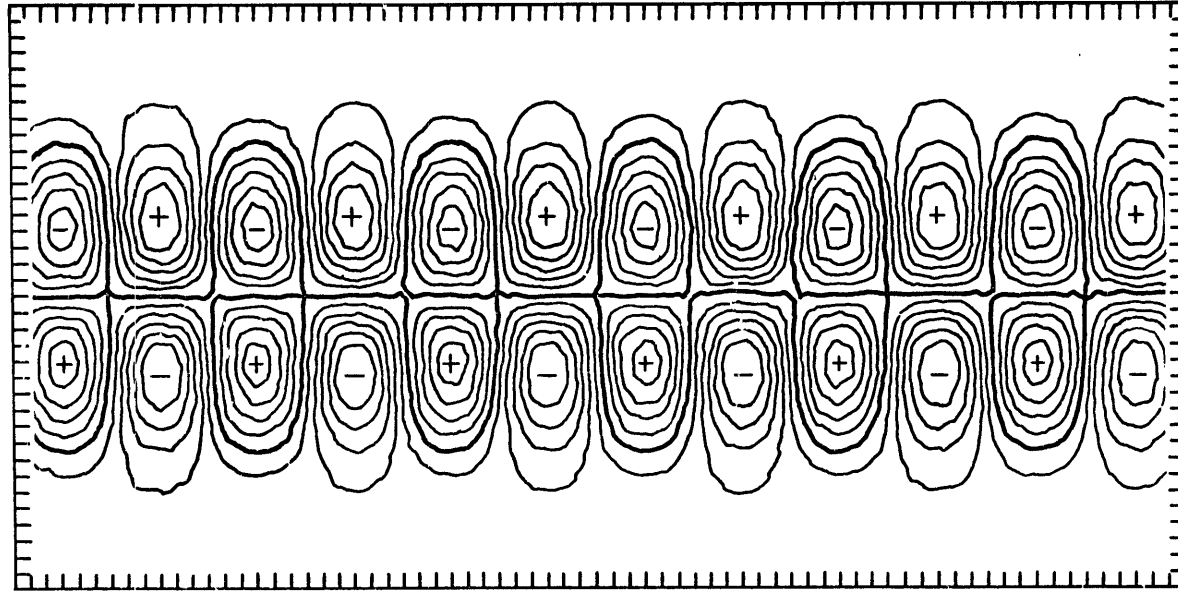


Fig. 3.5 Exact ψ values at time $t=0$. The dark line is the zero contour; contour interval is $7 \times 10^{-6} \text{ sec}^{-1}$. The figure was produced by the computer using linear interpolation within grid triangles. This causes the small irregularities in this and previous figures.

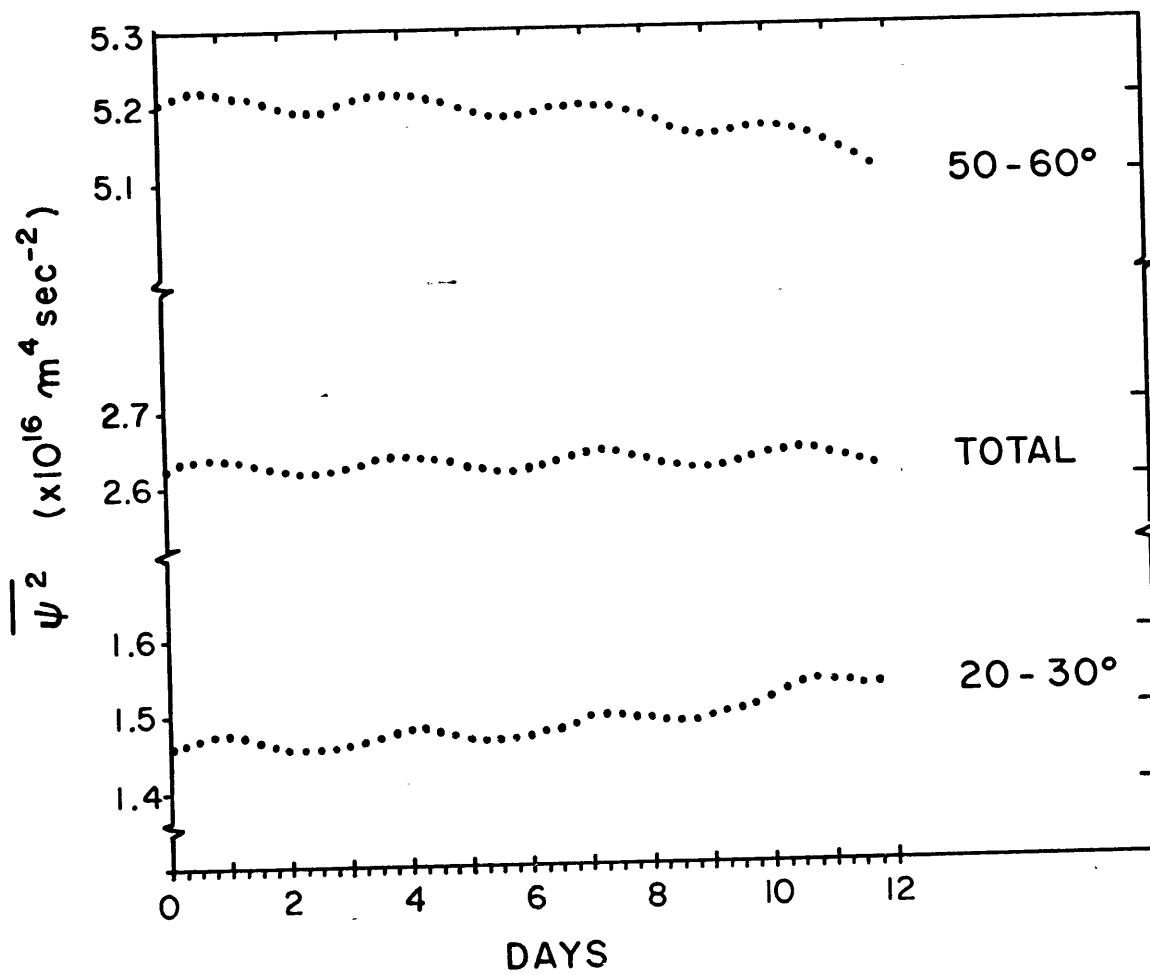
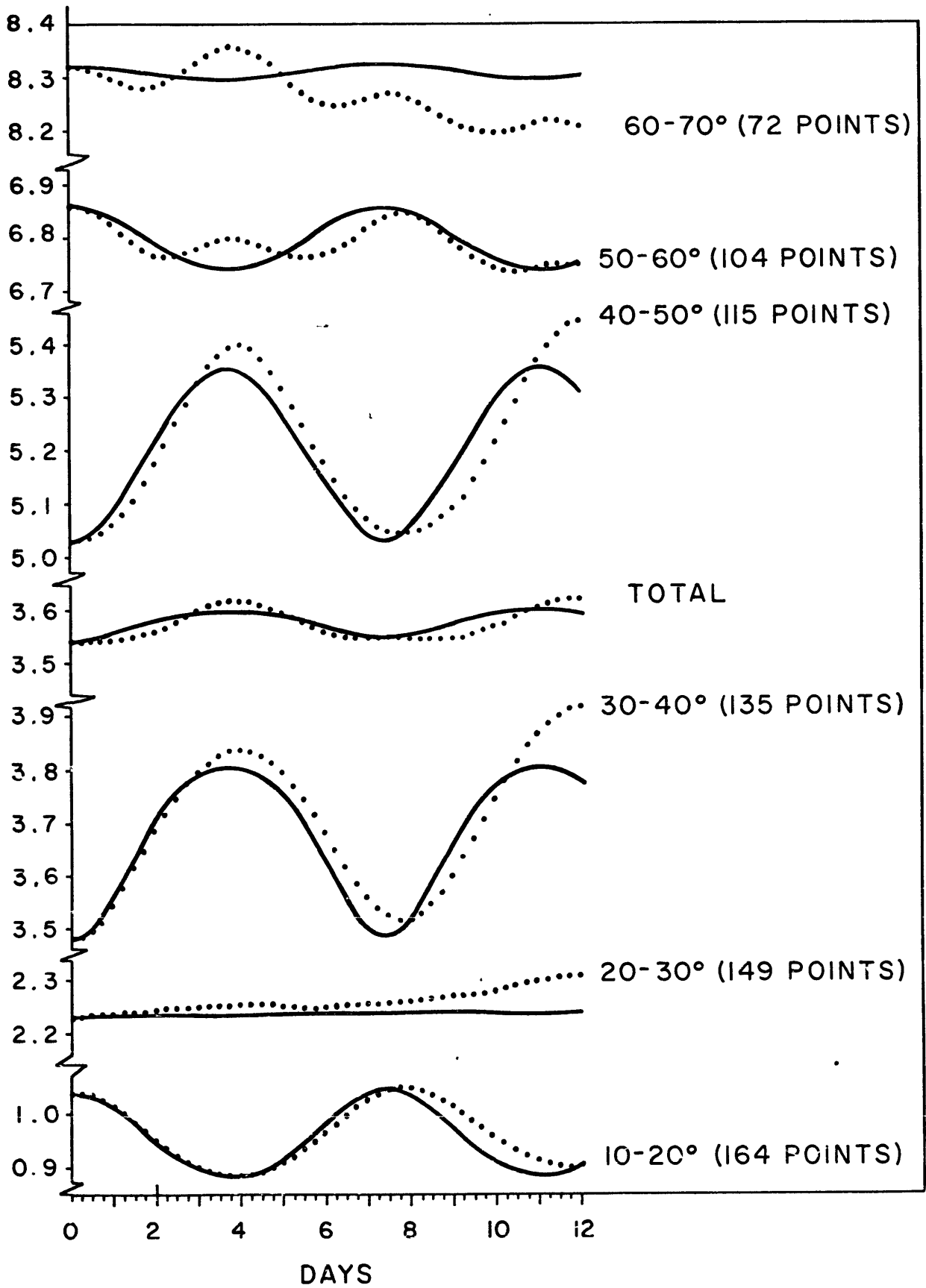


Fig. 3.6 Variation in $\overline{\psi^2}$ averaged over the entire earth and within the latitude bands 20-30°N and 50-60°N, for wave number six.

Fig. 3.7 Variation in ψ^2 averaged in latitude bands and over entire earth. The ordinate is $\overline{\psi^2}$ ($\times 10^{16} \text{ m}^4 \text{ sec}^{-2}$). The dotted lines are for numerical integration of wave number four. Solid lines are for analytic values indicating truncation error in the integration over latitude bands as opposed to truncation error in the model itself.



CHAPTER IV

PRIMITIVE BAROTROPIC MODEL ON A PLANE

We digress from the sphere for one chapter to consider difference approximations on a plane. Here we develop methods of approximation over triangular grids which will be useful to compare triangular approximations with the more usual square ones. Obviously, if triangular approximations are significantly worse than the square ones there would be no point in proceeding to the sphere. These schemes on the plane also have a side benefit for use as nonhomogeneous grids to deal with problems with spatially varying scales of motion.

The spatial scale of many geophysical fluid dynamics problems varies greatly over the domain of interest. The ocean circulation is such a problem. Western boundary currents such as the Gulf Stream or Kuroshio have a smaller scale than the remaining ocean circulation. Another example is the problem of fronts in the atmosphere, where relatively strong gradients exist in a narrow band with weak gradients elsewhere.

To study these problems numerically, a net of points must be defined over the domain. The density of the net must be great enough to resolve the smallest scales of interest. The size and speed of present computers does not allow a uniformly fine grid over the entire domain. Even if it were practical, such a grid would be inefficient since a fine grid is needed only over a small part of the domain.

For efficient use of the computer, it seems reasonable to use the optimum grid density for the spatial scale of the expected solution in each part of the domain. These various density grids must then be connected to each other in some manner and, in some cases, special difference equations must be designed for use at the interface.

If a coarse square grid is joined to a fine square grid, various difficulties can arise at the interface. For example, if a uniform wave is travelling parallel to the interface, the phase truncation error is smaller in the fine grid than in the coarse one, and a shearing soon develops in the wave structure. This numerical phenomenon is exhibited in the case of a wave on a sphere by Gates and Riegel (1962). If a wave is moving perpendicular to the interface, partial reflections might occur which are due solely to the numerical techniques and not to the physical problem.

To avoid these problems, a nonhomogeneous triangular grid seems ideal. Such grids have been used successfully for solving elliptic equations by the method of successive overrelaxation (Winslow, 1966). They permit a continuous, gradual transition from fine to coarse grid and permit construction of secondary polyhedral grid areas whose sides are common to only two such areas.

Masuda (1968) has developed finite difference schemes using the principle developed by A. Arakawa for use over a homogeneous triangular grid. He shows good results for integrations of the non-divergent barotropic model on a plane. Lorenz (1967) has developed

a finite difference approximation for a two level model on a beta plane when the governing equations are written in terms of a stream function. In the following, discrete approximations to the primitive equations governing frictionless two-dimensional flow are developed for use over arbitrary triangular grids. Cartesian geometry is assumed for this chapter. The modifications necessary for spherical geometry are discussed in Chapter V. Two approaches are considered. The first deals with the invariants of the continuous equations. A class of schemes is developed which conserves mass, momentum, and energy. The second approach approximates each term of the governing equations individually and examines the truncation error of all the schemes when applied to a homogeneous grid over a plane.

Results of test integrations of these schemes are then presented. The schemes are applied to an equilateral triangular (homogeneous) grid on a beta plane. No integrations over nonhomogeneous grids are performed. The results of the triangular schemes are compared with results of similar schemes applied to a square net and with results of integrations over a fine mesh.

The equations considered here are those for frictionless horizontal two-dimensional motion. For the derivation of the difference schemes, the Coriolis term will be neglected. Since all quantities will be defined at the same grid points, the Coriolis term can be differenced in a straightforward manner. The difference form of the Coriolis term is given in section 4.7. Using vector notation, the

governing equations can be written

$$\frac{\partial \vec{V}}{\partial t} + \vec{V} \cdot \nabla \vec{V} + g \nabla h = 0 \quad (4.1)$$

$$\frac{\partial h}{\partial t} + \nabla \cdot (h \vec{V}) = 0 \quad (4.2)$$

where \vec{V} is the vector velocity, h is the height of the free surface, g is gravity, and ∇ is the vector gradient operator. Equation (4.2) expresses conservation of mass.

The momentum equation can be formed from (4.1) and (4.2), and, using diadic notation, can be written as

$$\frac{\partial h \vec{V}}{\partial t} + \nabla \cdot (\vec{V} h \vec{V}) + \nabla (g \frac{h^2}{2}) = 0 \quad (4.3)$$

Thus, neglecting boundary effects, the system conserves momentum when integrated over the domain. The kinetic energy equation is obtained by combining (4.1) multiplied by $h \vec{V}$ with (4.2) multiplied by $\frac{1}{2} \vec{V} \cdot \vec{V}$.

$$\frac{\partial}{\partial t} \left(\frac{1}{2} \vec{V} \cdot \vec{V} h \right) + \nabla \cdot \left[\vec{V} \left(\frac{1}{2} \vec{V} \cdot \vec{V} h \right) \right] + g h \vec{V} \cdot \nabla h = 0 \quad (4.4)$$

This equation, together with gh times equation (4.2) yields the energy equation

$$\frac{\partial}{\partial t} \left[\frac{1}{2} (\vec{V} \cdot \vec{V} h + g h^2) \right] + \nabla \cdot \left[\vec{V} \left(\frac{1}{2} \vec{V} \cdot \vec{V} h + g h^2 \right) \right] = 0 \quad (4.5)$$

The total energy $\frac{1}{2} (\vec{\nabla} \cdot \vec{\nabla} h + g h^2)$ is seen to be conserved when integrated over the domain with boundary effects neglected.

We now wish to develop difference approximations to these partial differential equations and study their properties. Such approximations are easiest to develop from area integrals of the flux form of the equations. Consider integrals of equations (4.2) and (4.3) over some elementary grid area A yet to be defined.

$$\frac{\partial}{\partial t} \int_A h \vec{\nabla} dA = - \int_A \nabla \cdot (\vec{\nabla} h \vec{\nabla}) dA - \int_A \nabla g \frac{h^2}{2} dA \quad (4.6)$$

$$\frac{\partial}{\partial t} \int_A h dA = - \int_A \nabla \cdot (h \vec{\nabla}) dA \quad (4.7)$$

The area integrals on the right hand side can be transformed to line integrals along the boundary S of A .

$$\frac{\partial}{\partial t} \int_A h \vec{\nabla} dA = - \oint_S V_n h \vec{\nabla} ds - \oint_S g \frac{h^2}{2} \hat{n} ds \quad (4.8)$$

$$\frac{\partial}{\partial t} \int_A h dA = - \oint_S V_n h ds \quad (4.9)$$

Where V_n is the velocity component normal to the curve S and \hat{n} is the outward unit vector normal to S .

4.1 Conservative difference schemes

The difference schemes developed here are all written for a topologically regular grid in the sense that each grid point is surrounded by six triangles. Difference equations expressing the change of a variable at a grid point are written using local polar indexing. The value of some variable ψ at a central point is denoted by ψ_0 . The values at surrounding points are then denoted by $\psi_{ij} = \psi(r_i, \theta_j)$. r_i is the row radius of the point; $i=1$ for a grid point one triangle from the center, 2 for a point two triangles out, etc. θ_j is the azimuthal angle, $j=1$ for some reference line, 2 for a point 60° counterclockwise on a topological map of the grid, 3 for a point 120° , etc. See Fig. 4.1.

With this notation, a set of difference approximations to equations (4.8) and (4.9) conserving mass and momentum is given by

$$A_0 \frac{\partial}{\partial t} h_0 \vec{V}_0 + \sum_{i=1}^6 \delta_i (V_m h \vec{V})_{\frac{1}{2}i} + \sum_{i=1}^6 g \delta_i \left(\hat{m} \frac{h^2}{2} \right)_{\frac{1}{2}i} = 0 \quad (4.10)$$

$$A_0 \frac{\partial}{\partial t} h_0 + \sum_{i=1}^6 \delta_i (V_m h)_{\frac{1}{2}i} = 0 \quad (4.11)$$

A_0 is the area of the hexagon whose sides go through $(\frac{1}{2}, i)$ and are perpendicular to the grid lines, δ_i is the length of the side through $(\frac{1}{2}, i)$, $\hat{m}_{\frac{1}{2}i}$ is the outward unit vector normal to the side,

and V_m is the velocity component normal to the side. $(V_m h \vec{\nabla})_{\frac{1}{2}i}$, $(h^2/2)_{\frac{1}{2}i}$, and $(V_m h)_{\frac{1}{2}i}$ are to be related to grid point values from energy considerations.

Let $\bar{\Psi}$ denote the finite difference equivalent of integration of a quantity Ψ over the domain, i.e.,

$$\bar{\Psi} = \frac{1}{A_T} \sum A_o \Psi_o$$

where the summation is taken over all grid points, and A_T is the total area.

In order for (4.10) and (4.11) to conserve energy, the following relations must hold

$$\frac{1}{2} V_o^2 \sum_{i=1}^6 \delta_i (V_m h)_{\frac{1}{2}i} = \sum_{i=1}^6 \delta_i \vec{\nabla}_o \cdot (V_m h \vec{\nabla})_{\frac{1}{2}i} \quad (4.12)$$

$$\sum_{i=1}^6 g \delta_i \vec{\nabla}_o \cdot \hat{m}_{\frac{1}{2}i} \left(\frac{h^2}{2} \right)_{\frac{1}{2}i} = - \sum_{i=1}^6 g \delta_i h_o (V_m h)_{\frac{1}{2}i} \quad (4.13)$$

The first relation (4.12) insures that the space differences will not produce nonlinear instability; the second (4.13) provides for consistent conversion between kinetic and potential energy.

If we define

$$(\mathbf{v}_m h \vec{\nabla})_{\frac{1}{2}i} = \frac{1}{2} (\vec{\nabla}_0 + \vec{\nabla}_{1i}) (\mathbf{v}_m h)_{\frac{1}{2}i} \quad (4.14)$$

equation (4.12) holds because

$$\overline{\sum_{i=1}^6 \vec{\nabla}_0 \cdot \vec{\nabla}_{1i} (\mathbf{v}_m h)_{\frac{1}{2}i}} = 0$$

Differences with the form of (4.14) have been used by Lorenz (1960), Arakawa (1966), and Bryan (1966).

One possible definition of $(\mathbf{v}_m h)_{\frac{1}{2}i}$ is

$$(\mathbf{v}_m h)_{\frac{1}{2}i} = \frac{1}{2} [h_0 \vec{\nabla}_0 + h_{1i} \vec{\nabla}_{1i}] \cdot \hat{m}_{\frac{1}{2}i} \quad (4.15)$$

The energy conversion relation (4.13) then holds provided that

$$(h^2)_{\frac{1}{2}i} = h_0 h_{1i} \quad (4.16)$$

Substitution of (4.14), (4.15), and (4.16) into (4.10) and (4.11) results in one energy conservative difference scheme given as

Scheme I

$$\begin{aligned} \frac{\partial}{\partial t} h_o \vec{V}_o &= - \frac{1}{4A_o} \sum_{i=1}^6 \delta_i h_o \vec{V}_{1i} (\vec{V}_o \cdot \hat{m}_{\frac{1}{2}i}) \\ &\quad - \frac{1}{2A_o} \sum_{i=1}^6 \delta_i h_{1i} \left[\frac{1}{2} (\vec{V}_o + \vec{V}_{1i}) \right] (\vec{V}_{1i} \cdot \hat{m}_{\frac{1}{2}i}) - \frac{gh_o}{2A_o} \sum_{i=1}^6 \delta_i h_{1i} \hat{m}_{\frac{1}{2}i} \\ \frac{\partial h_o}{\partial t} &= - \frac{1}{2A_o} \sum_{i=1}^6 \delta_i h_{1i} \vec{V}_{1i} \cdot \hat{m}_{\frac{1}{2}i} \end{aligned} \quad (4.17)$$

If applied to a square grid this scheme is seen to be the same as scheme B of Grammelvedt (1968).

A second possible definition of $(V_m h)_{\frac{1}{2}i}$ is

$$(V_m h)_{\frac{1}{2}i} = \frac{1}{4} (h_o + h_{1i}) (\vec{V}_o + \vec{V}_{1i}) \cdot \hat{m}_{\frac{1}{2}i} \quad (4.18)$$

Relation (4.13) is now valid if

$$(h^2)_{\frac{1}{2}i} = \frac{1}{2} (h_o^2 + h_{1i}^2) \quad (4.19)$$

Substitution of (4.14), (4.18), and (4.19) into (4.10) and (4.11) results in a second energy conservative scheme given by

Scheme II

$$\begin{aligned} \frac{\partial}{\partial t} h_0 \vec{V}_0 = & - \frac{1}{8A_0} \sum_{i=1}^6 \delta_i (\vec{V}_0 + \vec{V}_{i,i}) (h_0 + h_{i,i}) \left[(\vec{V}_0 + \vec{V}_{i,i}) \cdot \hat{m}_{\frac{1}{2}i} \right] \\ & - \frac{g}{4A_0} \sum_{i=1}^6 \delta_i h_{i,i}^2 \hat{m}_{\frac{1}{2}i} \end{aligned} \quad (4.20)$$

$$\frac{\partial h_0}{\partial t} = - \frac{1}{4A_0} \sum_{i=1}^6 \delta_i (h_0 + h_{i,i}) (\vec{V}_0 + \vec{V}_{i,i}) \cdot \hat{m}_{\frac{1}{2}i}$$

We note that the mass flux of Scheme I is similar to Shuman's (1962) semi-momentum scheme and that of Scheme II is similar to his filtered factor form. These two schemes are also similar to those designed by Kurihara and Holloway (1967) for use over a quasi-homogeneous spherical grid.

4.2 Individual approximations

Difference approximations are now formulated for the individual terms of the governing equations without regard to energy conservation. First, grid vectors which are useful in writing the approximations are defined.

Let \vec{S}_i be the vector from the center point 0 to the surrounding point (1,i) (see Fig. 4.2a). The radial subscript is now dropped, all points considered being in the first row around the center point.

Two adjacent points along with the center point form a triangle with values ψ_0 , ψ_i , and ψ_{i+1} of some field ψ at its vertices. If ψ varies linearly over this triangle it can be written, following Winslow (1966), as

$$\psi = \psi_0 + \vec{S} \cdot \nabla \psi_{i+\frac{1}{2}} \quad (4.21)$$

where the gradient is a constant within the triangle and given by

$$\nabla \psi_{i+\frac{1}{2}} = \frac{(\psi_i - \psi_0) \vec{S}_{i+1}^T - (\psi_{i+1} - \psi_0) \vec{S}_i^T}{\vec{S}_i \cdot \vec{S}_{i+1}^T} \quad (4.22)$$

\vec{S} is the position vector with respect to the center point, and the superscript T denotes a 90° clockwise rotation of a vector (Fig. 4.2a).

A proof of (4.22) is straightforward. Since ψ is assumed to vary linearly in the triangle, it can be written in the following form

$$\psi = \psi_0 + \vec{S} \cdot \left[(\psi_i - \psi_0) \vec{f}(\vec{S}_i, \vec{S}_{i+1}) + (\psi_{i+1} - \psi_0) \vec{g}(\vec{S}_i, \vec{S}_{i+1}) \right]$$

where \vec{f} and \vec{g} are vector functions of \vec{S}_i and \vec{S}_{i+1} . Since

$$\psi_i = \psi_0 + (\psi_i - \psi_0) \quad \text{it follows that} \quad \vec{S}_i \cdot \vec{f} = 1 \quad \text{and} \quad \vec{S}_i \cdot \vec{g} = 0.$$

Similarly $\psi_{i+1} = \psi_0 + (\psi_{i+1} - \psi_0)$ implies $\vec{S}_{i+1} \cdot \vec{f} = 0$ and $\vec{S}_{i+1} \cdot \vec{g} = 1$.

Thus \vec{f} and \vec{g} have the form $\vec{f} = C_1 \vec{S}_{i+1}^T$ and $\vec{g} = C_2 \vec{S}_i^T$ where

$$C_1 = -C_2 = \left[\vec{S}_i \cdot \vec{S}_{i+1}^T \right]^{-1}$$

Define a secondary mesh for the grid to consist of the medians of the grid triangles (Fig. 4.3a). The elementary grid area associated with each grid point is then that of the secondary dodecagon surrounding it.

Pressure Gradient Term

Consider the integral of the pressure term over the dodecagonal grid area of Fig. 4.3a

$$I_2 = \int_A h \nabla h \, dA$$

and assume h varies linearly within each of the six grid triangles. The contribution to the integral from the area a formed by the intersection of one grid triangle and the dodecagon is

$$I = \int_a (h_0 + \vec{s} \cdot \nabla h) (\nabla h) \, da$$

where the position vector \vec{s} is the only variable in the integral.

Hence

$$I = \nabla h \{ a h_0 + \nabla h \cdot a \bar{\vec{s}} \}$$

$\bar{\vec{s}}$ is the average position vector of the area a .

In the grid triangle defined by \vec{S}_i and \vec{S}_{i+1} , the area a is that of the two triangles defined by $\frac{1}{2}\vec{S}_i$ and $\frac{1}{3}(\vec{S}_{i+1} + \vec{S}_i)$, and $\frac{1}{3}(\vec{S}_{i+1} + \vec{S}_i)$ and $\frac{1}{2}\vec{S}_{i+1}$ (see Fig. 4.3b). In these two triangles, $a\vec{S}$ is

$$a\vec{S} = \left(\frac{7}{6}\right)\left(\frac{1}{36}\right) |\vec{S}_i \times \vec{S}_{i+1}| (\vec{S}_i + \vec{S}_{i+1})$$

and $\nabla h \cdot a\vec{S}$ is

$$\nabla h_{i+\frac{1}{2}} \cdot a\vec{S} = \left(\frac{7}{6}\right)\left(\frac{1}{36}\right) |\vec{S}_i \times \vec{S}_{i+1}| \left[(h_i - h_o) + (h_{i+1} - h_o) \right]$$

Thus

$$I_2 = \sum_{i=1}^6 \nabla h_{i+\frac{1}{2}} \left\{ a_{i+\frac{1}{2}} h_o + \nabla h_{i+\frac{1}{2}} \cdot a\vec{S} \right\}$$

with the above values substituted.

Similarly, other approximations to the pressure term can be defined. Consider the integral

$$I_3 = \int_A \nabla \frac{h^2}{2} dA$$

and let h^2 vary linearly over the grid triangles. The integral then becomes

$$I_3 = \frac{1}{2} \sum_{i=1}^6 a_{i+\frac{1}{2}} \nabla h_{i+\frac{1}{2}}^2$$

where the expression for the gradient is given by (4.22).

Another approximation can be formulated from

$$I_4 = \oint \hat{m} \frac{h^2}{2} ds$$

where h^2 is assumed to vary linearly over grid triangles. In this case the line integral becomes simply the trapezoidal rule with values at the vertices of the dodecagon. The integral I_4 can be evaluated other ways, such as by assuming h varies linearly over grid triangles. The line integral does not reduce to the trapezoidal rule in this case.

Mass Flux

Difference approximations for the mass flux term, right hand side of (4.23), are now considered:

$$\frac{\partial h}{\partial t} = - \frac{1}{A} \oint_s (\vec{\nabla} h) \cdot \hat{m} ds \quad (4.23)$$

Let $\vec{\nabla} h$ vary linearly within grid triangles. The two outward normals along the two sides of the dodecagon (see Fig. 4.3b) within the grid triangle defined by \vec{s}_i and \vec{s}_{i+1} are given by

$$\hat{m}_i = \frac{\vec{s}_{i+1}^T - \frac{1}{2} \vec{s}_i^T}{|\vec{s}_{i+1}^T - \frac{1}{2} \vec{s}_i^T|}$$

and

$$\hat{m}_2 = \frac{\frac{1}{2} \overrightarrow{S_{i+1}^T} - \overrightarrow{S_i^T}}{\left| \frac{1}{2} \overrightarrow{S_{i+1}^T} - \overrightarrow{S_i^T} \right|}$$

Substituting these expressions for \hat{n}_1 and \hat{n}_2 , plus equations (4.21) and (4.22) for $\overrightarrow{\nabla} h$ into equation (4.23) along with some manipulation, leads to the difference equation

$$\frac{\partial h_0}{\partial t} = -\frac{1}{6A_0} \sum_{i=1}^6 \overrightarrow{\nabla}_i h_i \cdot (\overrightarrow{S_{i+1}^T} - \overrightarrow{S_{i-1}^T}) \quad (4.24)$$

Another approximation can be derived by assuming both h and $\overrightarrow{\nabla}$ vary linearly over grid triangles and approximating the line integral in (4.23) with the trapezoidal rule between vertices of the dodecagon. This approximation becomes

$$\begin{aligned} \frac{\partial h_0}{\partial t} = & -\frac{5}{72} \frac{1}{A_0} \sum_{i=1}^6 [h_i \overrightarrow{\nabla}_c + h_0 \overrightarrow{\nabla}_i + h_i \overrightarrow{\nabla}_i] \cdot (\overrightarrow{S_{i+1}^T} - \overrightarrow{S_{i-1}^T}) \\ & + \frac{1}{36} \frac{1}{A_0} \sum_{i=1}^6 (h_{i+1} \overrightarrow{\nabla}_i + h_i \overrightarrow{\nabla}_{i+1}) \cdot (\overrightarrow{S_{i+1}^T} - \overrightarrow{S_i^T}) \end{aligned} \quad (4.25)$$

Other approximations can be found by making assumptions similar to those made in approximating the pressure gradient term.

Momentum Flux

Approximations for the momentum flux term on the right hand side of the following equation

$$\frac{\partial h\vec{V}}{\partial t} = - \frac{1}{A} \oint_S (\vec{V}h)\vec{V} \cdot \hat{n} ds \quad (4.26)$$

can be obtained using the same methods as the mass advection. For example, if $\vec{V}h\vec{V}$ is assumed to vary linearly within grid triangles, the resulting expression for (4.26) becomes

$$\frac{\partial h\vec{V}}{\partial t} = - \frac{1}{6A} \sum_{i=1}^6 \vec{V}_i h_i \vec{V}_i \cdot (\vec{S}_{i+1}^T - \vec{S}_{i-1}^T) \quad (4.27)$$

By making approximations similar to those made for the mass flux, other difference schemes can be obtained.

4.3 Homogeneous grid

We now consider the form these schemes take when applied to an equilateral triangular (homogeneous) grid and determine the truncation error of such approximations. Consider Cartesian coordinates (x, y) with unit vectors (\hat{i}, \hat{j}) . Let δ be the constant distance between grid points, and define the grid vectors \vec{S}_i by

$$\vec{S}_1 = -\frac{1}{2} \delta \hat{i} + \frac{\sqrt{3}}{2} \delta \hat{j}$$

$$\vec{S}_2 = -\delta \hat{i}$$

$$\vec{S}_3 = -\frac{1}{2} \delta \hat{i} - \frac{\sqrt{3}}{2} \delta \hat{j}$$

$$\vec{S}_4 = \frac{1}{2} \delta \hat{i} - \frac{\sqrt{3}}{2} \delta \hat{j}$$

$$\vec{S}_5 = \delta \hat{i}$$

$$\vec{S}_6 = \frac{1}{2} \delta \hat{i} + \frac{\sqrt{3}}{2} \delta \hat{j}$$

See Fig. 4.4.

Consider first the pressure term on the right hand side of the following equation

$$\frac{\partial}{\partial t} (h \cdot \vec{V}_0) = -\frac{1}{A} \int_A g h \nabla h dA$$

or an equivalent form. We denote discrete approximations to the right hand side as P_j .

Since

$$\sum_{i=1}^6 \vec{S}_i = 0$$

and

$$\hat{m}_{\frac{1}{2}i} = \vec{S}_i / |\vec{S}_i|$$

the pressure gradient term of Scheme I can be written as

$$P_1 = -g \sum_{i=1}^6 h_0 \frac{h_i - h_0}{3\delta^2} \vec{S}_i$$

Noting that

$$\vec{S}_{i+1}^T - \vec{S}_{i-1}^T = \sqrt{3} \vec{S}_i$$

and

$$\vec{S}_{i+1}^T - \vec{S}_i^T = \frac{\sqrt{3}}{3} (\vec{S}_i + \vec{S}_{i+1})$$

the scheme corresponding to the integral I_2 is

$$P_2 = -g \sum_{i=1}^6 \left[\frac{73}{108} h_0 + \frac{21}{108} h_i + \frac{7}{108} h_{i+1} + \frac{7}{108} h_{i-1} \right] \frac{h_i - h_0}{3\delta^2} \vec{S}_i$$

The pressure gradient term of Scheme II and the scheme corresponding to I_3 both become

$$P_3 = -g \sum_{i=1}^6 \left(\frac{1}{2} h_0 + \frac{1}{2} h_i \right) \frac{h_i - h_0}{3\delta^2} \vec{S}_i$$

and that corresponding to I_4 becomes

$$P_4 = -g \sum_{i=1}^6 \frac{1}{6} \left[(h_{i-1}^2 + h_i^2 + h_0^2) + (h_i^2 + h_{i+1}^2 + h_0^2) \right] \frac{\vec{S}_i}{3\delta^2}$$

which can be shown to be the same as P_3 .

The mass flux scheme from the right hand side of (4.24), when applied to the homogeneous grid, becomes

$$Q_1 = - \frac{1}{3\delta^2} \sum_{i=1}^6 h_i \vec{V}_i \cdot \vec{S}_i$$

The mass flux term of Scheme I also reduces to this expression. The mass flux of Scheme II becomes

$$Q_2 = - \frac{1}{3\delta^2} \sum_{i=1}^6 \frac{1}{2} [h_0 \vec{V}_i + h_i \vec{V}_0 + h_i \vec{V}_i] \cdot \vec{S}_i$$

and the right hand side of (4.25) reduces to

$$Q_3 = \frac{5}{6} Q_2 - \frac{1}{3\delta^2} \sum_{i=1}^6 \frac{1}{18} [(h_{i+1} + h_{i-1}) \vec{V}_i + h_i (\vec{V}_{i+1} \cdot \vec{V}_{i-1})] \cdot \vec{S}_i$$

The momentum flux on the right hand side of (4.27) when applied to this grid becomes

$$M_1 = - \frac{1}{3\delta^2} \sum_{i=1}^6 (\vec{\nabla}_i h_i \vec{V}_i) \cdot \vec{S}_i$$

while the momentum flux of Scheme I reduces to

$$M_2 = - \frac{1}{3\delta^2} \sum_{i=1}^6 \frac{1}{2} h_0 \vec{V}_i (\vec{V}_0 \cdot \vec{S}_i) - \frac{1}{3\delta^2} \sum_{i=1}^6 h_i \left[\frac{1}{2} (\vec{V}_0 + \vec{V}_i) \right] (\vec{V}_i \cdot \vec{S}_i)$$

The momentum flux of Scheme II becomes

$$M_3 = -\frac{1}{3\delta^2} \sum_{i=1}^6 \frac{1}{4} (\vec{v}_0 + \vec{v}_i)(h_0 + h_i)(\vec{v}_0 + \vec{v}_i) \cdot \vec{s}_i$$

4.4 Truncation error

The truncation error of the approximations is determined by substituting Taylor's series expansions about the center point into the difference approximations and comparing the result with the continuous term. Let

$$h_{i\ell} = h_0 + \sum_{j=1}^{\infty} \frac{1}{j!} [(\vec{s}_{i\ell} \cdot \nabla)^j h_0] \tag{4.28}$$

$$\vec{v}_{i\ell} = \vec{v}_0 + \sum_{j=1}^{\infty} \frac{1}{j!} [(\vec{s}_{i\ell} \cdot \nabla)^j \vec{v}_0]$$

These expressions are substituted into schemes P_h , Q_h , and M_h , and like powers of δ are combined. Some relations prove useful in simplifying these combinations; these are listed in Appendix 1. All are easily verified by expansion into Cartesian components.

Using these relations, the Taylor's series expansions of schemes P_h simplify to

$$P_1 = -g h \nabla h - \delta^2 \frac{g}{8} h \nabla (\nabla^2 h) + O(\delta^4)$$

$$P_2 = -g h \nabla h - \delta^2 \frac{g}{144} \left[7 \nabla (\nabla \cdot h \nabla h) + 11 h \nabla (\nabla^2 h) + 7 \nabla^2 h \nabla h \right] + O(\delta^4)$$

$$P_3 = P_4 = -g h \nabla h - \delta^2 \frac{g}{8} \nabla (\nabla \cdot h \nabla h) + O(\delta^4)$$

These schemes are all seen to be second order.

The Taylor's series expansions of the mass advection schemes become

$$Q_1 = -\nabla \cdot (h \vec{v}) - \delta^2 \frac{1}{8} \left\{ \vec{v} \cdot \nabla (\nabla^2 h) + h \nabla^2 (\nabla \cdot \vec{v}) + 2 \nabla^2 h \nabla \cdot \vec{v} + 2 \nabla h \cdot \nabla^2 \vec{v} + 4 \nabla \cdot [(\nabla h \cdot \nabla) \vec{v}] \right\} + O(\delta^4)$$

$$Q_2 = -\nabla \cdot (h \vec{v}) - \delta^2 \frac{1}{8} \left\{ \vec{v} \cdot \nabla (\nabla^2 h) + h \nabla^2 (\nabla \cdot \vec{v}) + \nabla^2 h \nabla \cdot \vec{v} + \nabla h \cdot \nabla^2 \vec{v} + 2 \nabla \cdot [(\nabla h \cdot \nabla) \vec{v}] \right\} + O(\delta^4)$$

$$Q_3 = -\nabla \cdot (h \vec{v}) - \delta^2 \frac{1}{8} \left\{ \vec{v} \cdot \nabla (\nabla^2 h) + h \nabla^2 (\nabla \cdot \vec{v}) + \frac{7}{9} \nabla^2 h \nabla \cdot \vec{v} + \frac{7}{9} \nabla h \cdot \nabla^2 \vec{v} + \frac{5}{3} \nabla \cdot [(\nabla h \cdot \nabla) \vec{v}] \right\} + O(\delta^4)$$

All of these schemes are seen to be second order.

The expansions of the momentum advection terms are of the form

$$M_k = -\nabla \cdot (\vec{\nabla} h \vec{\nabla}) + \delta^2 \vec{F}_k(h, \vec{\nabla}) + O(\delta^4)$$

The expressions $\vec{F}_k(h, \vec{\nabla})$ are rather long and complicated and are not given here. These schemes are also seen to be second order.

4.5 Fourth order schemes

Straightforward extrapolation techniques can be applied to the second order schemes derived above to obtain fourth order schemes.

For example, consider the pressure term from the conservative Scheme I

$$P_1 = -g \sum_{i=1}^6 h_0 \frac{h_{1i} - h_0}{3\delta^2} \vec{S}_i$$

where we have resumed the use of the radial subscript. If this scheme is applied to the triangles formed by the points h_{2i} with h_0 , the approximation is the same as P_1 except δ is replaced by 2δ and \vec{S}_i by $2\vec{S}_i$. Hence we have a scheme

$$P_1' = -\frac{1}{2g} \sum_{i=1}^6 h_0 \frac{h_{2i} - h_0}{3\delta^2} \vec{S}_i$$

with a Taylor's series expansion

$$P_1' = -g h \nabla h - \delta^2 \frac{g}{2} h \nabla (\nabla^2 h) + O(\delta^4)$$

These two schemes can then be combined in the form $P_i^* = AP_i + BP_i'$, where A and B are found by requiring the coefficient of δ^2 in the Taylor expansion of P_i^* be zero and the coefficient of $-gh \nabla h$ be 1. The solution is $A = 4/3$, $B = -1/3$, and the fourth order approximation is

$$P_i^* = -g \sum_{i=1}^6 h_0 \left(\frac{4}{3} h_{1i} - \frac{1}{6} h_{2i} - \frac{7}{6} h_0 \right) \frac{\vec{S}_i}{3\delta^2}$$

This same extrapolation can be applied to all the terms of Scheme I. Such a fourth order scheme is also energy conservative since each of its two parts are.

Another possibility is to use the points $(2, i + \frac{1}{2})$ rather than $(2, i)$. These are closer to the center point than the points $(2, i)$, and are not lined up with the points $(1, i)$; and hence they might make a better approximation. In this case δ in the truncation error is replaced by $\sqrt{3} \delta$ and the combination coefficients become $A = 3/2$ and $B = -1/2$. The fourth order energy conservative scheme corresponding to Scheme I is given by

Scheme III

$$\frac{\partial h_0 \vec{V}_0}{\partial t} = - \frac{1}{4\delta} \sum_{i=1}^6 \left\{ h_0 \vec{V}_{1i} (\vec{V}_0 \cdot \hat{m}_{\frac{1}{2}i}) + h_{1i} \cdot (\vec{V}_0 + \vec{V}_{1i}) (\vec{V}_{1i} \cdot \hat{m}_{\frac{1}{2}i}) + 2gh_{1i} \hat{m}_{\frac{1}{2}i} \right\} \quad (4.29)$$

$$+ \frac{1}{12\sqrt{3}\delta} \sum_{i=1}^6 \left\{ h_0 \vec{V}_{2i+\frac{1}{2}} (\vec{V}_0 \cdot \hat{m}_{1i+\frac{1}{2}}) + h_{2i+\frac{1}{2}} (\vec{V}_0 + \vec{V}_{2i+\frac{1}{2}}) (\vec{V}_{2i+\frac{1}{2}} \cdot \hat{m}_{1i+\frac{1}{2}}) + 2gh_{2i+\frac{1}{2}} \hat{m}_{1i+\frac{1}{2}} \right\}$$

$$\frac{\partial h_0}{\partial t} = - \frac{1}{2\delta} \sum_{i=1}^6 h_{1i} \vec{V}_{1i} \cdot \hat{m}_{\frac{1}{2}i} + \frac{1}{6\sqrt{3}\delta} \sum_{i=1}^6 h_{2i+\frac{1}{2}} \vec{V}_{2i+\frac{1}{2}} \cdot \hat{m}_{1i+\frac{1}{2}}$$

4.6 Boundary conditions

We now consider the lateral boundary condition for an inviscid fluid when the boundary is a straight line coinciding with the sides of grid triangles. The boundary condition for the continuous equations is that there should be no normal flow across the boundary.

Denote the tangential and normal components of the velocity \vec{V} by u and v respectively. Define a row of grid points outside the boundary to be the mirror image of the first row of points inside

the boundary (see Fig. 4.5). Define a subscript (i, j) such that $j = B$ if the point is on the boundary, $j = B + 1$ ($j = B - 1$) if the point is in the first row inside (outside) the boundary, and i is an index along the boundary from some reference point. These subscripts, applied to the components u, v , and h should not be confused with the radial, azimuthal subscripts applied to the vectors.

With this notation, the discrete boundary condition becomes

$$\mathcal{N}_{i,B} = 0 \quad . \quad \text{If we define}$$

$$h_{i,B-1} = h_{i,B+1} \tag{4.30}$$

$$u_{i,B-1} = u_{i,B+1}$$

$$\mathcal{N}_{i,B-1} = -\mathcal{N}_{i,B+1}$$

difference equations of the form (4.10), (4.11) applied to the boundary points results in

$$\frac{\partial h_0 \mathcal{N}_0}{\partial t} = 0$$

if $(V_m h \vec{\nabla})_{\frac{1}{2}i}$, $(h^2/2)_{\frac{1}{2}i}$, and $(V_m h)_{\frac{1}{2}i}$ are evaluated using only values at (0) and $(1, i)$. Thus if $\mathcal{N}_{i,B}$ is initially zero, it will remain zero. It is also seen that the area weighted averages of mass and momentum over the domain are conserved when the boundary values are weighted by that part of their grid area inside the domain and that the energy conserving schemes (4.17) and (4.20) continue to conserve energy using these boundary conditions.

These boundary conditions hold only for pure gravity wave motions associated with (4.1) and (4.2). When the Coriolis term is included in the governing equations, the boundary conditions are no longer exact. Since the initial conditions for the test cases presented here are such that there is very little motion near the boundary and since the integrations are carried out for a relatively short time, little trouble is expected in using these boundary conditions.

4.7 Numerical integrations

Ten-day integrations were performed using several of the schemes developed here over an equilateral triangular grid on a beta plane. The Coriolis term was differenced by simply using the value of the velocity at the central point, thus the schemes remain energy conservative; i.e., in Schemes I, II, and III the X-momentum tendency equation has the additional term $f_0 h_0 v_0$ and the Y-momentum tendency equation has the additional term $-f_0 h_0 u_0$. When Scheme I is applied to the right triangles corresponding to a square net of points, it is seen to be the same as Grammelvedt's (1968) scheme B. For this reason it was decided to use the same initial conditions as he used. A direct comparison between four- and six-point differences is then possible. His initial condition I is given by

$$h(x,y) = H_0 + H_1 \tanh \frac{g(y_0 - y)}{2D} + H_2 \operatorname{sech}^2 \frac{g(y_0 - y)}{D} \sin\left(\frac{2\pi x}{L}\right)$$

where x is the eastward coordinate, y the northward, y_0 the center of the channel, L the length of the channel, and D the width. The initial velocity fields are assumed to be geostrophic.

The following values are adopted for the constants:

$$\begin{array}{ll} H_0 = 2000 \text{ m} & L = 6000 \text{ km} \\ H_1 = 220 \text{ m} & D = 3 \times 2600 \text{ km} \\ H_2 = 133 \text{ m} & f = 10^{-4} \text{ sec}^{-1} \\ g = 10 \text{ m sec}^{-2} & \beta = 10^{-11} \text{ sec}^{-1} \text{ m}^{-1} \end{array}$$

The length δ of the sides of the equilateral triangles forming the grid was taken to be either 100, 200, 231, or 270 km. The north-south boundary conditions are (4.30) with the additional requirement that v on the boundary be held at zero. These are equivalent to those used by Grammelvedt (1968). The east-west boundary conditions are cyclic. A ten minute time step is used when δ equals 200 km or more, and a five minute step when δ equals 100 km. Fig. 4.6 shows the initial height field.

The height fields after five days for eight different cases are shown in Fig. 4.7. The top left is obtained by Grammelvedt's square scheme F using a fine mesh with δ equal to 100 km, and the top right is due to Scheme I also using a fine mesh with δ equal to 100 km. Since these two solutions are almost identical, we can assume they represent the correct solution. The scheme used for the left of the second row is Grammelvedt's square scheme B with a coarser resolution of δ equal to 200 km, and the scheme used for

the right is triangular Scheme I with the same value of δ . The triangular scheme is seen to be better than the square scheme. Both the phase error and amplitude errors are less for the former.

From these results it is not clear whether or not the triangular scheme is better because it has slightly better resolution in the y direction. Since the base of a grid triangle is the same length as a side of the square grid, the height of the triangles is less than that of the squares, resulting in more grid points in the y direction in the triangular grid than in the square grid. To determine the effect of this difference in resolution, the triangular scheme was integrated over a grid with the height of the triangles equal to 200 km, or δ approximately equal to 231 km. The results are presented on the right side of the third row of Fig. 4.7. The solution hardly differs from the δ equals 200 km case and is again better than the square scheme. Scheme I was integrated with an even coarser resolution of δ approximately 273 km. The result is on the left of the third row of Fig. 4.7. This solution is seen to be at least as good as that for the square scheme B. Thus we conclude that the slightly better resolution in the y direction of the triangular schemes is not the main reason for their better solutions.

The bottom right of Fig. 4.7 is obtained from triangular Scheme II. The field is seen to be almost identical to that of Scheme I. The lower left is due to fourth order triangular Scheme III. The phase and amplitude have very little error when compared with the

fine resolution results. If the fourth order Scheme III is compared with Grammelvedt's fourth order square scheme J (his Fig. 8), the triangular scheme is again seen to be better.

Fig. 4.8 shows the height fields after ten days. Now the solutions of the two fine resolution schemes are beginning to diverge. The main feature is wave number two. The triangular schemes all exhibit this wave number two much better than the square scheme B. The phase error of the fourth order scheme is less than the second order schemes and is also less than the phase error for Grammelvedt's fourth order square scheme J as seen in his Fig. 4.8. These schemes can also be compared with Shuman's scheme (Grammelvedt's Fig. 9) which is seen to have a much greater phase truncation error.

The schemes compared here indicate that for numerical modelling of atmospheric-like fluid flow, triangular difference approximations provide better solutions than square approximations with similar resolution and the same order of truncation error. One would expect the same conclusion to hold on the sphere. With this in mind we turn to triangular difference approximations on the sphere.

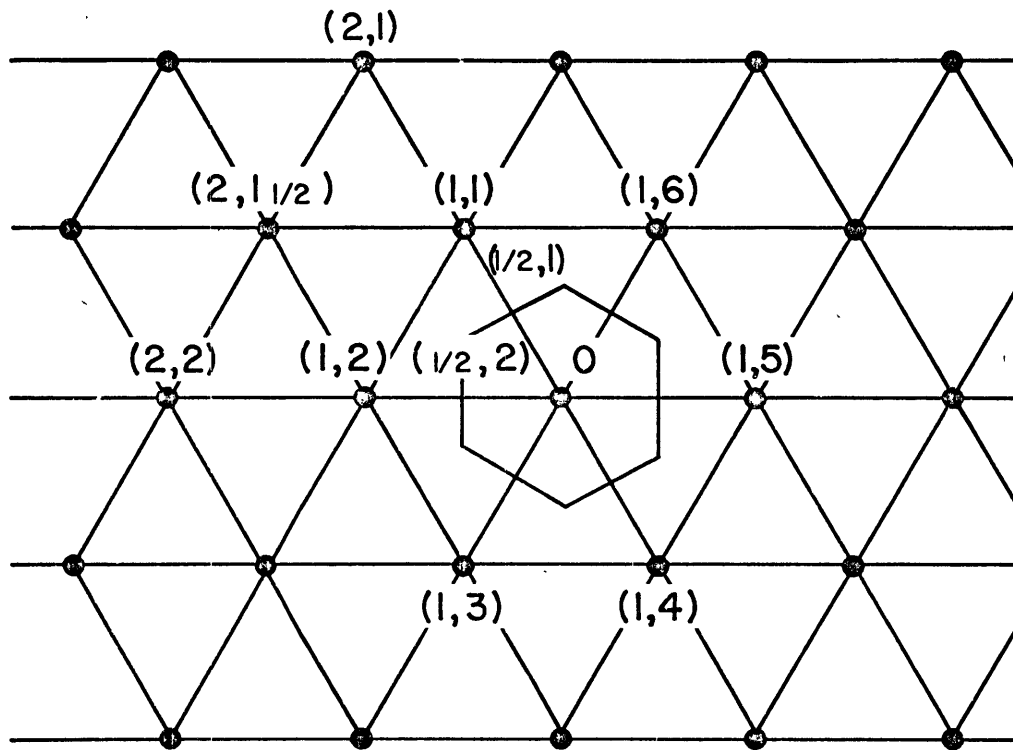


Fig. 4.1 Logical map of triangular grid.

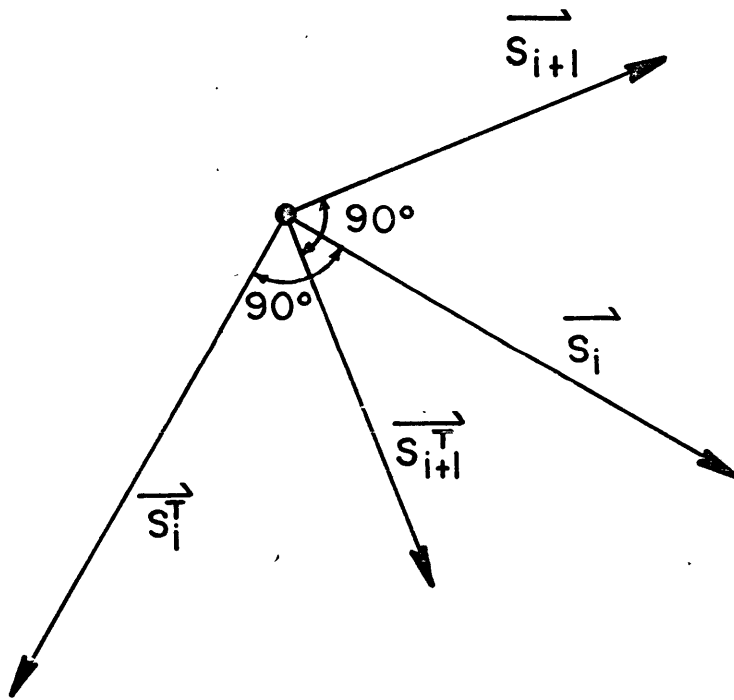
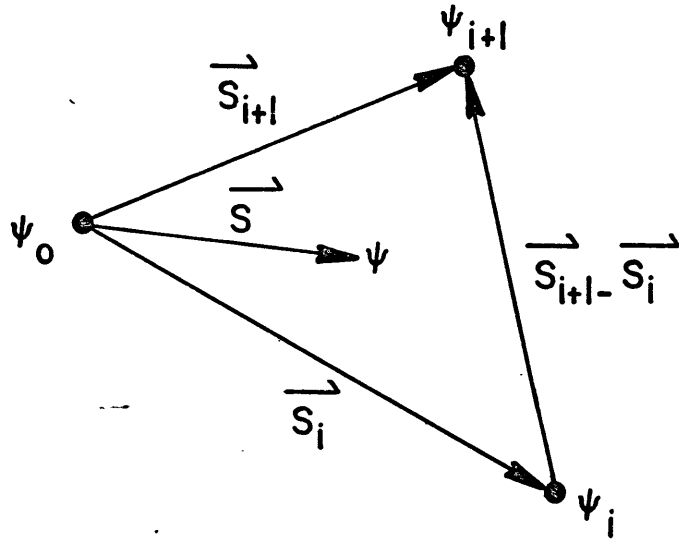


Fig. 4.2 Grid vectors

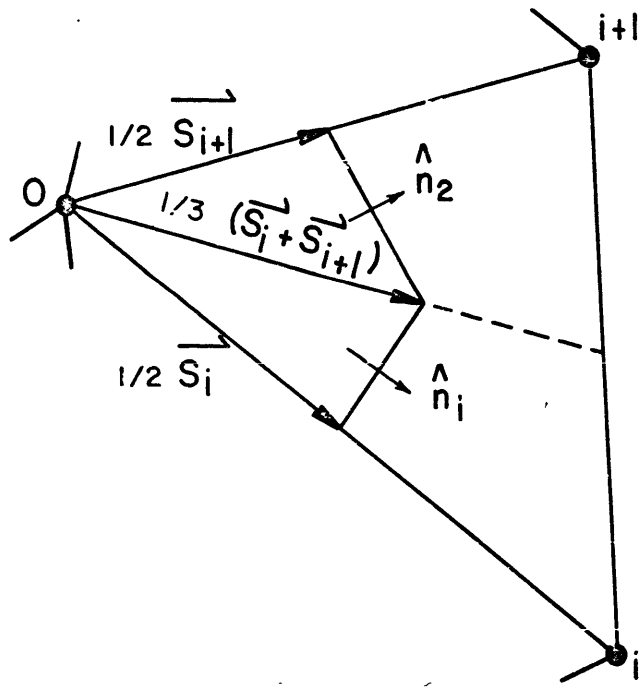
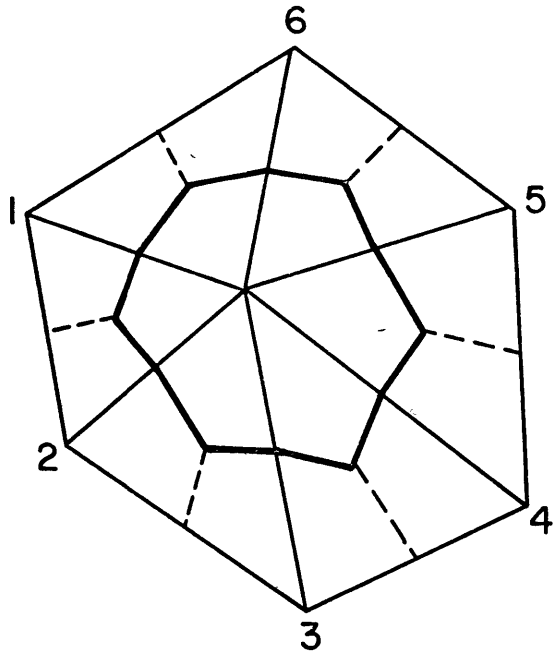


Fig. 4.3 Secondary dodecagonal grid area.

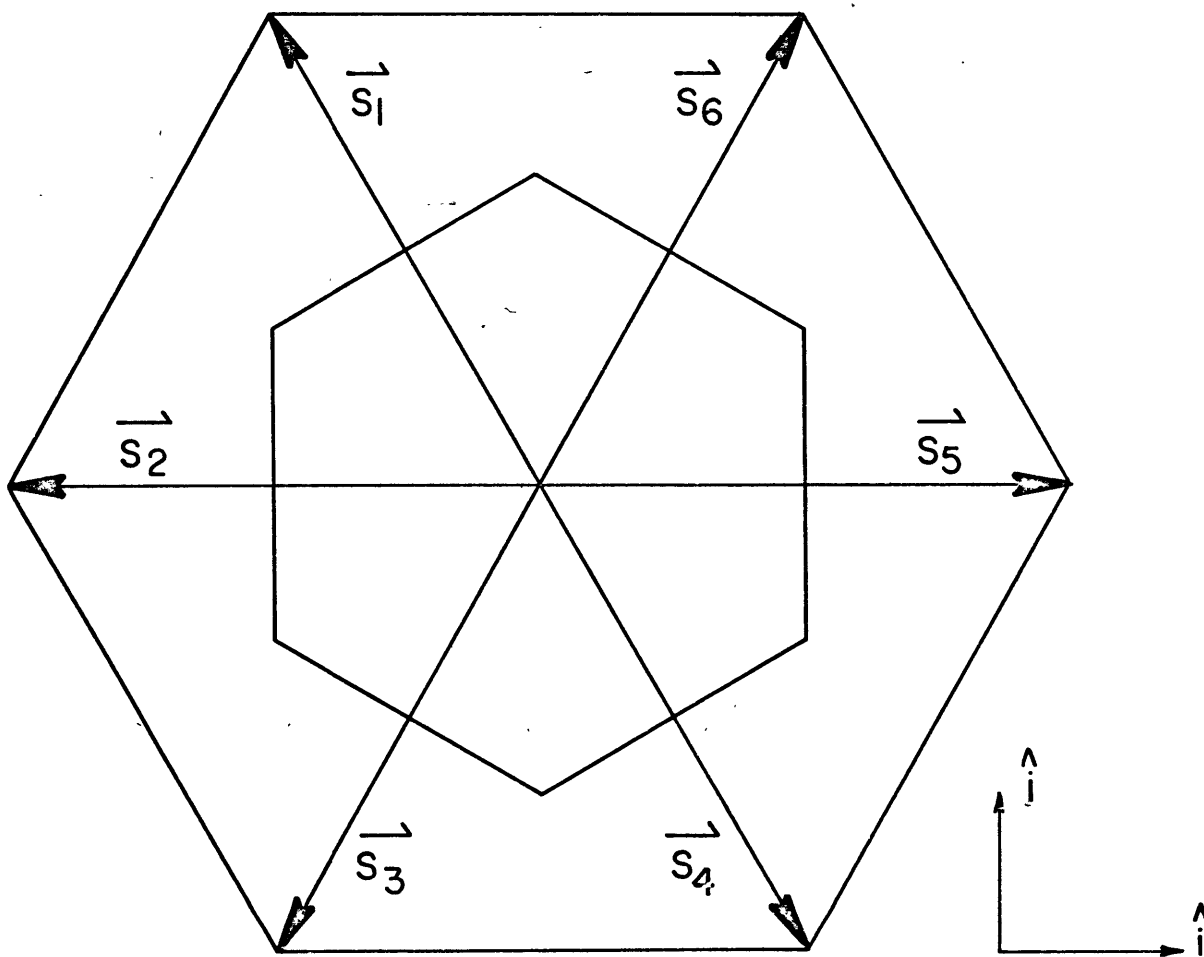


Fig. 4.4 Homogeneous grid vectors.

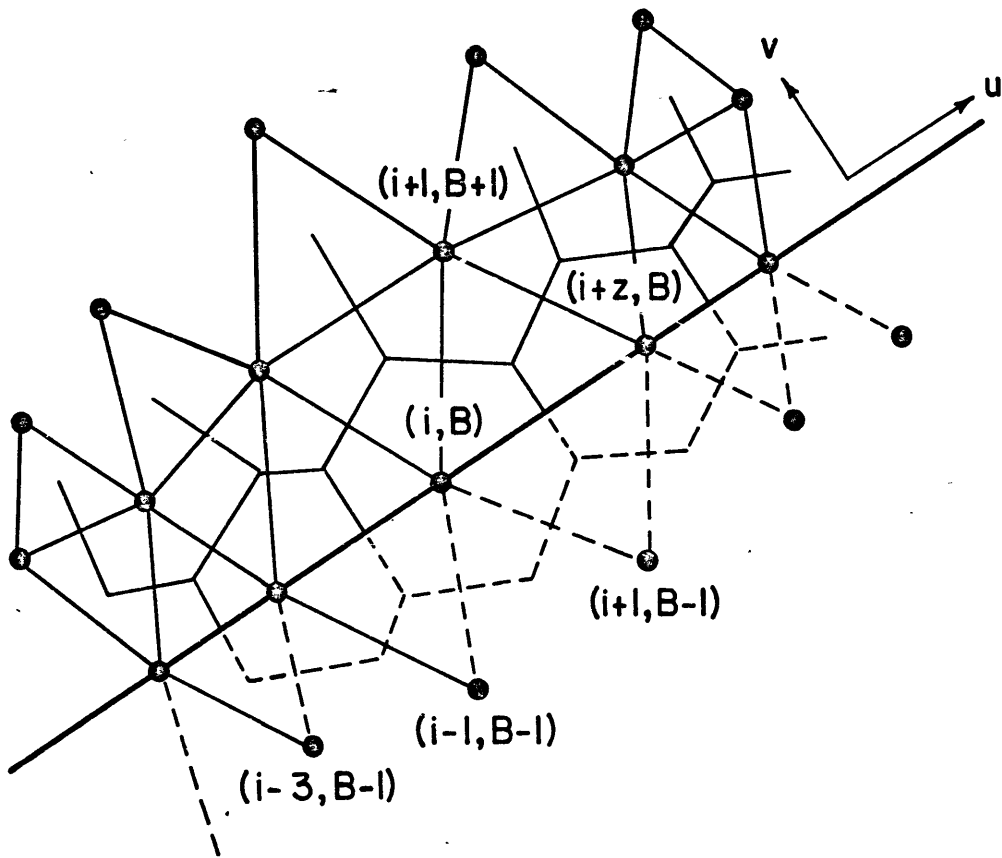


Fig. 4.5 Boundary grid points.

Fig. 4.6 Initial height field. Heights are given in meters;
contour interval is 500 meters.

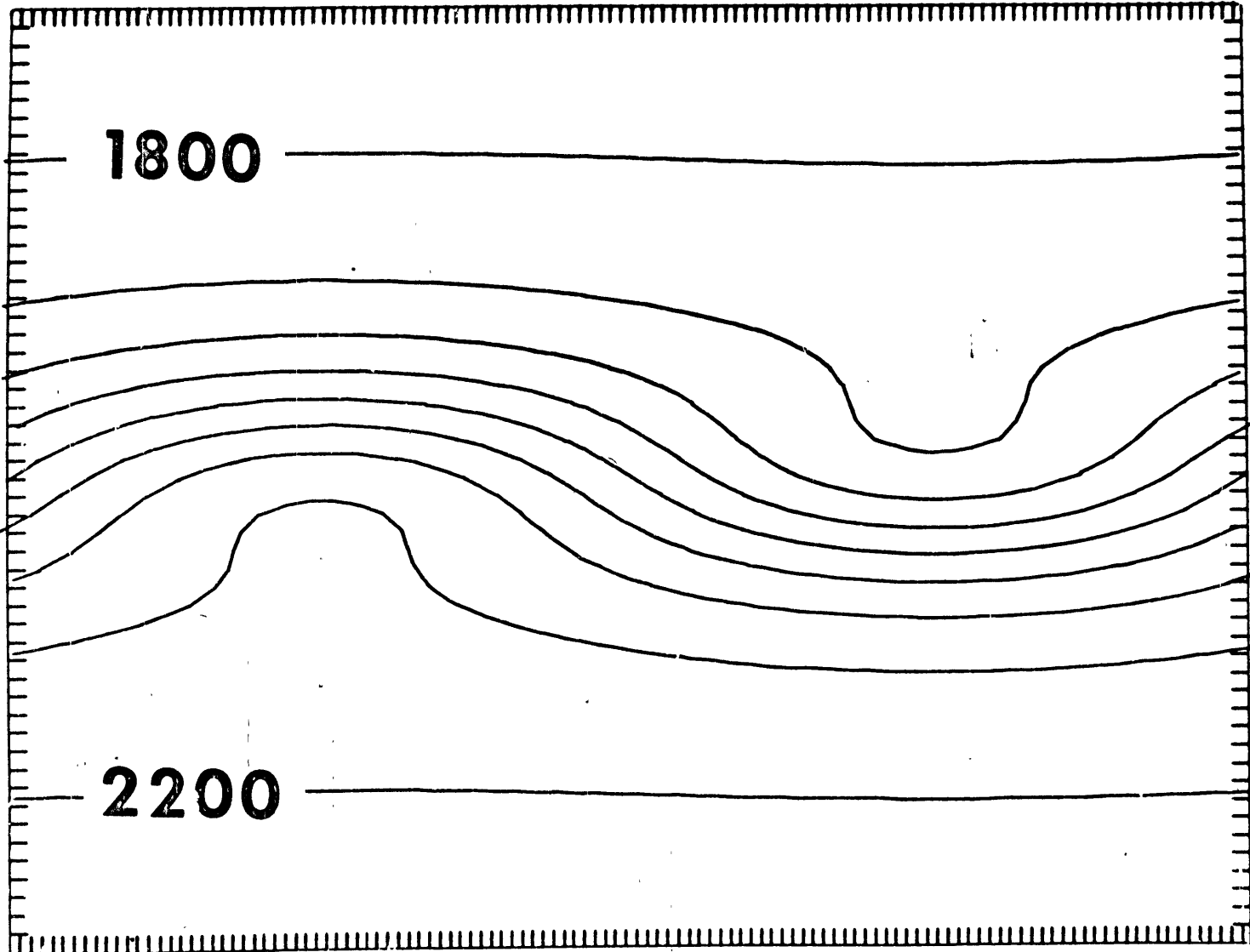
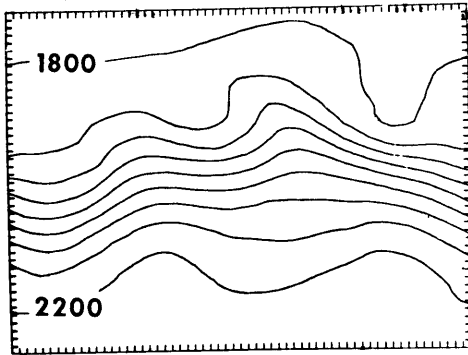
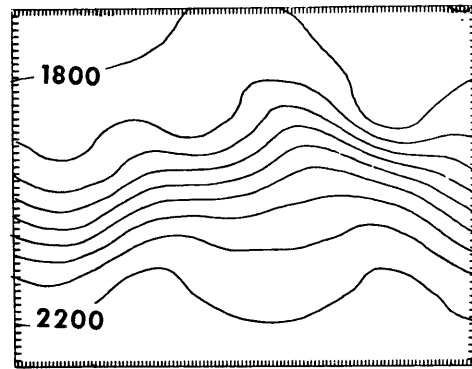


Fig. 4.7 Height fields after five days. Heights are given in meters; contour interval is 500 meters. See section 4.7 for explanation.

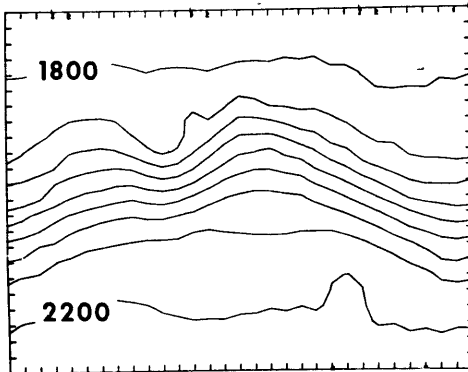
Square Scheme F, $\delta = 100\text{km}$



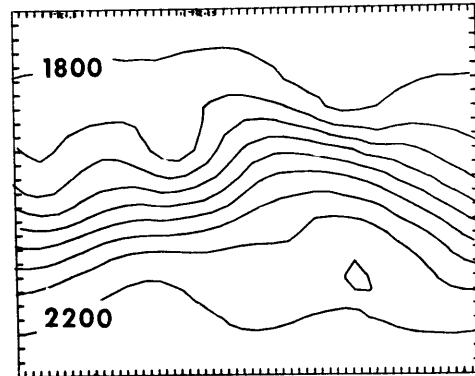
Triangular Scheme I, $\delta = 100\text{km}$



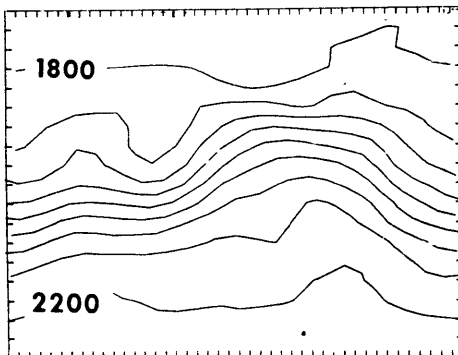
Square Scheme B, $\delta = 200\text{km}$



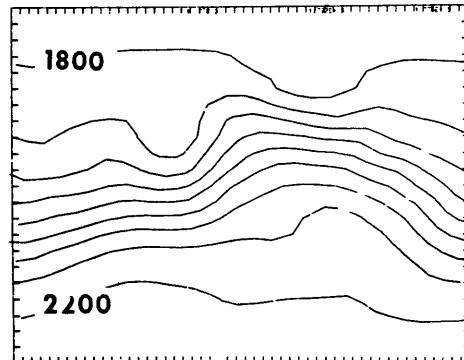
Triangular Scheme I, $\delta = 200\text{km}$



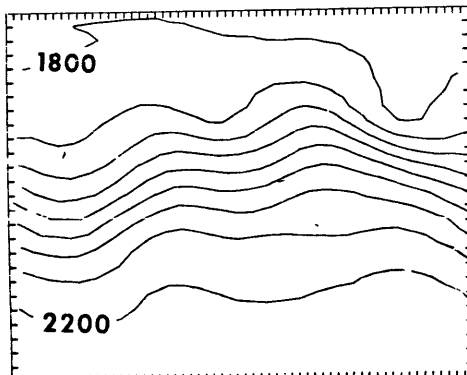
Triangular Scheme I, $\delta = 273\text{km}$



Triangular Scheme I, $\delta = 231\text{km}$



Triangular Scheme III, $\delta = 200\text{km}$



Triangular Scheme II, $\delta = 200\text{km}$

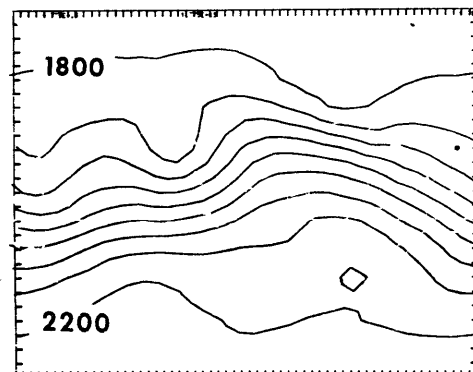
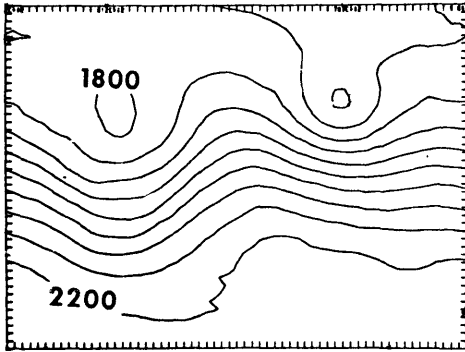
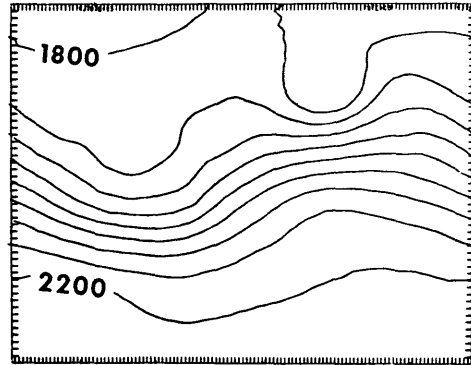


Fig. 4.8 Height fields after ten days. Heights are given in meters; contour interval is 500 meters. See section 4.7 for explanation.

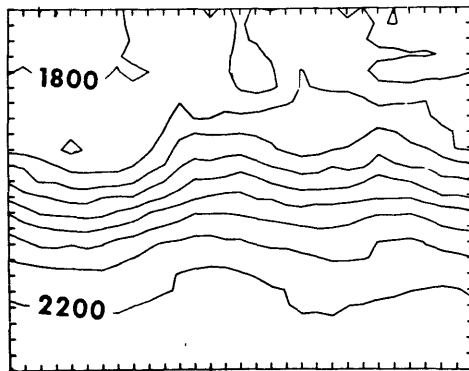
Square Scheme F, $\delta = 100\text{km}$



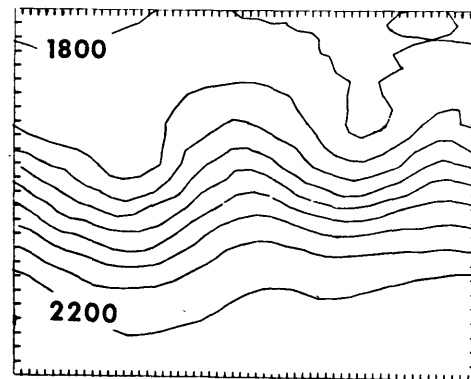
Triangular Scheme I, $\delta = 100\text{km}$



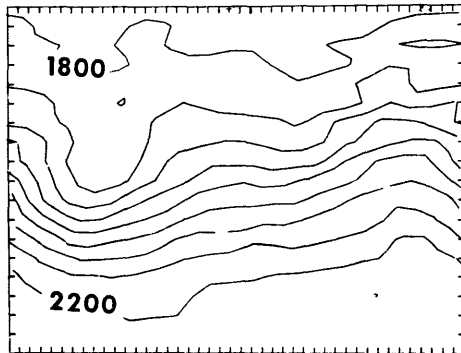
Square Scheme B, $\delta = 200\text{km}$



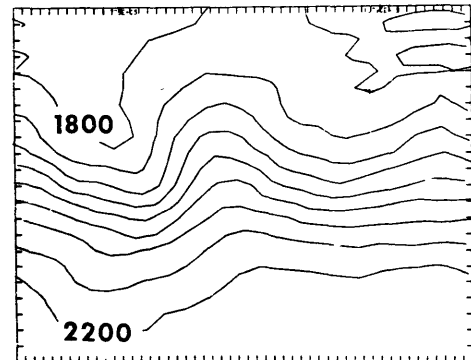
Triangular Scheme I, $\delta = 200\text{km}$



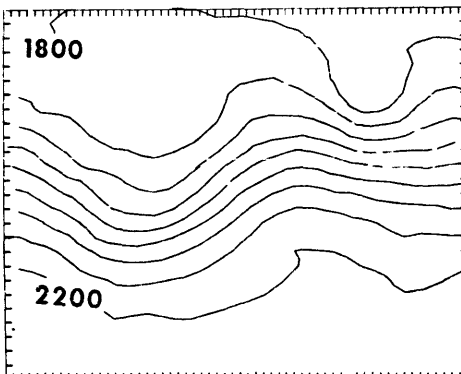
Triangular Scheme I, $\delta = 273\text{km}$



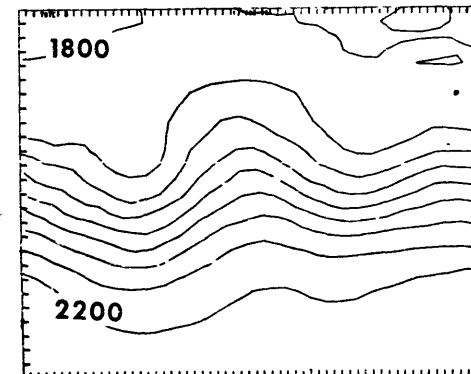
Triangular Scheme I, $\delta = 231\text{km}$



Triangular Scheme III, $\delta = 200\text{km}$



Triangular Scheme II, $\delta = 200\text{km}$



CHAPTER V

PRIMITIVE BAROTROPIC MODEL ON THE SPHERE

The derivation of discrete approximations in spherical geometry will follow very closely the development in cartesian geometry of Chapter IV. Let \hat{i} , \hat{j} , and \hat{k} be unit vectors on the sphere in the eastward, northward, and vertical directions respectively, and let ∇ be the spherical horizontal gradient operator. Then the equations governing frictionless, horizontal, two-dimensional motion on a sphere can be written

$$\frac{\partial h\mathbb{V}}{\partial t} = -\nabla \cdot (\mathbb{V}h\mathbb{V}) - \mathbb{F} \times h\mathbb{V} - \nabla (gh^2/2) \quad (5.1)$$

$$\frac{\partial h}{\partial t} = -\nabla \cdot (h\mathbb{V}) \quad (5.2)$$

where h is the height of the free surface, $\mathbb{V} = u\hat{i} + v\hat{j}$ is the vector velocity, and \mathbb{F} equals $(f + \frac{u}{a} \tan \theta)\hat{k}$, a is the radius of the sphere, f is the Coriolis parameter, θ is the latitude and g is gravity.

Again, as in the case of the plane, if $\mathbb{F} \times h\mathbb{V}$ is evaluated using values at the central grid point, this term will drop out when the discrete kinetic energy equation is formed. Thus it can be dropped in the energy considerations to follow.

5.1 Conservative difference approximations

The discrete approximations are based on area integrals over the secondary grid areas. The integrals of the divergence can be converted to line integrals using Gauss' theorem, resulting in

$$\frac{\partial}{\partial t} \int_A h \nabla dA = - \oint_S (\nabla h \nabla) \cdot \hat{n} ds - g \int_A \nabla \frac{h^2}{2} dA \quad (5.3)$$

$$\frac{\partial}{\partial t} \int_A h dA = - \oint_S (\nabla h) \cdot \hat{n} ds \quad (5.4)$$

where \hat{n} is the outward unit normal to the curve S bounding the area A.

A local polar indexing is used to write the difference equations. Let k denote the number of triangles surrounding the grid point in question. For the spherical geodesic grid, k is either five or six. Consider, first a general form of approximation to the divergence of some vector quantity \mathbb{B} .

$$D = \oint_S \mathbb{B} \cdot \hat{n} ds$$

If we assume the value of \mathbb{B} along the i^{th} segment S_i of S is constant and given by $\mathbb{B}_{\frac{1}{2}i}$, the approximation to the divergence becomes

$$D \doteq \sum_{i=1}^k \mathbb{B}_{\frac{1}{2}i} \cdot \int_{S_i} \hat{n} ds \quad (5.5)$$

where S_i denotes the great circle segments forming the grid area. It is easy to show that most approximations used in calculating fluid flow are of this general form. By the line integral of the unit normal vector we mean the line integral of the two components of the unit normal written in spherical polar coordinates. For a grid of the kind used by Washington and Kasahara (1968) the line integrals of the components reduce to the very simple forms $\pm \hat{\lambda} \Delta \theta$, or $\pm \hat{\lambda} \Delta \lambda$. In the case of the grid developed by Kurihara they take the form (in Gary's 1968 notation) $\pm \hat{\lambda} S_m$ or $\pm \hat{\lambda} S_m$. The line integrals of the components in the spherical geodesic grid do not reduce to anything quite so simple. In fact the expressions for the integrals along arbitrary great circle grid segments are difficult to calculate analytically. In this study they are calculated numerically (see Appendix 2). It should be pointed out that the coefficients can be calculated with a very high degree of precision since they need be calculated only once for each grid orientation and resolution. We denote these line integrals by \vec{C}_i , i.e.,

$$\vec{C}_i = \int_{S_i} \hat{n} ds \quad (3.6)$$

The components of \vec{C}_i are the integrals of the components of \hat{n} written in spherical polar coordinates.

Now we consider an approximation to the pressure gradient term

$$G = \int_A \nabla h dA.$$

Written in terms of spherical coordinates, the integral becomes

$$G = \iint_A \left[\frac{1}{a \cos \theta} \frac{\partial h}{\partial \lambda} \hat{i} + \frac{1}{a} \frac{\partial h}{\partial \theta} \hat{j} \right] a^2 \cos \theta \, d\theta \, d\lambda$$

or

$$G = \iint \left[a \frac{\partial h}{\partial \lambda} \hat{i} + a \frac{\partial (h \cos \theta)}{\partial \theta} \hat{j} \right] d\theta \, d\lambda + \iint a h \sin \theta \hat{j} \, d\theta \, d\lambda$$

Neglecting the spatial variation of the unit vectors within the secondary grid area, the first term on the right hand side can be shown to be a line integral of h times the outward unit normal and can be approximated by

$$\sum_{i=1}^k (h)_{\frac{1}{2}i} \vec{c}_i \quad (5.7)$$

If, in addition, the variation of h in the secondary grid area is neglected, the second term on the right hand side becomes

$$-\bar{h} \int_{\lambda} a \cos \theta \Big|_{\theta_1(\lambda)}^{\theta_2(\lambda)} \hat{j} \, d\lambda$$

where \bar{h} denotes some average value of h . This integral can be written approximately as

$$- \sum_{i=1}^k \bar{h} (\vec{c}_i \cdot \hat{j}) \hat{j} \quad (5.8)$$

Equations (5.7) and (5.8) can be combined for an approximation to the pressure gradient

$$G = \sum_{i=1}^k (h)_{\frac{1}{2}i} \vec{c}_i - \sum_{i=1}^k \bar{h} (\vec{c}_i \cdot \hat{j}) \hat{j} \quad (5.9)$$

We are now able to write a general approximation to equations (5.3) and (5.4). Using the approximations (5.5) and (5.9), the governing equations become

$$A_o \frac{\partial h_o \psi_o}{\partial t} = - \sum_{i=1}^k (\psi_h \psi)_{\frac{1}{2}i} \cdot \vec{c}_i - g \sum_{i=1}^k \left(\frac{h^2}{2}\right)_{\frac{1}{2}i} \vec{c}_i + g \sum_{i=1}^k \left(\frac{h^2}{2}\right) (\vec{c}_i \cdot \hat{j}) \hat{j} \quad (5.10)$$

$$A_o \frac{\partial h_o}{\partial t} = - \sum_{i=1}^k (h \psi)_{\frac{1}{2}i} \cdot \vec{c}_i \quad (5.11)$$

Let $\bar{\psi}$ denote the finite difference equivalent to integration of a scalar ψ over the sphere, i.e.,

$$\bar{\psi} = \frac{1}{A_T} \sum A_o \psi_o$$

where the summation is taken over all grid points and A_T is the area of the sphere. ψ is either h , u , or v .

Formation of the discrete energy equation shows that for (5.10) and (5.11) to conserve energy, the following relations must hold

$$\overline{\frac{1}{2} \mathbb{V}_0^2 \sum_{i=1}^k (\mathbb{V}h)_{\frac{1}{2}i} \cdot \vec{c}_i} = \overline{\mathbb{V}_0 \cdot \sum_{i=1}^k (\mathbb{V}h\mathbb{V})_{\frac{1}{2}i} \cdot \vec{c}_i} \quad (5.12)$$

$$\overline{\mathbb{V}_0 \cdot \sum_{i=1}^k \left(\frac{h^2}{2}\right)_{\frac{1}{2}i} \vec{c}_i} + \overline{\mathbb{V}_0 \cdot \sum_{i=1}^k \left(\frac{h^2}{2}\right) (\vec{c}_i \cdot \hat{j}) \hat{j}} = - \overline{h_0 \sum_{i=1}^k (\mathbb{V}h)_{\frac{1}{2}i} \cdot \vec{c}_i} \quad (5.13)$$

Again, the first relation (5.12) insures that the space differences will not produce nonlinear instabilities; the second (5.13) provides for consistent average conversion between kinetic and potential energy.

We note that when the curvilinear coordinate system reduces to a cartesian system, equations (5.10) through (5.13) reduce to the corresponding cartesian equations (4.10) through (4.13).

Relation (4.12) can be satisfied if we take

$$(\mathbb{V}h\mathbb{V})_{\frac{1}{2}i} = \frac{1}{2} (\mathbb{V}_0 + \mathbb{V}_{1i}) (\mathbb{V}h)_{\frac{1}{2}i} \quad (5.14)$$

since, as in the Cartesian case,

$$\overline{\sum_{i=1}^k \mathbb{V}_0 \cdot \mathbb{V}_i (\mathbb{V}h)_{\frac{1}{2}i} \cdot \vec{c}_i} = 0$$

One possible definition of $(\mathbb{V}h)_{\frac{1}{2}i}$ is

$$(\nabla h)_{\frac{1}{2}i} = \frac{1}{2} (h_o \nabla_o + h_i \nabla_i) \quad (5.15)$$

The energy conversion relation (4.13) then holds provided that

$$(h^2)_{\frac{1}{2}i} = h_o h_i \quad (5.16)$$

and

$$(\overline{h^2}) = h_o^2 \quad (5.17)$$

Substitution of (5.14), (5.15), (5.16) and (5.17) into (5.10) and (5.11) results in

Scheme Is

$$\begin{aligned} \frac{\partial h_o \nabla_o}{\partial t} = & - \frac{1}{4A_o} \sum_{i=1}^k (\nabla_o + \nabla_i) (h_o \nabla_o + h_i \nabla_i) \cdot \vec{c}_i \\ & - \frac{g}{2A_o} \sum_{i=1}^k h_o h_i \vec{c}_i + \frac{g}{2A_o} h_o^2 \sum_{i=1}^k (\vec{c}_i \cdot \hat{j}) \hat{j} \end{aligned}$$

$$\frac{\partial h_o}{\partial t} = - \frac{1}{2A_o} \sum_{i=1}^k (h_o \nabla_o + h_i \nabla_i) \cdot \vec{c}_i$$

The special form this scheme takes when applied to a regular spherical grid is the same as the scheme of Grimmer and Shaw (1967).

A second possible definition of $(\Psi h)_{\frac{1}{2}i}$ is

$$(\Psi h)_{\frac{1}{2}i} = \frac{1}{4} (h_o + h_i)(\Psi_o + \Psi_i) \quad (5.18)$$

Relation (5.13) is now valid if

$$(h^2)_{\frac{1}{2}i} = \frac{1}{2} (h_o^2 + h_i^2) \quad (5.19)$$

and

$$\overline{(h^2)} = h_o^2 \quad (5.20)$$

Substitution of (5.14), (5.18), (5.19) and (5.20) into (5.10) and (5.11) results in a second energy conservative scheme given by

Scheme IIs

$$\begin{aligned} \frac{\partial h_o \Psi_o}{\partial t} = & - \frac{1}{8A_o} \sum_{i=1}^k (\Psi_o + \Psi_i)(h_o + h_i)(\Psi_o + \Psi_i) \cdot \vec{c}_i \\ & - \frac{g}{4A_o} \sum_{i=1}^k (h_o^2 + h_i^2) \vec{c}_i + \frac{g}{2A_o} h_o^2 \sum_{i=1}^k (\vec{c}_i \cdot \vec{j}) \vec{j} \end{aligned}$$

$$\frac{\partial h_o}{\partial t} = - \frac{1}{4A_o} \sum_{i=1}^k (h_o + h_i)(\Psi_o + \Psi_i) \cdot \vec{c}_i$$

The special form Scheme IIs takes when applied to a regular spherical grid is the same as Kurihara's scheme as studied by Gary (1968).

5.2 Numerical experiments

Several simple numerical experiments are performed to test the suitability of the difference schemes for use with fluid flow problems. For these tests the grid is oriented so that the north and south poles are grid points. This orientation is useful for our evaluation runs since with this orientation, the grid has a period of five around the sphere. If the initial conditions also have a period of five, only one fifth of the computations need be performed. Most of our experiments will take advantage of this feature.

This orientation is not desirable for general usage since the poles must be treated separately when spherical polar coordinates are used. In this case the velocity components, u and v , are not defined at the poles. Since the cases we consider here have little happening at the pole, the velocity, \mathbf{V} , is set equal to zero there and the height, h , is assigned the average value of the five closest points when these values are needed by the difference operators. We note that for general integrations, the poles do not have to be treated separately if they are not grid points or do not lie on a side of a secondary grid area. This follows from the application of Gauss' theorem to convert the area integrals to line integrals for the fundamental approximations. This relation is a vector relation independent of the particular coordinate system chosen. In this case the difference operators defined in the previous section can be applied at every grid point. Also, if spherical polar coordinates are not used this difficulty does not arise.

For instance, if a streamfunction is used as in Chapter III there is no difficulty at the poles.

The results of the experiments are all shown on a cylindrical projection where intersections of 5° latitude and longitude lines are mapped onto a square grid. In such a projection the pole points are distorted into straight lines. Fig. 5.1 shows the 5° grid on such a projection. Grid points on the sides of the icosahedral triangles are indicated by 0, points interior to icosahedral triangles are indicated by +. The continent outlines furnish some idea of the distortions near the poles.

Gravity Waves

To establish whether or not the difference schemes introduced any gross errors when dealing with gravity wave motion, a short integration was performed with the Coriolis term set equal to zero. The initial conditions are ψ equal to 0, and h equal to a constant 8,000 m with an additional cone of fluid of height 800 m and radius 10° centered at $\theta = 0^\circ$, $\lambda = 180^\circ$. Fig. 5.2 shows the ensuing height and velocity fields at 2, 4, and 6 hours for the 5° grid. The figures cover the area of -90° to $+90^\circ$ latitude and $+90^\circ$ to 270° longitude. The contours of the initial height field are then circles centered in the figure with a maximum radius of 10° . Because of the distortion of the projection, a circular wave front will transform into the square outline of the figure as the radius approaches 90° .

Centered time differences are used with a 75 second time step. A forward difference is taken every 96 (48) time steps for the 5° ($2\frac{1}{2}^{\circ}$) grid to eliminate one of the two solutions associated with the centered time differences.

The linear gravity wave speed, \sqrt{gh} , for a fluid of depth 8,000 m is approximately 9.1° /hour. The wave front in the numerical solution is seen to agree very well with this. The circular wave front does become square on this projection as the radius approaches 90° and passes over the poles shortly before the 8th hour. The computation could not be carried out further because of the method of treating the poles.

A similar computation was performed with the $2\frac{1}{2}^{\circ}$ grid. This time a conical depression of 800 m was placed at the north pole. Fig. 5.3 shows the resulting h and v patterns at 4, 8, and 12 hours. The area covered in the figure is slightly more than two cycles of the grid. With this projection the wave fronts should appear as straight horizontal lines and move down the figure. The source is damped out very fast because of the averaging at the pole. The speed of the waves is seen to agree very well with the linear speed. The wave fronts do remain as straight horizontal lines.

Fig. 5.4 shows the kinetic energy as a function of time for these two cases. Both show a rapid increase in kinetic energy initially, then a decrease as the wave spreads out. The 5° curve shows a series of peaks corresponding to new waves being sent out

from the center point. These peaks are missing in the $2\frac{1}{2}^{\circ}$ curve because the center point is so strongly damped.

Neamtan waves

In order to evaluate these schemes for use with more atmospheric-like motions we use the initial conditions used by Phillips (1959) and subsequently by other investigators. These conditions are those of a Neamtan (1946) wave, which, in a nondivergent barotropic atmosphere, propagates eastward with a constant angular velocity and without change of shape. For the divergent model considered here there is no analytic solution; however, several investigators, namely Grimmer and Shaw (1967) and Gary (1968) have used the same initial conditions to test difference approximations for the same model. Our results can be compared with theirs and hence the difference schemes can be compared with each other. These initial conditions have another advantage; since they are analytic, the exact initial tendencies can be calculated and compared to the discrete initial tendencies.

The initial velocity $\nabla\psi$ is nondivergent and given by the stream function

$$\psi = -a^2 \omega \sin \Theta + a^2 K \cos^R \Theta \sin \Theta \cos R\lambda$$

where ω , K , R and a are constants. The initial height field is

determined so that h and ψ satisfy the balance equation

$$gh = gh_0 + \alpha^2 A(\theta) + \alpha^2 B(\theta) \cos R\lambda + \alpha^2 C(\theta) \cos 2R\lambda$$

$$A(\theta) = \frac{1}{2} \omega (2\Omega + \omega) c^2 + \frac{1}{4} K^2 c^{2R} [(R+1)c^2 + (2R^2 - R - 2) - 2R^2 c^{-2}]$$

$$B(\theta) = \frac{2(\Omega + \omega)K}{(R+1)(R+2)} c^R [(R^2 + 2R + 2) - (R+1)^2 c^2]$$

$$C(\theta) = \frac{1}{4} K^2 c^{2R} [(R+1)c^2 - (R+2)]$$

$$c = \cos \theta$$

The constants are given the following values

$$\omega = K = 7.848 \times 10^{-6} \text{ sec}$$

$$h_0 = 8 \times 10^3 \text{ m}^2 \text{ sec}^{-2}$$

R is taken to be either 4 or 5.

A six day (6912 time step) integration was carried out over the 5° grid. The h , u , and v fields are shown in Fig. 5.5 at one day intervals. The region covered by each figure is -90° to $+90^\circ$ latitude and 0° to 150° longitude, a little over two periods. The wave speed is a little over 17 degrees per day compared with an analytic value for the nondivergent case of 19.8. The fields become very jagged and the solution is not good at day 6.

Fig. 5.6 shows the results of an 8 day (18432 time step) integration over a $2\frac{1}{2}^\circ$ grid. The most noticeable feature is the two-grid

interval noise superimposed on the pattern. Such phenomena are present in other schemes (Okamura, 1968) and can be avoided by changing the space phasing of the variables (Masuda, 1968; Okamura, 1968) or by adding a diffusion term or space smoothing.

Disregarding this two-grid interval noise, these results can be smoothed by eye and compared with previous investigations. For the first four or five days, when the original wave is still clearly defined in the pattern, the wave moved with a speed slightly greater than 18 degrees per day. Again, the analytic value for the nondivergent model is about 19.8.

Gary (1968) compared two schemes currently being used for general circulation models: Kurihara's (1965b) and Kasahara and Washington's (1967), hereafter referred to as Centered. Gary concluded that the Kurihara scheme is more accurate than the centered scheme for a given $\Delta\theta$. However, because of the space-time phasing of the variables he says the Kurihara scheme at $\Delta\theta$ should be compared with the centered scheme at approximately $\Delta\theta/\sqrt{2}$. Further information he gives suggests that under these conditions the schemes are probably equally good. Gary also concluded that the Kurihara scheme with a "uniform mesh spacing," in which the number of grid points on a latitude circle decreases uniformly from equator to pole, produces less accurate results than one in which $\Delta\lambda$ was constant and equal to $\Delta\theta$ up to around $\theta = 65^\circ$, then increased.

With this in mind, we will compare our results with those of the Kurihara scheme over a regular spherical mesh, not the "uniform mesh." We will consider his case where the resolution at the equator is approximately equal to ours. This is his case 503.1, or his Fig. 11. This has a grid size of about 2.65° at the equator with the resolution increasing up to about 65° latitude. This grid has 7044 points compared with 7682 points in the $2\frac{1}{2}^\circ$ spherical geodesic grid.

Our patterns evolved very closely to his. The main difference being that by the eighth day his patterns become very weak due to a diffusion term he added for stability. Essentially, these two schemes produce very similar results for this type of initial condition, and we conclude that in this respect the schemes are equally good.

We can also compare our results to Gary's Fig. 12 which is the solution from Kurihara's scheme applied to his "uniform grid." Our results are seen to be better than these.

Gary's Figs. 28-32 show the evolution of the centered scheme for six days over a grid of 7048 points (about 2.8° at equator). Again, our scheme produces better results than this scheme.

We cannot compare the energy conservation properties of these schemes since Gary always used a diffusion term for stability. Hence, the energy in his cases always decreased. The total energy

per unit area in our $2\frac{1}{2}^{\circ}$ integration remained in the range 4.61564×10^8 to 4.61588×10^8 during the entire eight days. The energy variation in the 5° integration was of the same order, about .003%.

From these comparisons we conclude that the space differences over the spherical geodesic grid are at least as good as those in use today for general circulation models when applied to a simple wave. However, when these schemes are combined with centered time differencing, a very small time step is required for linear stability. One of the reasons for using a quasi-homogeneous grid is to eliminate the convergence of grid points at the pole and the very small time step this convergence imposes.

The Matsuno or Euler-backward time differencing (Kurihara, 1965a) was tried to determine its effect on the linear stability. A 20 minute time step was found to be stable for the 5° grid and correspondingly a 10 minute step for the $2\frac{1}{2}^{\circ}$ grid. This is up to four times longer than would be necessary for the present general circulation models at a similar resolution. Time steps that have been used are: Mintz (1964), $\Delta t = 12$ min. for $\Delta\Theta = 7^{\circ}$; Kasahara and Washington¹, $\Delta t = 6$ min. for $\Delta\Theta = 5^{\circ}$; Kurihara and Holioway (1967), $\Delta t = 7.5$ min. for $\Delta\Theta = 4^{\circ}$. This could mean a saving of computer time of a factor of four.

¹Private communication

Height fields for various days are shown in Fig. 5.7 for the 5° and $2\frac{1}{2}^{\circ}$ grid using Matsuno time differences. The time steps used are 20 minutes and 7.5 minutes for the 5° and $2\frac{1}{2}^{\circ}$ grids respectively. With a 10 minute time step on the $2\frac{1}{2}^{\circ}$ grid, two-grid-interval wiggles appeared in limited areas at various times and then disappeared. No sign of this phenomenon was seen with the 7.5 minute time step. Fig. 5.7 can be compared with Figs. 5.5 and 5.6. The height field patterns are very similar. The same can be said for the u and v fields (not shown). The Matsuno schemes produce a slightly slower phase speed than the centered scheme. The Matsuno scheme also produces a slight damping. The total energy decreased by 0.4% during the 8 day run over the $2\frac{1}{2}^{\circ}$ grid. Other than these slight differences, the same conclusions can be made for the Matsuno scheme as were made for the centered scheme.

5.3 Initial tendencies

In order to better understand how these schemes work we consider the initial tendencies. The analytic initial conditions permit the initial tendencies to be calculated analytically and compared with the discrete tendencies. This will help explain why the 5° grid produced poor results. First it will prove useful to introduce another approximation to the mass flux.

The mass flux can be written as the sum of an advection and a divergence term

$$\nabla \cdot (h\mathbb{V}) = \mathbb{V} \cdot \nabla h + h \nabla \cdot \mathbb{V}$$

and each term can be differenced independently. From (5.9) and (5.5) we have approximations for ∇h and $\nabla \cdot \mathbb{V}$, namely

$$\nabla \cdot \mathbb{V} = \frac{1}{A_0} \sum_{i=1}^k \frac{1}{2} (\mathbb{V}_0 + \mathbb{V}_i) \cdot \vec{c}_i$$

$$\nabla h = \frac{1}{2A_0} \sum_{i=1}^k (h_i - h_0) \vec{c}_i$$

Thus we can write an approximation IIIs as

Scheme IIIs

$$\mathbb{V} \cdot \nabla h = \frac{\mathbb{V}_0}{2A_0} \cdot \sum_{i=1}^k (h_i - h_0) \vec{c}_i$$

$$h \nabla \cdot \mathbb{V} = \frac{h_0}{2A_0} \sum_{i=1}^k (\mathbb{V}_i - \mathbb{V}_0) \cdot \vec{c}_i$$

$$\nabla \cdot (h\mathbb{V}) = \frac{1}{2A_0} \sum_{i=1}^k (\mathbb{V}_0 h_i + \mathbb{V}_i h_0) \cdot \vec{c}_i$$

This approximation has the same general form as Is and IIs, and, as will be seen, gives very similar results.

To study the initial tendencies we use a wave number four initial condition rather than a wave number five. This prevents the grid pattern and wave pattern from coinciding.

The left column of Fig. 5.8 shows the initial analytic flux fields. The two other columns show the flux fields as calculated by Scheme IIs over a 10° and 5° grid. The momentum fluxes are seen to be quite good but the mass fluxes only begin to resemble the analytic field with the 5° grid. The pressure approximations, not shown, are at least as good as the momentum flux approximations. Thus we will confine the ensuing discussion to the momentum and mass flux. The question we wish to consider is why the mass flux approximations are so much poorer than the momentum fluxes.

Fig. 5.9 shows the approximations of Scheme IIIs for the 10° and 5° grids. The mass flux is almost identical with that from Scheme IIs. Of the two individual parts of the mass flux, the advection term is a good approximation to the mass flux but the divergence term, which should be zero, is very poor. In fact, the approximation values of the divergence are larger than the mass flux for the 10° grid and almost as large for the 5° grid. The question now is why the divergence approximation is so poor.

To study this question we apply the difference schemes over a stencil of points more naturally suited to polar spherical coordinates. Consider four grid points around a central point such that two have the same latitude as the central point and two have the same longitude, although they need not be the same distance from the central point (Fig. 5.10). To apply the schemes to this stencil, the line integrals of the normal vectors and the area are needed.

These are given by

$$\vec{c}_1 = a \Delta\theta^* \hat{i}$$

$$\vec{c}_2 = a \cos(\theta_0^* + \frac{\Delta\theta^*}{2}) \Delta\lambda^* \hat{j}$$

$$\vec{c}_3 = -a \Delta\theta^* \hat{i}$$

$$\vec{c}_4 = -a \cos(\theta_0^* - \frac{\Delta\theta^*}{2}) \Delta\lambda^* \hat{j}$$

$$A_0 = 2a^2 \sin \frac{\Delta\theta^*}{2} \cos \theta_0^* \Delta\lambda^*$$

where

$$\Delta\lambda^* = \frac{1}{2} (\Delta\lambda_1 + \Delta\lambda_3)$$

$$\Delta\theta^* = \frac{1}{2} (\Delta\theta_2 + \Delta\theta_4)$$

$$\theta_0^* = \theta_0 + \frac{1}{4} (\Delta\theta_2 - \Delta\theta_4)$$

When $\Delta\lambda_1 = \Delta\lambda_3$ and $\Delta\theta_2 = \Delta\theta_4$ we have the common spherical stencil. In the following we will consider differences over two cases of this stencil. The first will be called regular spherical differences. At each grid point of the 5^0 spherical geodesic grid we define the stencil so that $\Delta\lambda_1 = \Delta\lambda_3 = \Delta\theta_2 = \Delta\theta_4 = D$. At each of these newly defined stencil points, the appropriate analytic values are assigned to h, u and v. The difference schemes are applied over this new stencil. We note that this is not appropriate for integrating in time, but rather is appropriate for studying the approximations to the initial tendencies.

The second case we will consider is called random spherical differences. In this case $\Delta\lambda_1$, $\Delta\lambda_3$, $\Delta\theta_2$, $\Delta\theta_4$ are given by $\Delta = D(1.0 + 0.1R)$ where D is the mean value and R is a random number between -1 and 1 with a rectangular distribution. In the following we will refer to 10° , 5° and $2\frac{1}{2}^\circ$ stencils. This indicates the value of D for both the regular and random stencils.

Fig. 5.11 shows the momentum flux calculated with both the regular and random differences over a 10° stencil. Both cases are seen to be good approximations. As would be expected, the 5° and $2\frac{1}{2}^\circ$ stencils (not shown) produce even better results.

Fig. 5.12 shows the mass flux calculated over the 10° , 5° and $2\frac{1}{2}^\circ$ regular spherical stencils. The top row is Scheme IIIs, the second row is Scheme IIIIs. Again, both schemes produce very similar results. The third row is the advection part of Scheme IIIIs. It is very close to the analytic values just as in the previous cases. The last row is the divergence which analytically is zero. It is seen to be as large as the advection term with the 10° stencil but becomes negligible with the $2\frac{1}{2}^\circ$ stencil. These regular spherical differences give us the first indication of what the trouble is. The differences over a regular stencil are second-order. When the stencil is not regular, the schemes become first-order and the divergence is not calculated with enough accuracy until the mesh becomes very fine. This is seen in Fig. 5.13 where the schemes are applied to the random spherical stencil. This figure has the same format as Fig. 5.12. Here, again,

the advection term is satisfactory but the divergence error is very large. It is not until $2\frac{1}{2}^0$ resolution that the mass flux pattern begins to resemble the analytic value.

We get a better understanding of why the error in the divergence affects only the mass flux in the next section, where the truncation error is calculated for these schemes over a random spherical stencil.

5.4 Truncation error

Schemes Is and IIs produce results that are almost identical. Therefore, for truncation error studies we will consider Scheme Is since it is a little simpler. The terms considered are

Scheme Is, momentum flux, Q_1

$$Q_1 = -\frac{1}{4A_0} \sum_{i=1}^k (\mathbb{V}_0 + \mathbb{V}_i) (h_0 \mathbb{V}_0 + h_i \mathbb{V}_i) \cdot \vec{C}_i$$

Scheme Is, mass flux, M_1

$$M_1 = -\frac{1}{2A_0} \sum_{i=1}^k (h_0 \mathbb{V}_0 + h_i \mathbb{V}_i) \cdot \vec{C}_i$$

Scheme IIIs, advection term A_2

$$A_2 = -\frac{1}{2A_0} \sum_{i=1}^k \mathbb{V}_0 (h_i - h_0) \cdot \vec{C}_i$$

Scheme IIIs, divergence term, D_2

$$D_2 = -\frac{1}{2A_0} \sum_{i=1}^k h_0 (V_0 + V_i) \cdot \vec{c}_i$$

Scheme IIIs, mass flux, $M_2 = A_2 + D_2$

$$M_2 = -\frac{1}{2A_0} \sum_{i=1}^k (h_i V_0 + h_0 V_i) \cdot \vec{c}_i$$

The quantities in the difference equations are expanded in Taylor's Series around the centerpoint

$$\psi_i = \psi_0 + \sum_{j=1}^{\infty} \frac{1}{j!} \Delta \lambda_i^j \frac{\partial^j \psi_i}{\partial \lambda^j} \text{ for } \psi = V \text{ or } h, i = 1 \text{ or } 3$$

$$\psi_i = \psi_0 + \sum_{j=1}^{\infty} \frac{1}{j!} \Delta \theta_i^j \frac{\partial^j \psi_i}{\partial \theta^j} \text{ for } \psi = V \text{ or } h, i = 2 \text{ or } 4$$

The following simplifications are made in the expansions

$$4 \sin \frac{\Delta \theta_2 + \Delta \theta_4}{4} \doteq \Delta \theta_2 + \Delta \theta_4$$

$$\cos \frac{\Delta \theta_2 + \Delta \theta_4}{2} \doteq 1$$

These simplifications affect the results by less than one percent, not by orders of magnitude.

The Taylor's Series' expansions for the approximations are

then

$$Q_1 = -\nabla \cdot (\nabla h \nabla) - \frac{(\Delta \lambda_1 - \Delta \lambda_3)}{2} Q_{1\lambda} \\ - \frac{(\Delta \theta_2 - \Delta \theta_4)}{2} Q_{1\theta} + O(\Delta^2)$$

$$M_1 = -\nabla \cdot (h \nabla) - \frac{(\Delta \lambda_1 - \Delta \lambda_3)}{2} M_{1\lambda} \\ - \frac{(\Delta \theta_2 - \Delta \theta_4)}{2} M_{1\theta} + O(\Delta^2)$$

$$A_2 = -\nabla \cdot \nabla h - \frac{(\Delta \lambda_1 - \Delta \lambda_3)}{2} A_{2\lambda} \\ - \frac{(\Delta \theta_2 - \Delta \theta_4)}{2} A_{2\theta} + O(\Delta^2)$$

$$D_2 = -h \nabla \cdot \nabla - \frac{(\Delta \lambda_1 - \Delta \lambda_3)}{2} D_{2\lambda} \\ - \frac{(\Delta \theta_2 - \Delta \theta_4)}{2} D_{2\theta} + O(\Delta^2)$$

where

$$Q_{1\lambda} = \frac{1}{2a \cos \theta} \left\{ hu \frac{\partial^2 V}{\partial \lambda^2} + V \frac{\partial^2 hu}{\partial \lambda^2} + \frac{\partial^2}{\partial \lambda^2} (huV) \right\}$$

$$Q_{1\theta} = \frac{1}{2a} \left\{ h\nu \frac{\partial^2 V}{\partial \theta^2} + V \frac{\partial^2 h\nu}{\partial \theta^2} + \frac{\partial^2}{\partial \theta^2} (h\nu V) - 2 \tan \theta \frac{\partial}{\partial \theta} (h\nu V) \right\}$$

$$M_{1\lambda} = \frac{1}{a \cos \theta} \frac{\partial^2}{\partial \lambda^2} (hu)$$

$$M_{1\theta} = \frac{1}{a} \left\{ \frac{\partial^2}{\partial \theta^2} (h\nu) - \frac{1}{2} \tan \theta \frac{\partial}{\partial \theta} (h\nu) \right\}$$

$$A_{2\lambda} = \frac{u}{a \cos \theta} \frac{\partial^2 h}{\partial \lambda^2}$$

$$A_{2\theta} = \frac{\nu}{a} \left\{ \frac{\partial^2 h}{\partial \theta^2} - \frac{1}{2} \tan \theta \frac{\partial h}{\partial \theta} \right\}$$

$$D_{2\lambda} = \frac{h}{a \cos \theta} \frac{\partial^2 u}{\partial \lambda^2}$$

$$D_{2\theta} = \frac{h}{a} \left\{ \frac{\partial^2 \nu}{\partial \theta^2} - \frac{1}{2} \tan \theta \frac{\partial \nu}{\partial \theta} \right\}$$

Table 3 gives a bound for the first order error terms for Schemes Is and IIIs. With the random stencil defined in the previous section $|(\Delta\lambda_1 - \Delta\lambda_3)/2|$ and $|(\Delta\theta_2 - \Delta\theta_4)/2|$ are less than $.1\Delta\lambda^*$ and $.1\Delta\theta^*$ respectively. Thus, the maximum value of the truncation error for the advection term of Scheme IIIs is bounded by $.1\Delta\lambda^* |A_2|$ or $.1\Delta\theta^* |A_{2\theta}|$. Table 1 also lists these error bounds for the 10° , 5° , and $2\frac{1}{2}^\circ$ random stencils. For comparison, Table 4 lists the maximum analytic values of momentum and mass fluxes and advection term for wave number five.

Table 3

	Analytic	Error Bound		
		10°	5°	$2\frac{1}{2}^{\circ}$
$Q_{1\lambda}$	3.9×10^2	6.8×10^0	3.4×10^0	1.7×10^0
	1.2×10^3	2.1×10^1	1.1×10^1	5.3×10^0
$Q_{1\theta}$	9.4×10^1	1.7×10^0	8.2×10^{-1}	4.1×10^{-1}
	1.6×10^2	2.8×10^0	1.4×10^0	7.0×10^{-1}
$M_{1\lambda}$	2.0×10^0	3.7×10^{-2}	1.9×10^{-2}	9.2×10^{-3}
$M_{1\theta}$	1.3×10^0	2.3×10^{-2}	1.2×10^{-2}	5.7×10^{-3}
$A_{2\lambda}$	1.9×10^{-1}	3.3×10^{-3}	1.7×10^{-3}	8.3×10^{-4}
$A_{2\theta}$	8.6×10^{-2}	1.5×10^{-3}	7.5×10^{-4}	3.8×10^{-4}
$D_{2\lambda}$	2.1×10^0	3.7×10^{-3}	1.9×10^{-2}	9.2×10^{-3}
$D_{2\theta}$	1.3×10^0	2.3×10^{-2}	1.2×10^{-2}	5.7×10^{-3}

Table 4

	Analytic Bound
$ \nabla \cdot (h \mathbb{V}) $	1.3×10^{-2}
$ \nabla \cdot (\mathbb{V} h u) $	2.4×10^1
$ \nabla \cdot (\mathbb{V} h w) $	3.4×10^1
$ \nabla \cdot (h \mathbb{V}) $	1.3×10^{-2}
$ \mathbb{V} \cdot \nabla h $	1.3×10^{-2}
$ h \nabla \cdot \mathbb{V} $	0

Comparison shows that the maximum possible errors in the momentum flux approximations are less than the analytic values even for the 10° stencil and are at least an order of magnitude smaller for the $2\frac{1}{2}^{\circ}$ stencil. This is not the case for the mass flux. Here the maximum possible errors are the same size as the mass flux even with the 5° grid and the numerical examples in the previous section bear out that the actual errors are almost as large. Examination of Scheme IIIs in the table shows this error can be attributed to the error in the divergence term. The reason the error in the divergence does not adversely affect the momentum flux is that the momentum flux is three orders of magnitude larger than the mass flux. But since $hu \nabla \cdot \mathcal{V} = u(h \nabla \cdot \mathcal{V})$ and u is less than 100 m sec^{-1} , if the error in the divergence term is the same order as the advection term in the mass flux, the error in the divergence term is at least one order smaller than the momentum flux.

Essentially these tables say the maximum possible errors will not be small enough for satisfactory integration of the continuity equation unless the resolution of the grid is at least $2\frac{1}{2}^{\circ}$. This agrees with the conclusions from the numerical experiments.

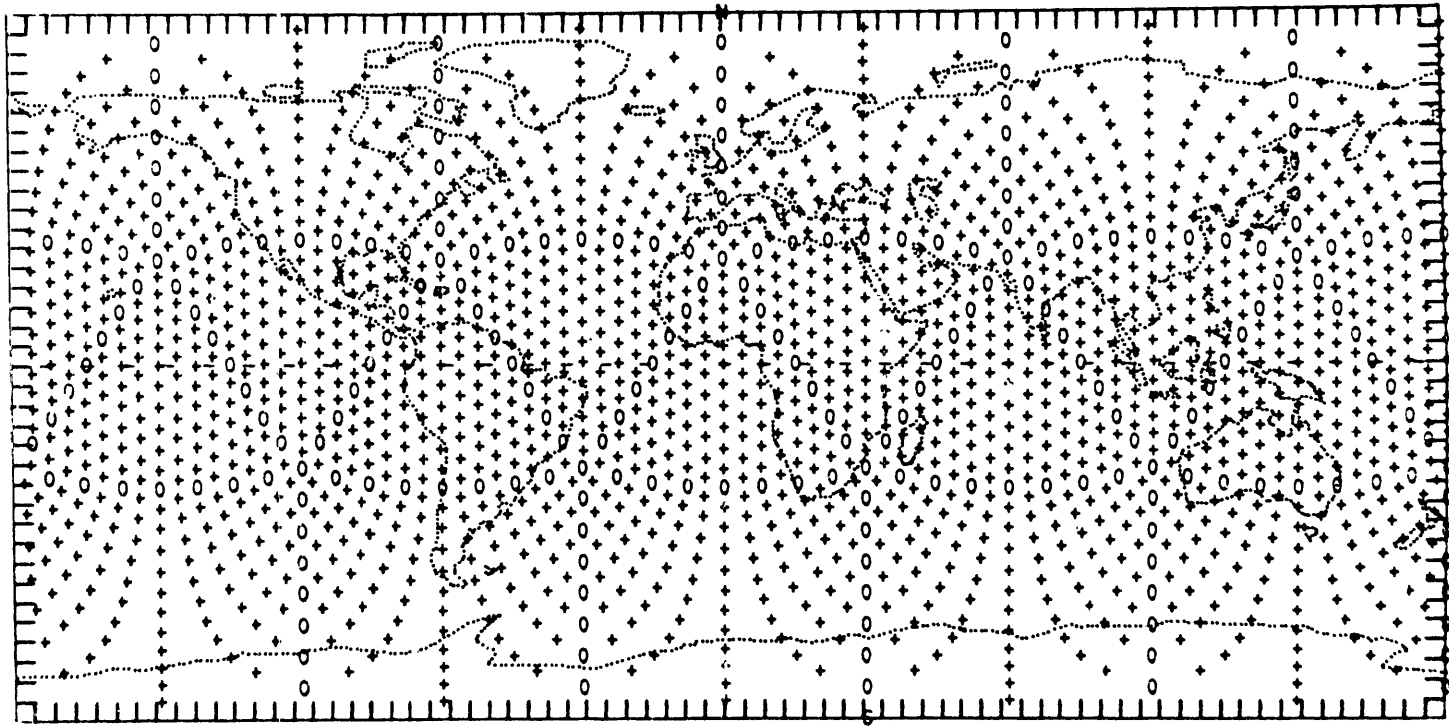
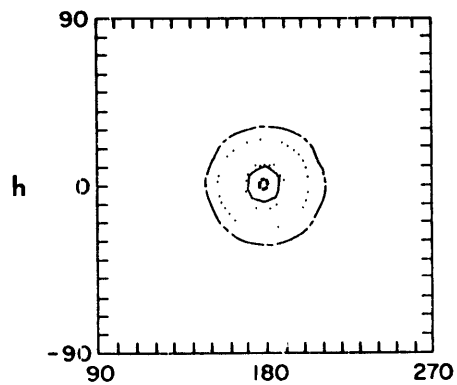


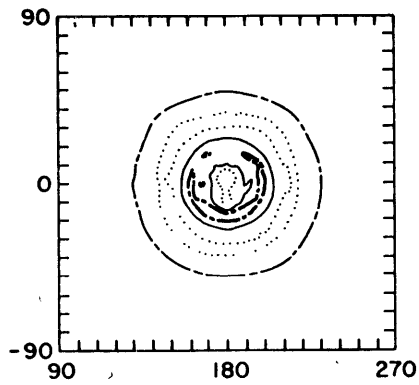
Fig. 5.1 5° grid on a cylindrical projection.

Fig. 5.2 h, u, and v fields for gravity wave solution
over $2\frac{1}{2}^\circ$ grid.

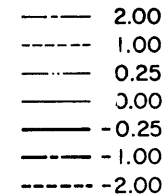
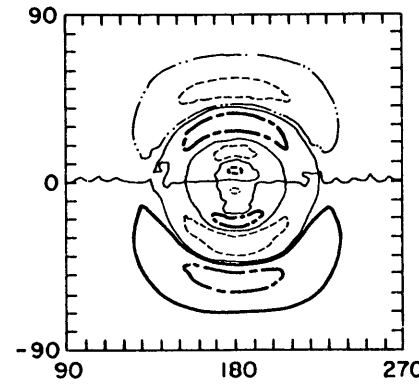
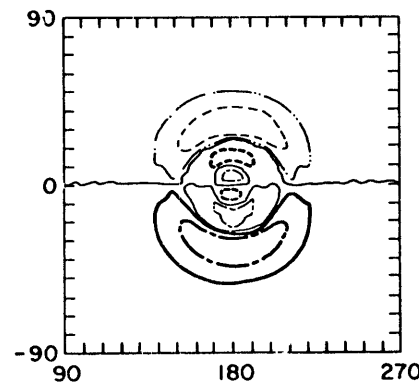
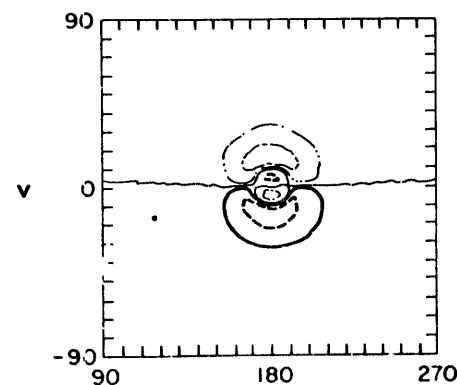
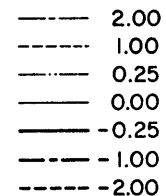
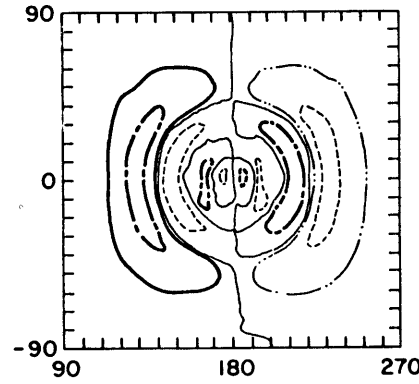
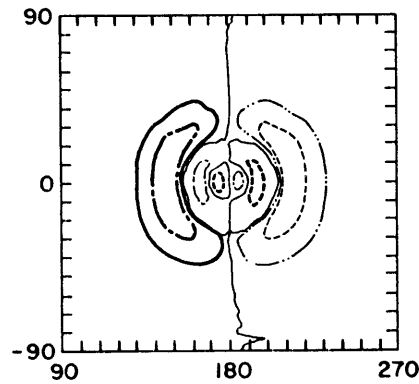
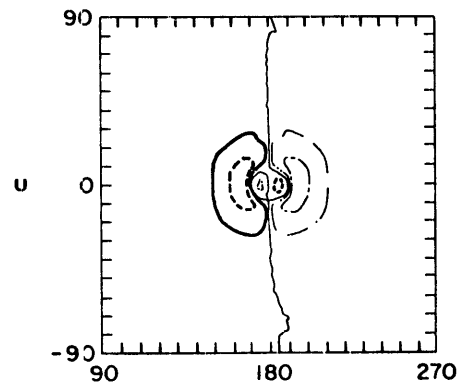
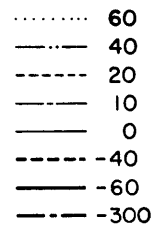
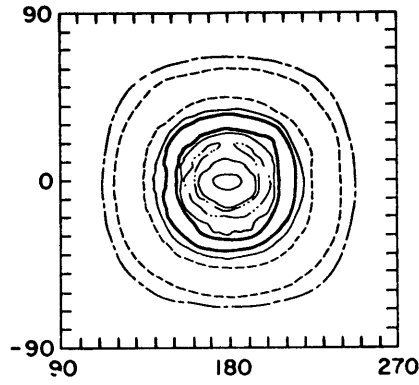
2 Hours



4 Hours



6 Hours



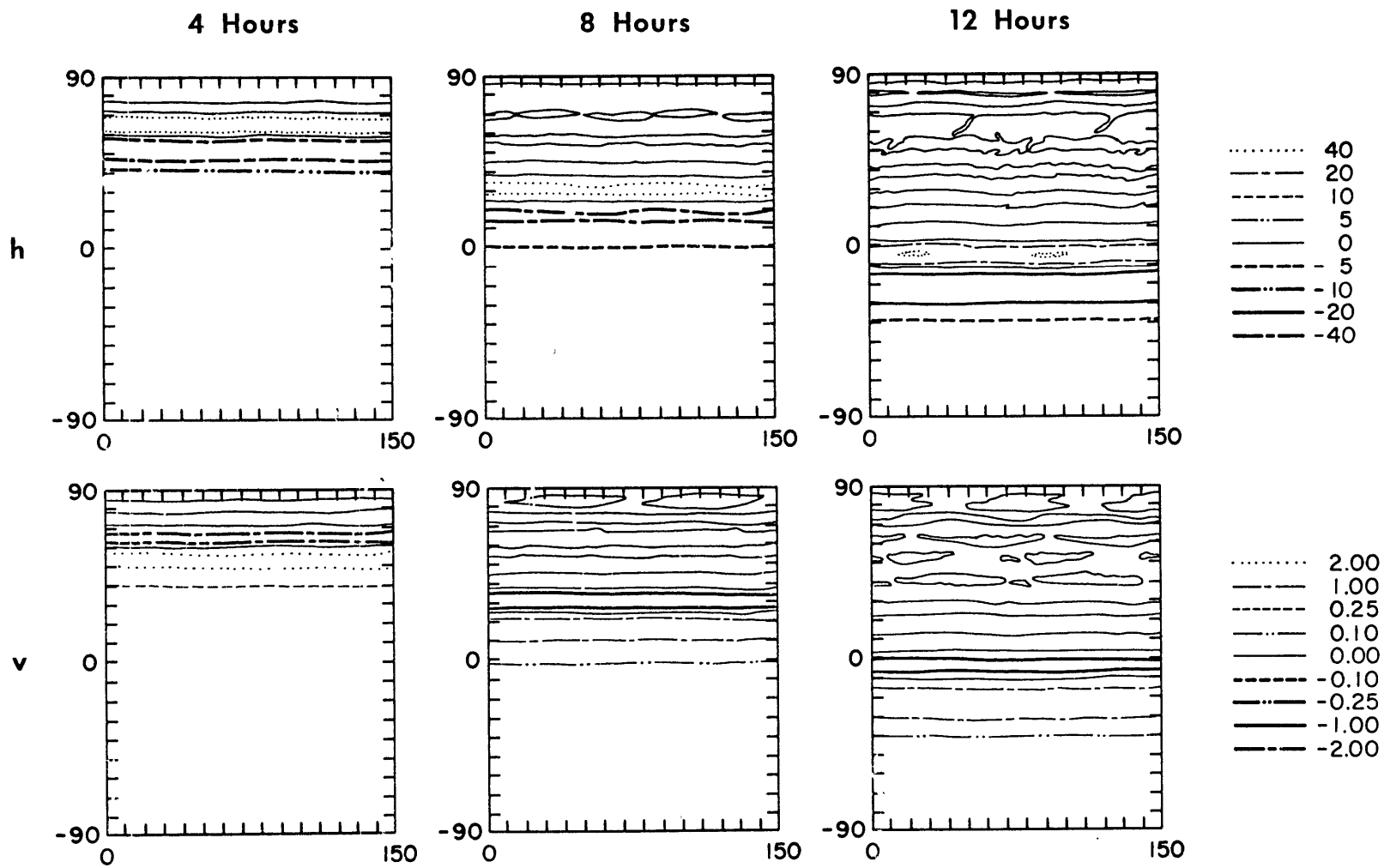
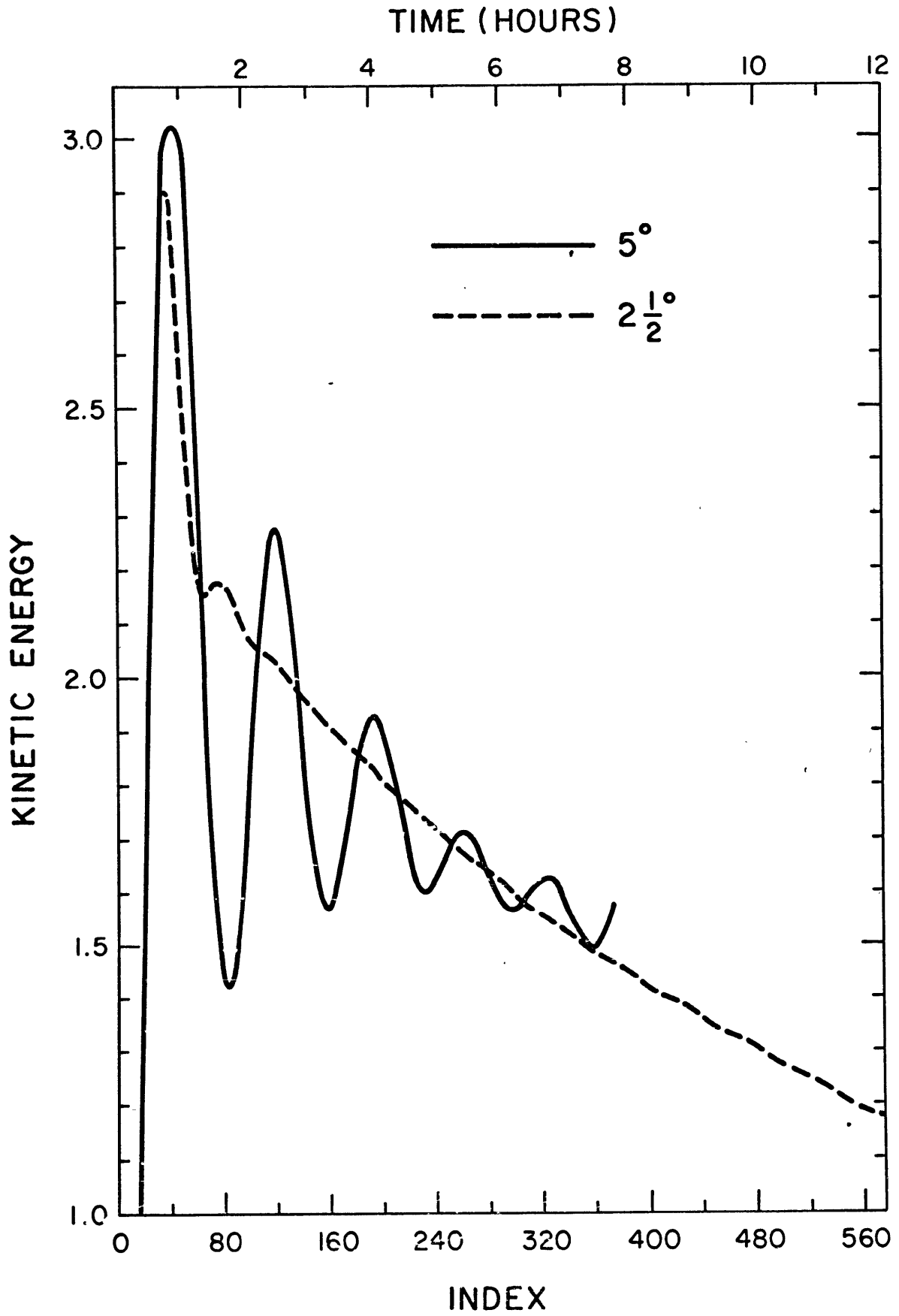


Fig. 5.3 h and v fields for gravity wave solution over $2\frac{1}{2}^\circ$ grid.

Fig. 5.4 Kinetic energy variation for 5° and $2\frac{1}{2}^{\circ}$ integrations.



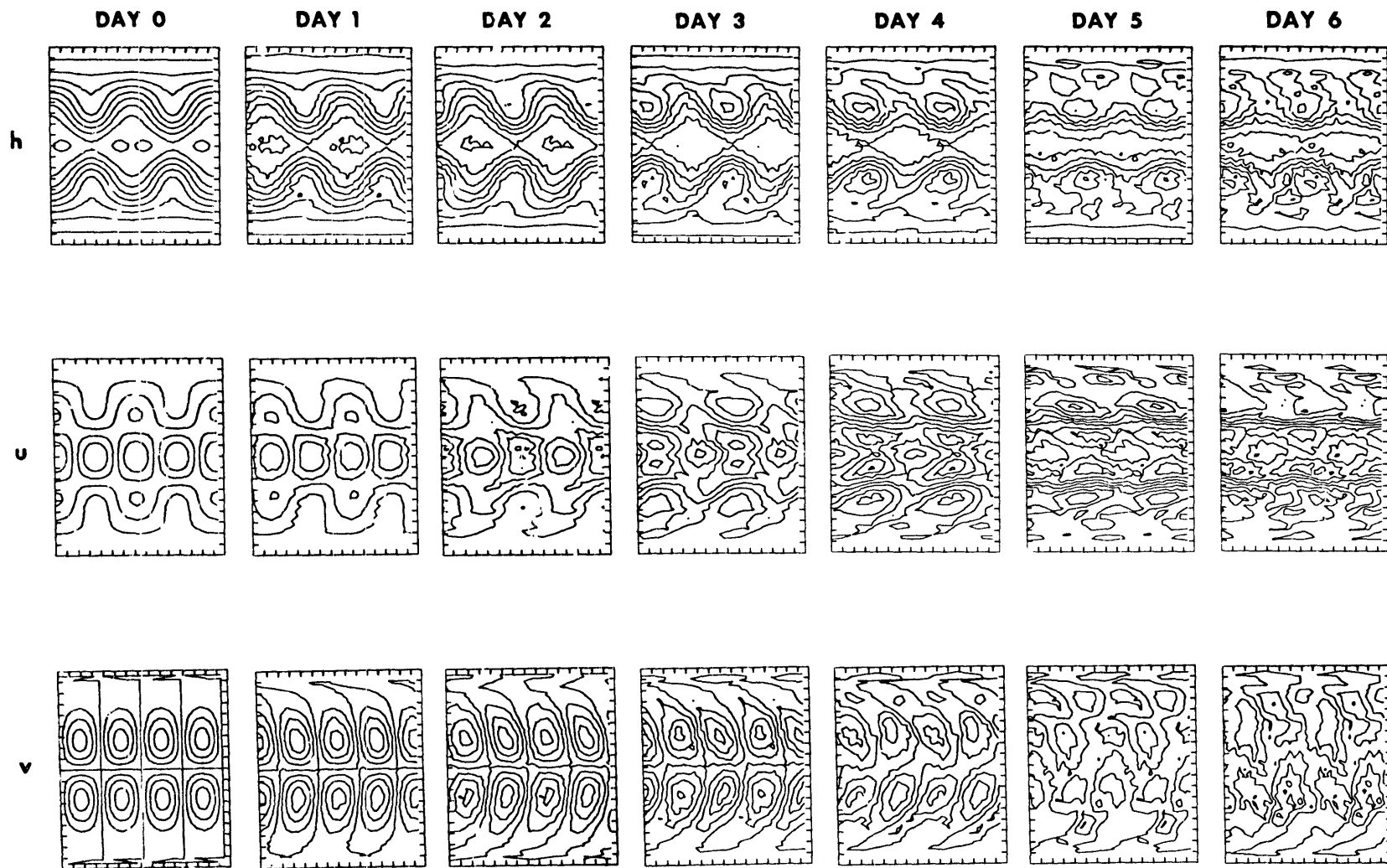


Fig. 5.5 Neamtan wave solution over 5° grid using centered time step. The figures contain a little over two wavelengths of the solutions.

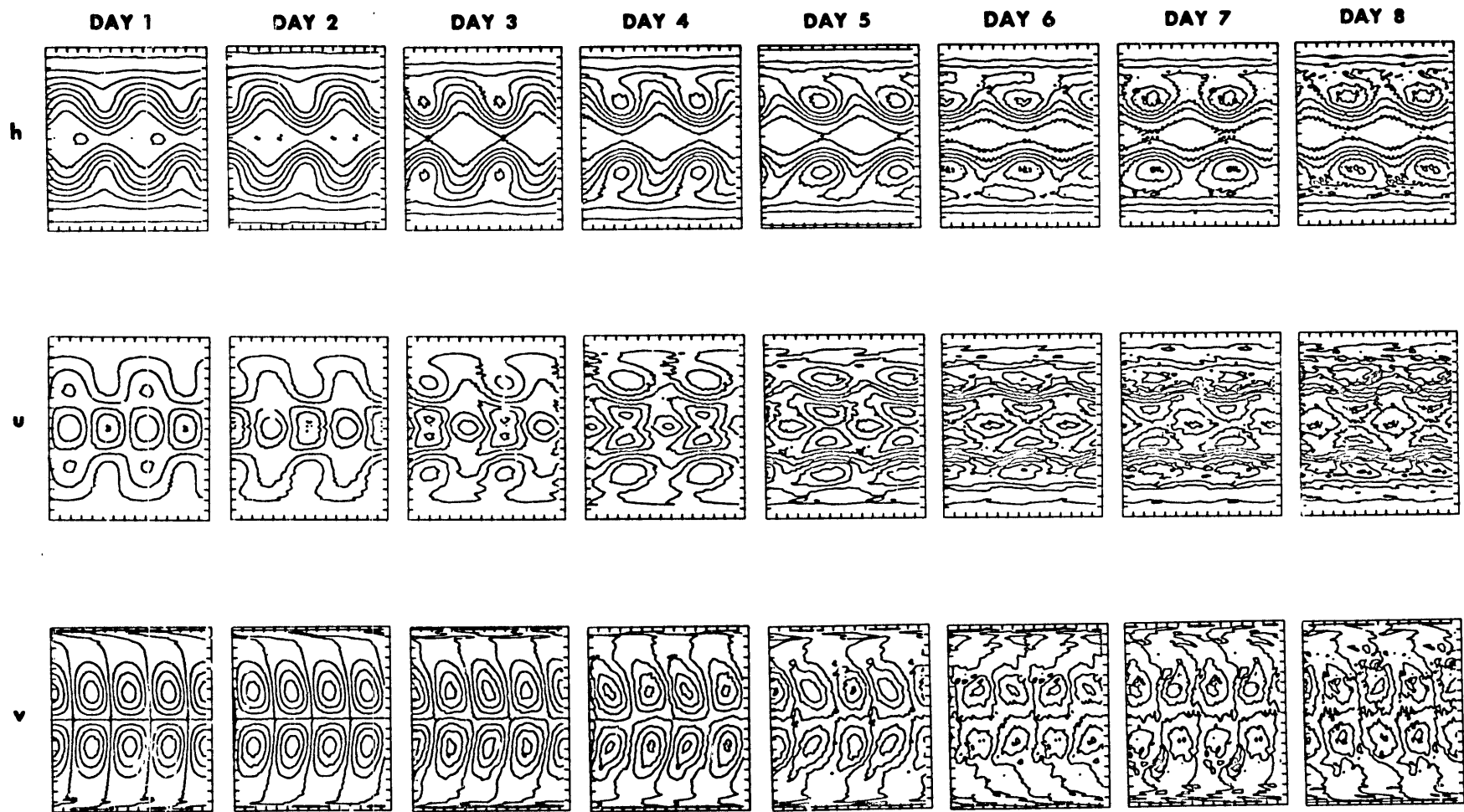
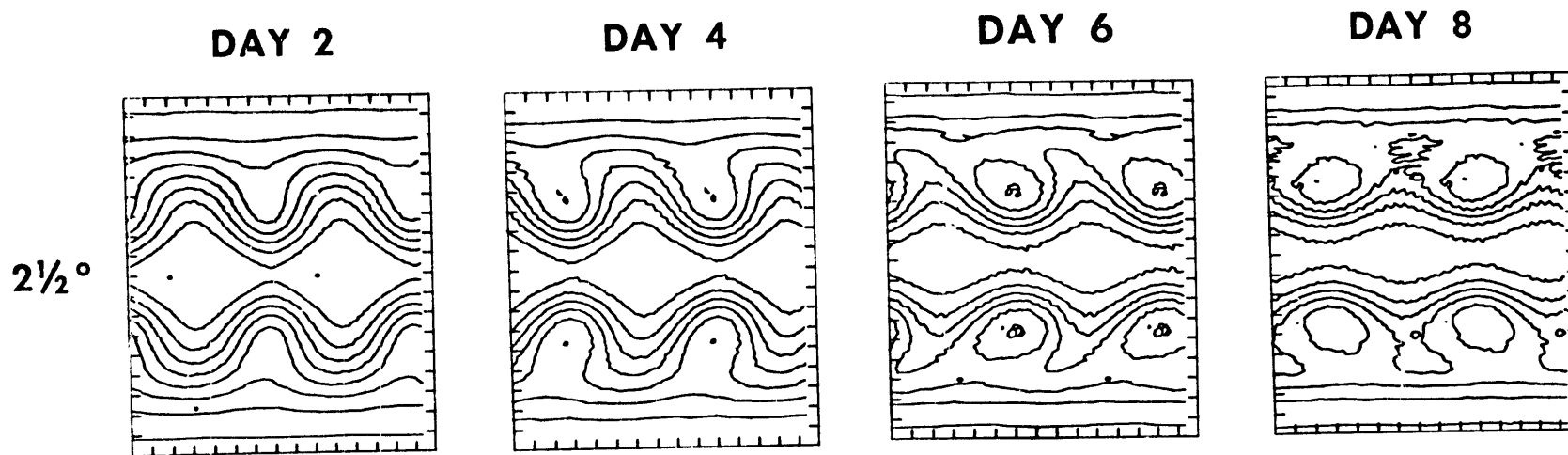
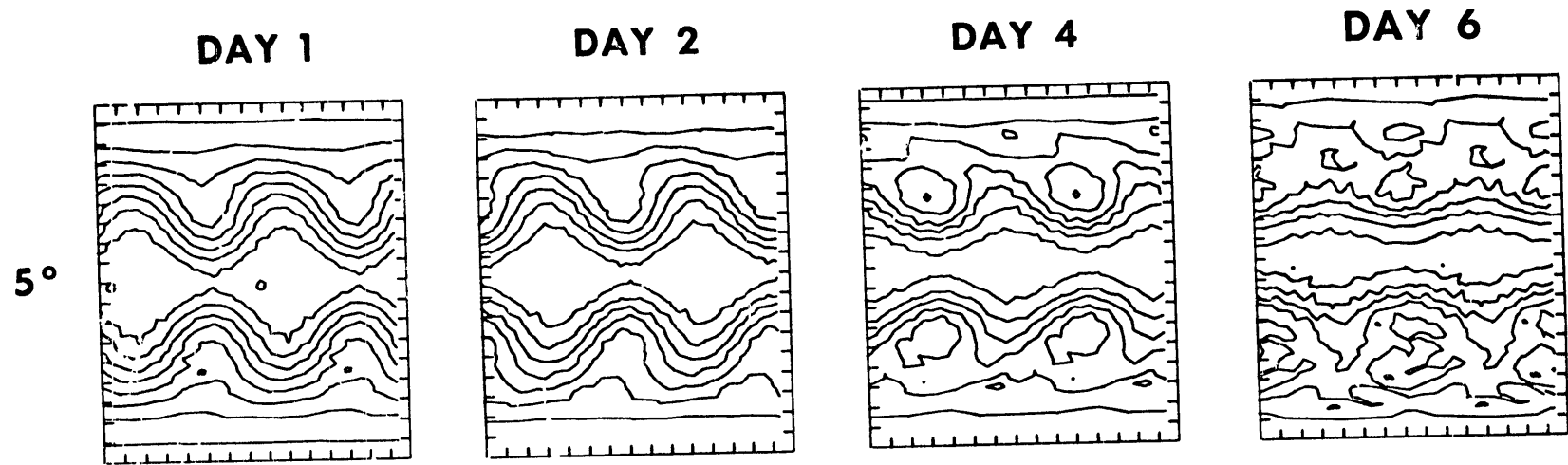


Fig. 5.6 Neamtan wave solution over $2\frac{1}{2}^\circ$ grid using centered grid.

Fig. 5.7 Height field of Neamtan wave solution over
 5° and $2\frac{1}{2}^{\circ}$ grids using Matsuno time step.



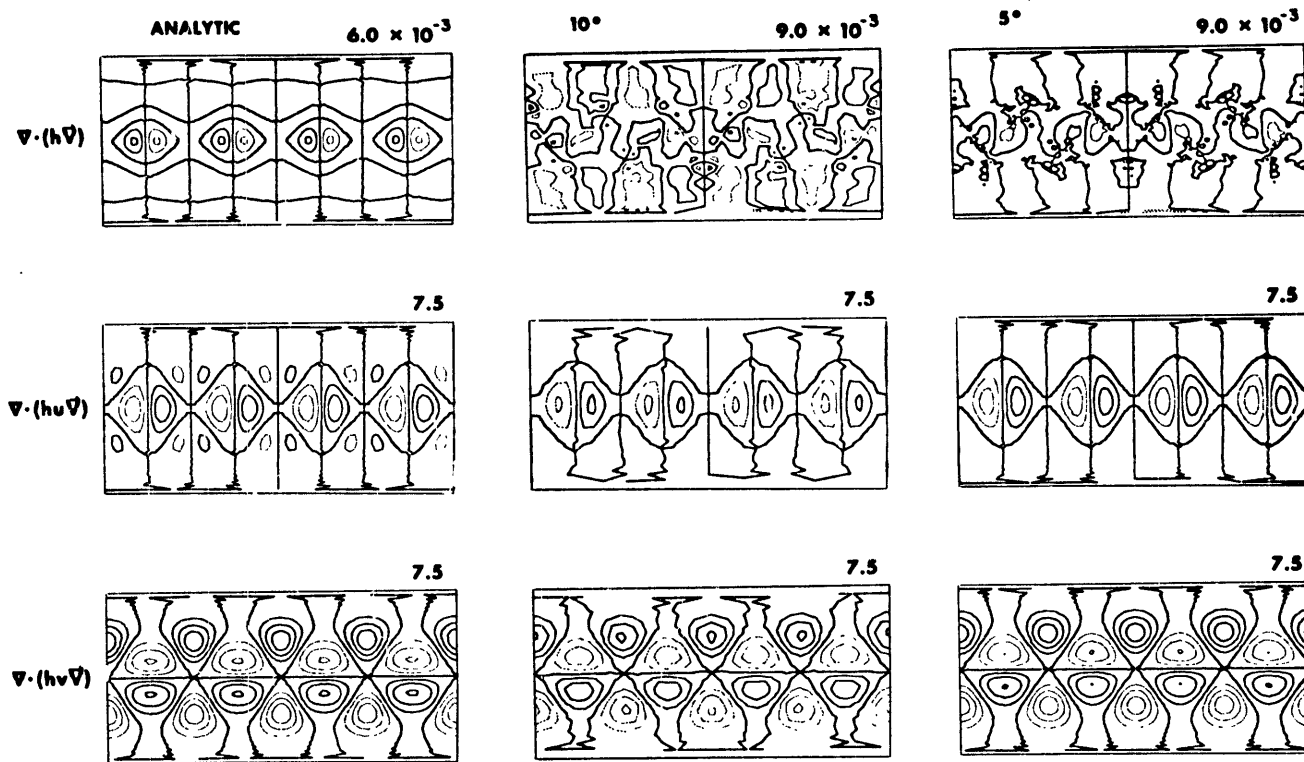


Fig. 5.8 Analytic and discrete flux terms. The contour interval is given in the upper right corner of each plot in units of meters and seconds.

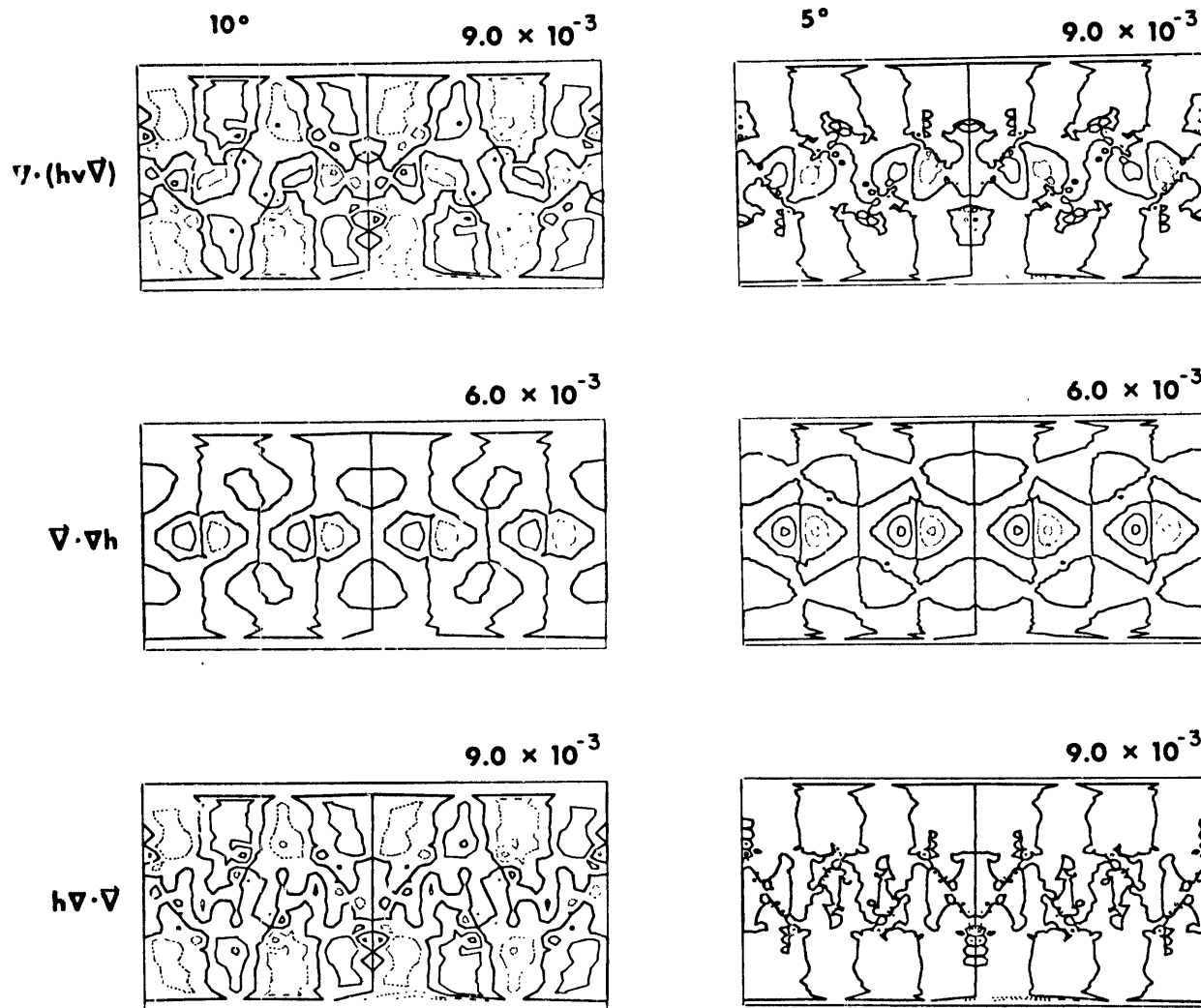


Fig. 5.9 Scheme IIIs over 10° and 5° grids. The contour intervals are given in the upper right corners. The dark contour has zero value, solid lines positive, and dashed lines negative.

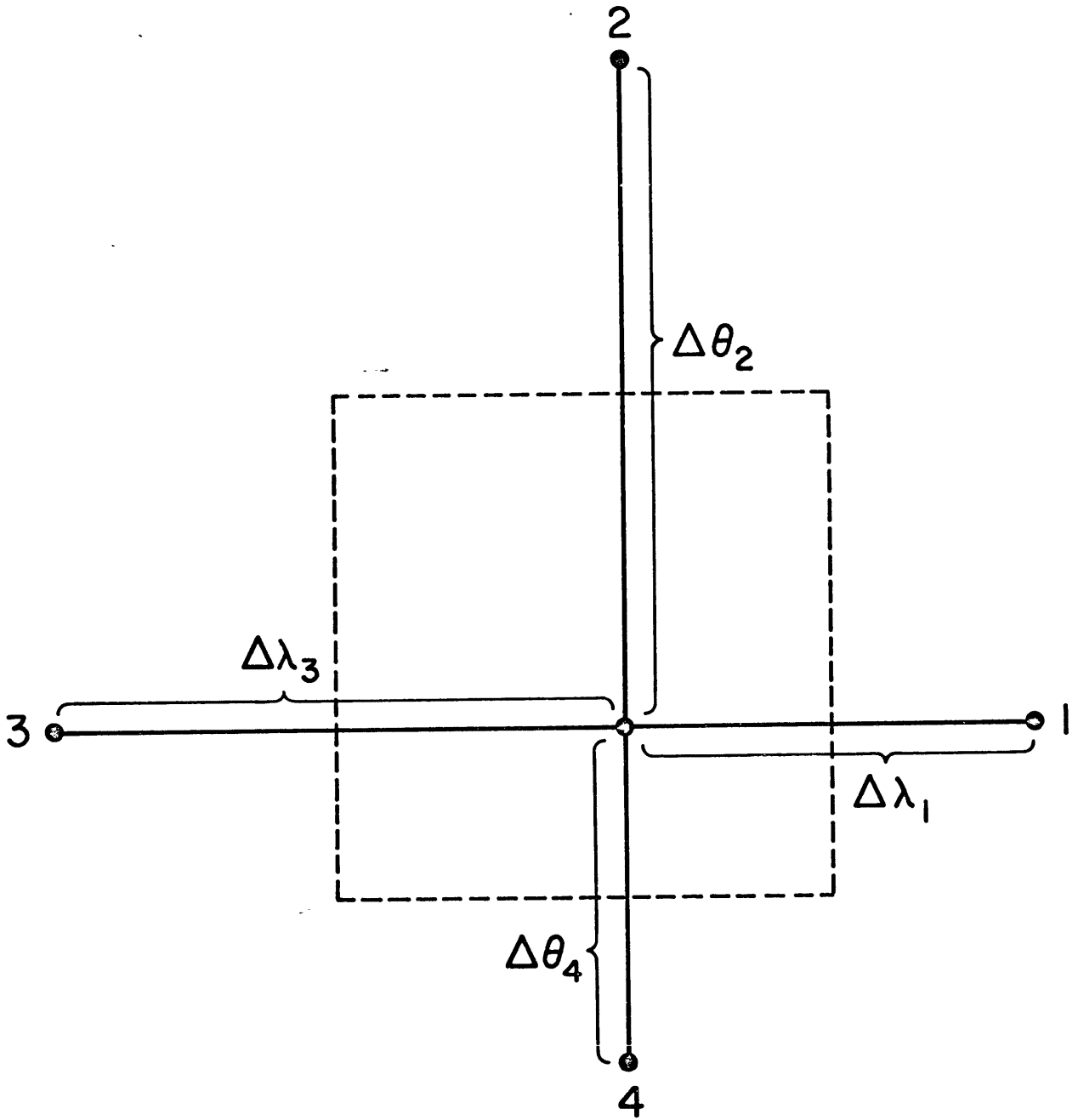


Fig. 5.10 Random Spherical Stencil

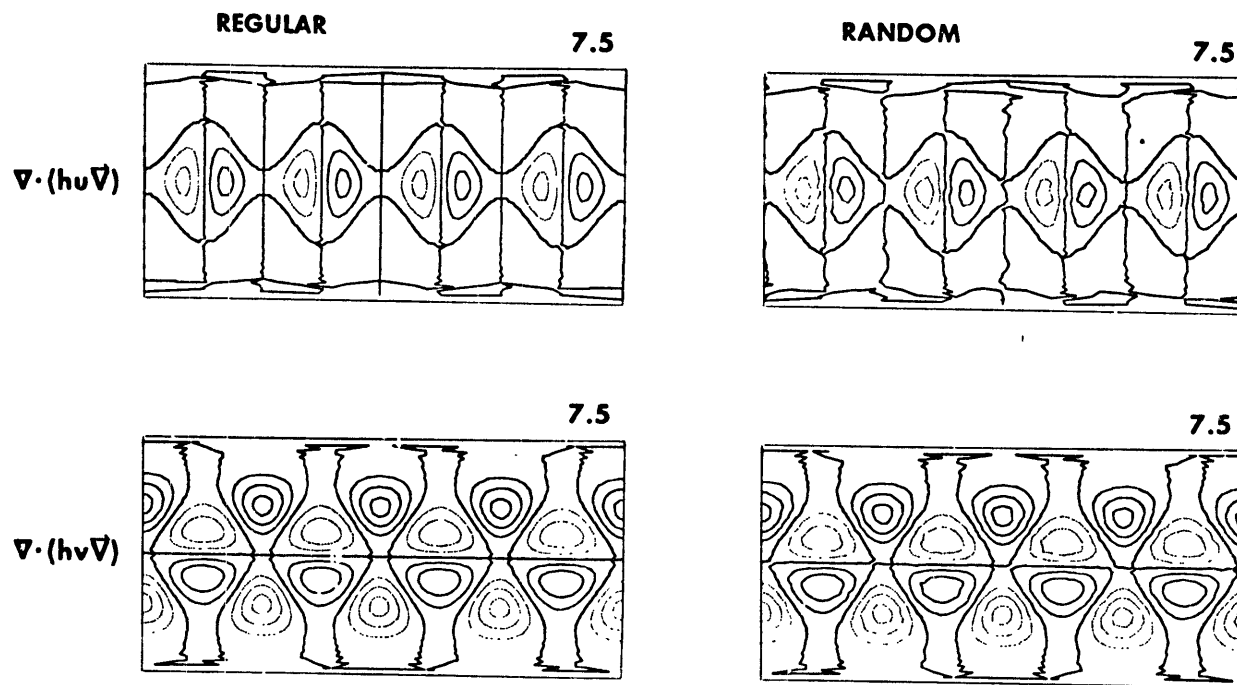


Fig. 5.11 Momentum flux calculated over regular and random spherical stencils. Contour intervals are given in the upper right corners.

Fig. 5.12 Fluxes computed over regular spherical stencil.
Contour intervals are given in the upper right
corners.

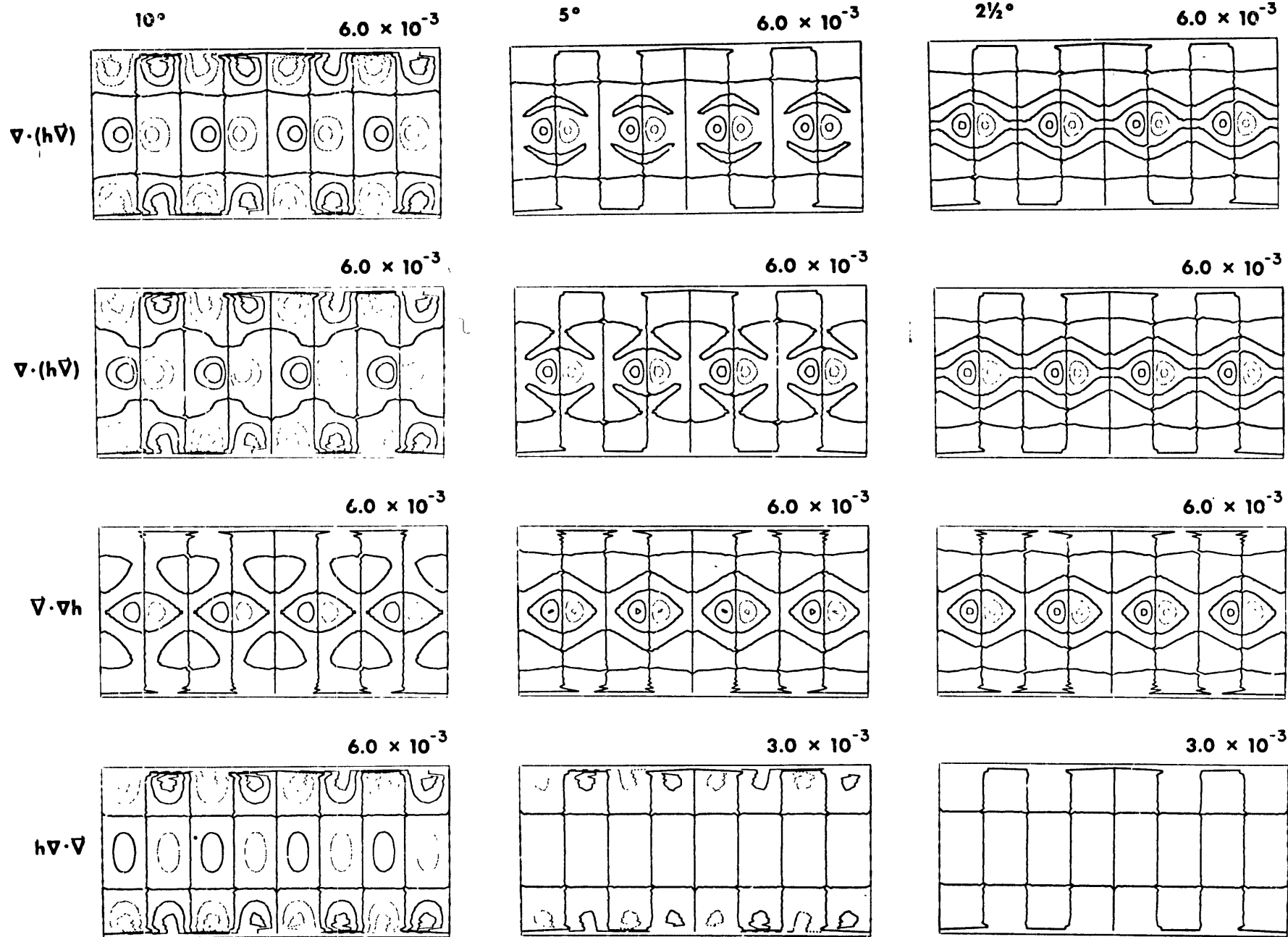
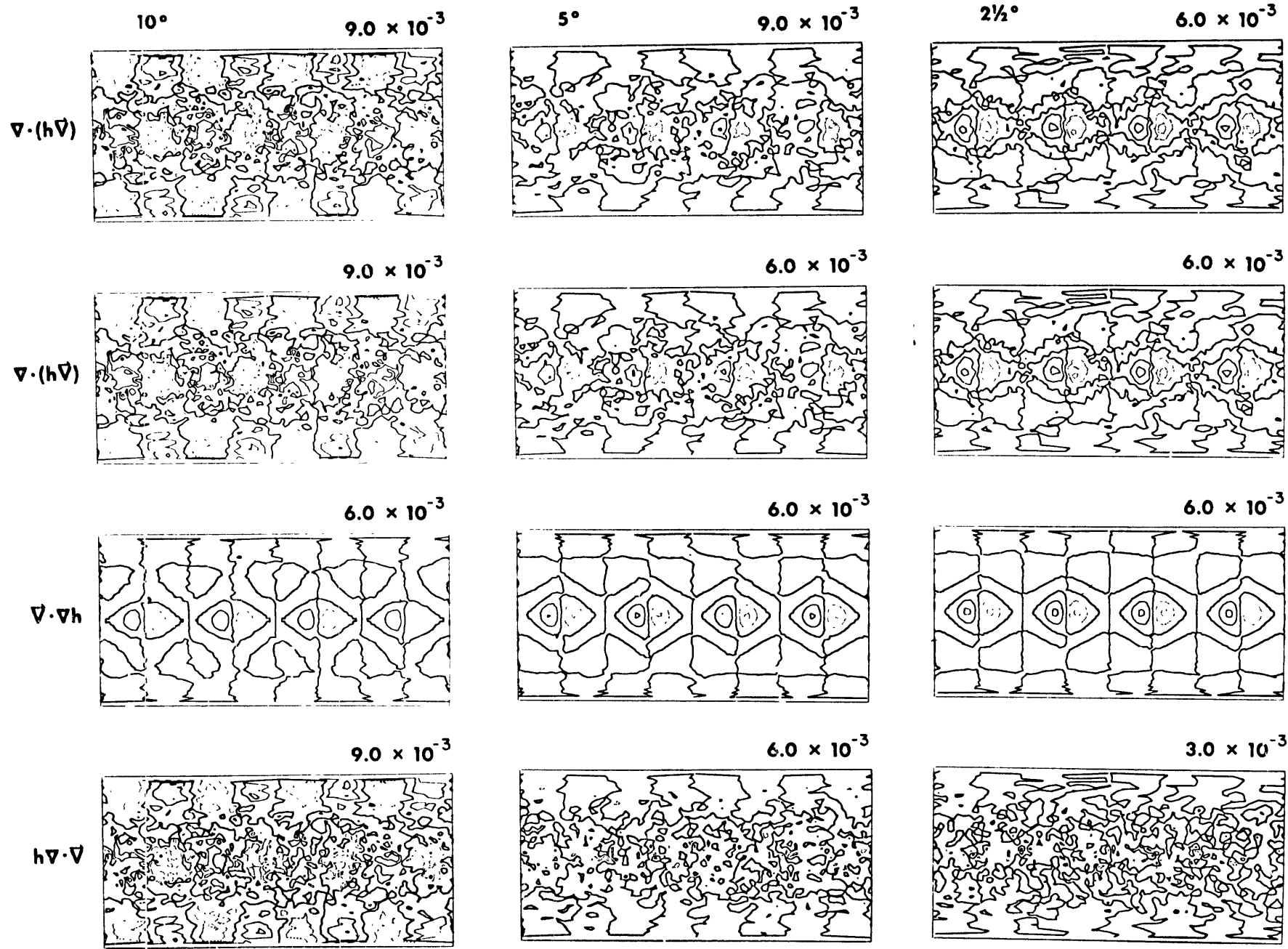


Fig. 5.13 Fluxes computed over random spherical stencil.
Contour intervals are given in the upper right
corners.



CHAPTER VI

CONCLUSIONS

6.1 Conclusions

The properties of spherical grids are reviewed and compared with one another. Grids based on conformal coordinates have the problem of interpolating between overlapping grids on two or more different projections. Grids based on spherical polar coordinates have difficulties associated with the convergence of meridians approaching the poles. Heuristically, the spherical geodesic grid has the most desirable properties for numerical integration over a sphere. This type of grid is quasi-homogeneous in that the grid interval has about a 10 percent variation over the sphere. Compared to other grids, this quasi-homogeneity increases the minimum grid interval used to determine the maximum time step allowed by linear stability conditions.

Integrations over homogeneous grids on a beta-plane show that six-point differences associated with triangular grids produce better solutions for the primitive barotropic model than square differences with similar resolution and the same order of truncation error. Masuda's (1968) figures show that the same conclusion holds for approximations of the nondivergent barotropic vorticity equation. It should be pointed out that the triangular schemes require slightly more computer time than square schemes if both grids contain the same number

of points. This follows from the fact that the number of computations required to calculate the time derivatives depends on the number of grid points times the number of surrounding points. However, since a triangular grid integrated over a coarser grid produces results as good as those from a square scheme over a less coarse grid, the triangular schemes actually produce a saving of computer time for the same quality of solution. One would expect these same conclusions to hold in spherical geometry as well.

As a first test of the spherical geodesic grid the nondivergent barotropic vorticity equation was integrated for 12 days over a 10° and a 5° grid. The grids were oriented so that no grid point coincided with the poles. This model was chosen for the first test since it approximates large scale atmospheric behavior yet for certain initial conditions has a known analytic solution with which to compare the numerical solution. The triangular difference approximations to this model work quite well. The only observable error in the contoured output after 12 days was a small phase error. No indication of a tilt of the wave with increasing latitude was observed. Such a tilt has plagued other schemes. Examination of the mean square streamfunction reveals small truncation errors in the amplitude, with little accumulation in the 12 days.

Integrations of the primitive model show that the small variation in grid interval does introduce an unexpected problem. Conservative difference schemes which are second order when applied to a regular grid

become first order when applied to a non-regular grid. In the models we consider, the first order error is significant only in calculating the divergence. Thus there is no trouble in integrating the nondivergent barotropic vorticity equation. When the divergence is relatively large, such as for gravity wave motions, the relative error in the divergence becomes acceptably small. This is seen in the gravity wave problem integrated over a 5° grid. For more atmospheric like motions, such as a Neamtan wave where the divergence is small, the error can be significant. This is seen in the integration of a Neamtan wave over a 5° grid.

This same truncation error will be present in any non-regular spherical grid for conservative difference approximations of the type presented here. Any spherical grid with more than twelve points cannot be completely homogeneous. Gary (1968) points out that Kurihara's (1965b) and the Centered schemes are first order at the latitudes where the mesh size increases. In these schemes, the error is concentrated in latitude bands; in the spherical geodesic grid it is spread out over the entire grid.

The truncation error of the spherical geodesic grid can be made insignificant by taking a fine enough mesh. This is seen with the $2\frac{1}{2}^{\circ}$ integration. The need for a fine mesh for a satisfactory approximation is not necessarily a handicap. Studies by Grammelvedt (1968) and Gary (1968) indicate that at least 16 points per wavelength are needed for a satisfactory approximation to the phase velocity even

with second and fourth order schemes. Thus the $2\frac{1}{2}^{\circ}$ grid is suitable up to wave number nine. An even finer grid is needed for smaller waves.

Once the mesh size is small enough, the spherical geodesic schemes are seen to produce good results. Compared to Kurihara's scheme over his "uniform" grid, the spherical geodesic schemes are seen to be much better. On the other hand, the spherical geodesic schemes produce the same results as the Kurihara scheme over a regular spherical grid. The spherical geodesic schemes are also slightly better than the scheme of Kasahara and Washington.

The particular time differencing combined with the spherical geodesic difference is important. Centered time differences produce very good results, especially with regard to energy conservation. However, a very small time step is needed for stability. In fact, the time step must be almost as small as would be needed with a regular spherical grid if there were no skipping of grid points near the poles.

The Matsuno time difference, on the other hand, remains stable for a much larger time step. A time step up to four times longer than the time step of the other schemes is possible. Depending on the complexity of the other schemes, this could mean a saving of four in computer time. A more realistic figure is probably a little less than three because the spherical geodesic schemes use six surrounding points rather than the more normal four.

6.2 Suggestions for further research

There is much that can be done to continue the development and evaluation of the difference approximations over the spherical geodesic grid. Schemes with a different space phasing of the variables could eliminate the two-grid interval noise present in the primitive model schemes presented here. In schemes of the type presented here, the two-grid interval waves are treated as inertial motion and hence they are not damped. By spatially separating the height and velocity vector, these small waves could be treated as gravity waves and hence damped by the spatial dispersion. The Matsuno time step also damps this type of motion.

The development of higher order schemes would also be useful. Second order schemes would not require as fine a mesh size as $2\frac{1}{2}^{\circ}$ to produce acceptable truncation errors. Such schemes would be useful to study large scale phenomena for which phase truncation error requirements do not require a $2\frac{1}{2}^{\circ}$ grid.

The integrations performed here indicate that the particular time step scheme used is very important. It would be useful to have comparative studies of the various possible time steps combined with the spatial spherical geodesic schemes.

It would also be desirable to have comparative experiments of spherical grids using real atmospheric data.

Another approach to the problem might be taken. The vector velocity can be broken up into two scalar fields; a streamfunction for the nondivergent part and a potential function for the irrotational part. This approach would be an extension of Chapter III, and does not require the use of spherical polar coordinates with the polar singularity. A disadvantage of this system, however, is that Poisson's equation must be solved at each time step. This could be very time consuming for multi-level models.

Acknowledgements

The author would like to express his gratitude to his advisor Professor Edward N. Lorenz for his continual interest and advice during the course of this study. Thanks are also due to Drs. A. Kasahara, P. Thompson, and W. Washington of the National Center for Atmospheric Research for discussions about discrete approximations and to Dr. Grammelvedt for permission to use his figures showing results of the square difference schemes. The author also had the pleasure of having discussions with many other people in the field too numerous to mention individually. He is very grateful for these opportunities.

The major part of the computer time used for this study was provided by the Computer Facility of the National Center for Atmospheric Research. Additional computations were performed at the MIT Computation Center.

During his graduate studies the author was supported by UCAR and Ford Foundation fellowships and by research assistantships under contract AF 19(628)-5826 sponsored by the Air Force Cambridge Research Laboratories and contract Cwb-11392 sponsored by the Environmental Sciences Service Administration.

The author wishes to thank Mrs. Marie L. Gabbe for typing this manuscript.

APPENDIX 1

Relations used to simplify truncation error expressions

Relation 1

$$\begin{aligned} \frac{1}{3\delta^2} \sum_{i=1}^6 (\vec{S}_i \cdot \nabla)^k h \vec{S}_i &= 0 \text{ for even } k \\ &= \nabla h \text{ for } k=1 \\ &= \frac{3}{4} \delta^2 \nabla (\nabla^2 h) \text{ for } k=3 \\ &\leq O(\delta^{k-1}) \text{ for odd } k > 3 \end{aligned}$$

$$\begin{aligned} \frac{1}{3\delta^2} \sum_{i=1}^6 (\vec{S}_i \cdot \nabla)^k \vec{V}_0 \cdot \vec{S}_i &= 0 \text{ for even } k \\ &= \nabla \cdot \vec{V} \text{ for } k=1 \\ &= \frac{3}{4} \delta^2 \nabla \cdot (\nabla^2 \vec{V}) \text{ for } k=3 \\ &\leq O(\delta^{k-1}) \text{ for odd } k > 3 \end{aligned}$$

Relation 2

$$\begin{aligned}
 \sum_{\substack{j+k=l \\ j,k \neq 0}} \frac{1}{3\delta^2} \sum_{i=1}^6 [(\vec{S}_i \cdot \nabla)^j h][(\vec{S}_i \cdot \nabla)^k h] \vec{S}_i &= 0 \text{ for } l \text{ even} \\
 &= \frac{1}{2} \delta^2 \left\{ \nabla^2 h \nabla h + \nabla [(\nabla h)^2] \right\} \text{ for } l=3 \\
 &\leq O(\delta^{l-1}) \text{ for odd } l > 3
 \end{aligned}$$

$$\begin{aligned}
 \sum_{\substack{j+k=l \\ j,k \neq 0}} \frac{1}{3\delta^2} \sum_{i=1}^6 [(\vec{S}_i \cdot \nabla)^j h][(\vec{S}_i \cdot \nabla)^k \vec{V}] \cdot \vec{S}_i &= 0 \text{ for } l \text{ even} \\
 &= \frac{1}{2} \delta^2 \left\{ \nabla^2 h \nabla \cdot \vec{V} + \nabla h \cdot \nabla^2 \vec{V} + 2 \nabla \cdot [(\nabla h \cdot \nabla) \vec{V}] \right\} \text{ for } l=3 \\
 &\leq O(\delta^{l-1}) \text{ for odd } l > 3
 \end{aligned}$$

$$\begin{aligned}
 \sum_{\substack{j+k=l \\ j,k \neq 0}} \frac{1}{3\delta^2} \sum_{i=1}^6 [(\vec{S}_i \cdot \nabla)^j \vec{V}][(\vec{S}_i \cdot \nabla)^k h] \vec{V} \cdot \vec{S}_i &= 0 \text{ for } l \text{ even} \\
 &= \frac{1}{4} \delta^2 \left\{ \nabla^2 \vec{V} (\vec{V} \cdot \nabla h) + \nabla^2 h (\vec{V} \cdot \nabla \vec{V}) \right. \\
 &\quad \left. + 2 \vec{V} \cdot \nabla (\nabla h \cdot \nabla \vec{V}) \right\} \text{ for } l=3 \\
 &\leq O(\delta^{l-1}) \text{ for odd } l > 3
 \end{aligned}$$

Relation 3

$$\frac{1}{3\delta^2} \sum_{i=1}^6 [(\vec{S}_{i+1} \cdot \nabla)^j + (\vec{S}_{i-1} \cdot \nabla)^j] \vec{S}_i = 0 \text{ for } j \text{ even}$$

$$= \nabla h \text{ for } j=1$$

$$= \frac{3}{4} \delta^2 \nabla(\nabla^2 h) \text{ for } j=3$$

$$\leq O(\delta^{j-1}) \text{ for odd } j > 3$$

$$\frac{1}{3\delta^2} \sum_{i=1}^6 [(\vec{S}_{i+1} \cdot \nabla)^j + (\vec{S}_{i-1} \cdot \nabla)^j] \nabla \cdot \vec{S}_i = 0 \text{ for } j \text{ even}$$

$$= \nabla \cdot \vec{V} \text{ for } j=1$$

$$= \frac{3}{4} \delta^2 \nabla \cdot (\nabla^2 \vec{V}) \text{ for } j=3$$

$$\leq O(\delta^{j-1}) \text{ for odd } j > 3$$

Relation 4

$$\sum_{\substack{j+k=l \\ j,k \neq 0}} \frac{1}{3\delta^2} \sum_{i=1}^6 [(\vec{S}_{i+1} \cdot \nabla) h + (\vec{S}_{i-1} \cdot \nabla) h] (\vec{S}_i \cdot \nabla)^k h \vec{S}_i$$

$$= 0 \text{ for } l \text{ even}$$

$$= \frac{3}{2} \delta^2 \nabla^2 h \nabla h \text{ for } l=3$$

$$\leq O(\delta^{l-1}) \text{ for odd } l > 3$$

$$\sum_{\substack{j+k=l \\ j,k \neq 0}} \frac{1}{3\delta^2} \left\{ \sum_{i=1}^6 [(\vec{S}_i \cdot \nabla)^j h] [(\vec{S}_{i+1} \cdot \nabla)^k + (\vec{S}_{i-1} \cdot \nabla)^k] \vec{\nabla} \cdot \vec{S}_i \right. \\ \left. + \sum_{i=1}^6 [(\vec{S}_{i+1} \cdot \nabla)^j h + (\vec{S}_{i-1} \cdot \nabla)^j h] (\vec{S}_i \cdot \nabla)^k \vec{\nabla} \cdot \vec{S}_i \right\}$$

$$= 0 \text{ for } l \text{ even}$$

$$= \frac{3}{2} \delta^2 [\nabla^2 \vec{\nabla} \cdot \nabla h + \nabla^2 h \nabla \cdot \vec{\nabla}] \text{ for } l=3$$

$$\leq O(\delta^{l-1}) \text{ for odd } l > 3$$

Relation 5

$$\sum_{\substack{j+k+l=m \\ j,k,l \neq 0}} \frac{1}{3\delta^2} \sum_{i=1}^6 [(\vec{s}_i \cdot \nabla)^j \vec{V}] [(\vec{s}_i \cdot \nabla)^k h] (\vec{s}_i \cdot \nabla)^l \vec{V} \cdot \vec{s}_i$$

$$= 0 \text{ for } m \text{ even}$$

$$= \frac{1}{4} \left\{ (\nabla \cdot \vec{V})(\nabla h \cdot \nabla \vec{V}) + (\nabla h \cdot \nabla \vec{V}) \cdot \nabla \vec{V} \right. \\ \left. + \nabla(\vec{V} \cdot \nabla h) \cdot \nabla h - [(\vec{V} \cdot \nabla) \nabla h] \cdot \nabla \vec{V} \right\} \text{ for } m=3$$

$$\leq O(\delta^{m-1}) \text{ for odd } m > 3$$

APPENDIX 2

COMPUTATION OF \vec{C}_i

Denote the latitude and longitude of the end points of a great circle segment of a secondary grid area by (θ_1, λ_1) and (θ_2, λ_2) . The equation of the great circle through them is

$$a \cos \lambda + b \sin \lambda = \tan \theta$$

where a and b are determined by substituting in (θ_1, λ_1) and (θ_2, λ_2) . The longitude, λ_0 , of the intersection of this great circle with the equator is given by

$$\tan \lambda_0 = -\frac{a}{b}$$

The angle, θ_0 , the great circle makes with the equator is given by

$$\tan \theta_0 = a \cos \left(\lambda_0 + \frac{\pi}{2} \right) + b \sin \left(\lambda_0 + \frac{\pi}{2} \right)$$

Now define a new coordinate system such that its equator is the great circle through (θ_1, λ_1) and (θ_2, λ_2) . Denote coordinates in this new system by primes. The coordinates of points on the great circle are related in the two systems by

$$\begin{aligned} \cos \lambda' &= \cos(\lambda - \lambda_0) \cos \theta \\ \theta' &= 0 \end{aligned}$$

and

$$\begin{aligned} \sin \theta &= \sin \lambda' \sin \theta_0 \\ \tan(\lambda - \lambda_0) &= \tan \lambda' \cos \theta_0 \end{aligned}$$

At any point on the great circle, the unit normal vector in the primed coordinate system is \hat{j}' . We now perform a series of transformations to write this normal in the unprimed coordinate system. First transform the primed system to a cartesian system, then rotate down through an angle of θ_0 , rotate around by an angle of λ_0 , and return to spherical polar coordinates (unprimed). The product of the transformation matrices is the total transformation and the unit normal is given by

$$\hat{m} = \left\{ \begin{array}{l} (\sin \lambda \sin \theta_0 \sin \lambda_0 + \cos \lambda \cos \theta_0 \cos \lambda_0) \hat{i} \\ (\cos \lambda \sin \theta_0 \sin \lambda_0 - \sin \lambda \sin \theta_0 \cos \lambda_0 - \cos \theta_0 \cos \lambda_0) \hat{j} \end{array} \right\}$$

The line integral can now be calculated numerically. In the experiments reported here, the trapezoidal rule was used over 10 equally spaced points on each grid side. Experiments using 40 divisions indicated that 10 were sufficiently accurate.

References

- Arakawa, A., 1966: "Computational Design for Long-Term Numerical Integration of the Equations of Atmospheric Motion," Journal of Computational Physics. Vol. 1, No. 1, pp 119-143.
- Baer, F., 1964: "Integration with the Spectral Vorticity Equation," Journal of the Atmospheric Sciences," Vol. 21, No. 3, pp 260-276.
- Bryan, K., 1966: "A Scheme for Numerical Integration of the Equations of Motion on an Irregular Grid free of Nonlinear Instability," Monthly Weather Review, Vol. 94, No. 1, 39-40.
- Ellsaesser, H.W., 1966: "Evaluation of Spectral Versus Grid Methods of Hemispherical Numerical Weather Prediction," Journal of Applied Meteorology, Vol. 5, No. 3, pp 246-262.
- Gary, J.M., 1968: "A Comparison of Two Finite Difference Schemes Used for Numerical Weather Prediction," NCAR Manuscript No. 68-215, National Center for Atmospheric Research, Boulder, Colorado.
- Gates, W.L., and Riegel, C.A., 1962: "A Study of Numerical Errors in the Integration of Barotropic Flow on a Spherical Grid," Journal of Geophysical Research, Vol. 67, No. 2, pp 773-784.
- Gates, W.L., and Riegel, C.A., 1963a: "Further Studies of Numerical Errors in the Integration of Barotropic Flow on a Spherical Grid," Journal of Geophysical Research, Vol. 68, No. 17, pp 4949-4952.
- Gates, W.L., and Riegel, C.A., 1963b: "Comparative Numerical Integration of Simple Atmospheric Models on a Spherical Grid," Tellus, Vol. 15, No. 4, pp 406-423.
- Grammeltvedt, A., 1968: "A Survey of Finite Difference Schemes for the Primitive Equations for a Barotropic Fluid," submitted to Monthly Weather Review.

- Grimmer, M., and Shaw, D.B., 1967: "Energy-Preserving Integrations of the Primitive Equations on the Sphere," Quarterly Journal of the Royal Meteorological Society, Vol. 93, No. 397, pp 337-349.
- Haurwitz, B., 1940: "The Motion of Atmospheric Disturbances on the Spherical Earth," Journal of Marine Research, Vol. 3, pp 254-267.
- Kasahara, A., and Washington, W.M., 1967: "NCAR Global General Circulation Model of the Atmosphere," Monthly Weather Review, Vol. 95, No. 7, pp 389-402.
- Kuo, H.L., 1956: "On Quasi-Nondivergent Prognostic Equations and their Integration," Tellus, Vol. 8, pp 373-383.
- Kuo, H.L., and Nordø, J., 1959: "Integration of Four-Level Prognostic Equations over the Hemisphere," Tellus, Vol. 11, No. 4, pp 412-424.
- Kurihara, Y., 1965a: "On the Use of Implicit and Iterative Methods for the Time Integration of the Wave Equation," Monthly Weather Review, Vol. 93, No. 1, pp 33-46.
- Kurihara, Y., 1965b: "Numerical Integration of the Primitive Equations on a Spherical Grid," Monthly Weather Review, Vol. 93, No. 7, pp 399-415.
- Kurihara, Y., and Holloway, J.L., Jr., 1967: "Numerical Integration of a Nine-Level Global Primitive Equations Model Formulated by the Box Method," Monthly Weather Review, Vol. 95, No. 8, 509-530.
- Lorenz, E.N., 1960: "Energy and Numerical Weather Prediction," Tellus, Vol. 12, No. 4, 364-373.
- Lorenz, E.N., 1967: "Persistence of Atmospheric Circulation," Progress Report No. 2, Contract CWB-11392, ESSA.
- Mac Neal, R.H., 1953: "An Asymmetrical Finite Difference Network," Quarterly of Applied Math., Vol. 11, pp 295-310.

- Masuda, Y., 1968: "A Finite Difference Scheme by Making Use of Hexagonal Mesh-Points," Proceedings of the WMO/IUGG Symposium on Numerical Weather Prediction, Tokyo, 1968.
- McHale, J., 1962: R. Buckminster Fuller, New York, George Brazeller, pp 127.
- Mintz, Y., 1964: "Very Long-Term Global Integration of the Primitive Equations of Atmospheric Motion," WMO/IUGG Symposium on Research and Development Aspects of Long-Range Forecasting, Boulder, Colo.
- Miyakoda, K., 1960: "Test of Convergence Speed of Iterative Methods for Solving 2- and 3-dimensional Elliptic Type Differential Equations," Journal of the Meteorological Society of Japan, Vol. 38, pp 107-122.
- Neamtan, S.M., 1946: "The Motion of Harmonic Waves in the Atmosphere," Journal of Meteorology, Vol. 3, 53-56.
- Okamura, Y., 1968: "A Finite Difference Scheme for the Primitive Equation Model with Special Emphasis on the Suppress of the Two-Grid Interval Noise," Proceedings of the WMO/IUGG Symposium on Numerical Weather Prediction, Tokyo, 1968.
- Pfeffer, R.L., 1960: "On the Design of a Numerical Experiment for the Study of the General Circulation of the Atmosphere," Dynamics of Climate, Pergamon Press, New York, pp 26-31.
- Phillips, N.A., 1959: "Numerical Integration of the Primitive Equations on the Hemisphere," Monthly Weather Review, Vol. 87, No. 9, pp 333-345.
- Phillips, N.A., 1962: "Numerical Integration of the Hydrostatic System of Equations with a Modified Version of the Eliassen Finite-Difference Grid," Proceedings of the International Symposium on Numerical Weather Prediction, Tokyo, 1960, Meteorological Society of Japan, pp 109-120.
- Richardson, L.F., 1922: Weather Prediction by Numerical Process. Cambridge University Press, pp 236.

- Robert, A., 1966: "The Integration of a Low Order Spectral Form of the Primitive Meteorological Equations," Journal of the Meteorological Society of Japan, Vol. 44, pp 237-245.
- Robert, A., 1968: "The Treatment of Moisture and Precipitation in Atmospheric Models Integrated by the Spectral Method," Journal of Applied Meteorology, Vol. 7, No. 5, pp 730-735.
- Sadourny, R., Arakawa, A., and Mintz, Y., 1968: "Integration of the Nondivergent Barotropic Vorticity Equation with an Icosahedral-Hexagonal Grid for the Sphere," Monthly Weather Review, Vol. 96, No. 6, pp 351-356.
- Shuman, F.G., 1962: "Numerical Experiments with the Primitive Equations," Proceedings of the International Symposium on Numerical Weather Prediction, Tokyo, 1960, Meteorological Society of Japan, pp 85-107.
- Smagorinsky, J., Manabe, S., and Holloway, J.L., 1965: "Numerical Results from Nine-Level General Circulation Model of the Atmosphere," Monthly Weather Review, Vol. 93, No. 12, pp 727-768.
- Thompson, P.D., 1961: Numerical Weather Analysis and Prediction, New York, The Macmillan Company, pp 170.
- Vestine, E.H., Sibley, W.L., Kern, J.W., and Carlstedt, J.L., 1963: "Integral and Spherical-Harmonic Analysis of the Geomagnetic Field for 1955.0, Part 2," Journal of Geomagnetism and Geoelectricity, Vol. 15, No. 2, pp 73-89.
- Williamson, D., 1968: "Integration of the Barotropic Vorticity Equation on a Spherical Geodesic Grid," Tellus, Vol. 20, No. 4, pp 642-653.
- Winslow, A.M., 1966: "Numerical Solution of the Quasilinear Poisson Equation in a Nonuniform Triangular Mesh," Journal of Computational Physics, Vol. 1, No. 2, pp 149-172.

Biography

The author was born on Friday, March 13, 1942. He graduated from the Sayre (Pa.) High School in 1960 whereupon he matriculated at The Pennsylvania State University. That institution awarded him a B.S. with highest distinction in Meteorology in June 1963 and a M.A. in Mathematics in March 1965. He entered the Graduate School of MIT in September 1965.

He is a member of the American Meteorological Society and of Sigma Xi.

His publications to date are:

Stability of Difference Approximations to Certain Partial Differential Equations of Fluid Dynamics, Journal of Computational Physics, Vol. 1, No. 1, July 1966, pp 51-67.

Integration of the Barotropic Vorticity Equation on a Spherical Geodesic Grid, Tellus, Vol. 20, No. 4, 1968, pp 642-653.